

Minimal Glacier Models

by

Johannes Oerlemans

Institute for Marine and Atmospheric Research Utrecht
Utrecht University
Utrecht
The Netherlands

Igitur, Utrecht Publishing & Archiving Services, Universiteitsbibliotheek Utrecht
ISBN 978-90-6701-022-1
Published in May 2008
Second print in March 2011 (with some revisions)
© J. Oerlemans

Cover: On the way to a weather station on Hardangerjökulen, Norway (photo K. Stuermer)

Minimal glacier models

1. Basics	5
1.1 Introduction	
1.2 Minimal glacier models	
1.3 The mass balance field	
1.4 Perfect plasticity	
2. Equilibrium states	13
2.1 The simplest glacier model	
2.2 More complex geometry	
2.3 Including feedback of length on ice thickness (nonlinear model)	
2.4 Calving glaciers I (constant accumulation rate)	
2.5 Calving glaciers II (mass-balance field depending on altitude)	
3. Time-dependent modelling	31
3.1 Introduction	
3.2 The simple dynamic glacier model	
3.3 Model for a glacier of varying width	
3.4 Climate change experiments	
3.5 Application to Nordenskiöldbreen, Svalbard	
4. Surging glaciers	49
4.1 Introduction	
4.2 Describing a surge in the minimal glacier model	
5. Varying bed slope	55
5.1 Introduction	
5.2 Modifying the continuity equation	
5.3 A simple concave bed	
5.4 Overdeepening	
6. Calving glaciers	63
6.1 Introduction	
6.2 Constant balance rate	
6.3 Balance rate depending on altitude	
6.4 Application to Hansbreen, Svalbard	
6.5 A note on more complicated bed profiles	
7. Linear modelling	73
7.1 Introduction	
7.2 A first-order linear model for glacier length	
7.3 Backward modelling	
7.4 Estimating response times from length records with linear theory	

8. Further applications	83
8.1 Introduction	
8.2 Model formulation	
8.3 Application to McCall Glacier, Alaska	
8.4 Application to the Vadret da Morteratsch	
Epilogue	95
Acknowledgements	97
References	99



Piz Bernina (left) and Piz Morteratsch (right)

1. Basics

1.1 Introduction

During the past few decades the study of glaciers and their response to climate change has shown a strong development. Early theoretical work in the fifties and sixties has been complemented by the construction of numerical models of glaciers and ice sheets with various degrees of complexity. Observations of glaciers from space have given us a much better view on where the glaciers are and what they look like. More recently, advanced techniques like SAR interferometry have revealed an unexpectedly rich dynamic behaviour of many ice bodies. Fast flow (intermittent or continuous) has been observed on a large number of glaciers, and this finding suggests that many glaciers may adjust to climate change more quickly than hitherto assumed.

In view of these developments it may seem a bit odd to write a text on “Minimal Glacier Models”. Why play around with simple quasi-analytical models if computer power is virtually unlimited to run codes on very high resolution? Well, digging into to numerical models and codes for more than 20 years has revealed to me that numerical modelling also has negative sides. First of all, documentation of codes (including my own) is normally inadequate, details of how boundary conditions are implemented in a numerical scheme are generally not described, and altogether reproducibility is poor. An outstanding problem is the dependence of numerical solutions on the resolution of a computational mesh or grid, in particular when the balance rate depends on surface elevation (e.g. Van den Berg et al., 2006), or when the position of the grounding line plays an important role in the evolution of an ice sheet. This criticism is not meant to claim that one should stick with simpler models, but it helps to appreciate that there are more lines along which glaciers can be studied.

Simple models are first of all learning tools. There is an intrinsic value in models that can be solved analytically or coded by a student in a couple of days. Simple models have the advantage that the parameter space can be explored in great detail. This means that a better feeling can be developed for what matters and what is fairly insignificant.

Simple models are also very useful to find out how robust the dynamic behaviour of complex numerical models is. Subtle instabilities may be lost when going from many degrees of freedom (in a numerical model with spatial resolution) to a few (in a minimal model). It is useful to have knowledge about the “dimensionality“ of a particular process.

In this text the focus is on the interaction between glaciers and climate - not on the mechanics of glacier flow. This interaction involves a number of feedbacks mechanism that can be captured by simple models. The dependence of the balance rate on surface altitude is the most obvious example, and leads to nonlinear behaviour that can be studied well with simple models.

1.2 Minimal glacier models

I use the term minimal glacier models to indicate a class of models that normally have no spatial resolution, i.e. that do not explicitly describe how quantities like ice thickness, basal water pressure, sliding velocity, etc., vary in space. State variables are typically glacier length L (or ice-cap radius R), mean ice thickness, ice thickness at the glacier front or grounding line, etc. Like in glacier models with spatial resolution, the evolution of a glacier is always calculated from an integrated continuity equation. Normally this integration is done over a vertical coordinate to find a prognostic equation for local ice thickness. In the case of minimal models the integration is done over the entire glacier:

$$\frac{dV}{dt} = \int b dx dy + C . \quad (1.2.1)$$

Here V is ice volume, t is time, b is the balance rate, x and y are horizontal coordinates, and C is the mass change associated with processes at the glacier front (e.g. calving of icebergs) or the mass flux across a grounding line (when changes in the volume of grounded ice are considered). Throughout this text it is assumed that ice density is constant, which implies that volume and total mass are equivalent concepts.

In many cases we want to work with a prognostic equation for glacier length rather than glacier volume. In general we will seek for a simple relation between length (or radius) and volume which makes it possible to derive an explicit expression for dL/dt . For instance, if $V = aL^\eta$, where a and η are suitable constants, we have

$$\frac{dL}{dt} = a^{-1} \eta^{-1} L^{1-\eta} \frac{dV}{dt} . \quad (1.2.2)$$

Ultimately, the driving force for any glacier is the mass balance. Because the balance rate varies in space, any change in the shape of a glacier will affect its total mass budget. In fact, it is this interaction that may give rise to some interesting nonlinear behaviour.

1.3 The mass balance field

The balance rate \dot{b} is defined as the net annual gain or loss of mass at the glacier surface (Østrem and Brugman, 1991). It should be noted that the specific balance rate is always defined with respect to the vertical (i.e. not perpendicular to the glacier surface).

On glaciers the balance rate is first of all depending on altitude (Figure 1.1). The accumulation zone of a glacier is the zone where $\dot{b} > 0$. Here none or only part of the accumulated snow melts and runs off in summer. The accumulation zone is normally the highest part of a glacier. When going downglacier sooner or later the ablation zone is found where $\dot{b} < 0$. Here the winter snowpack is melted in late spring and early summer, and then the underlying ice is exposed to high air temperatures and a positive radiation balance throughout the summer.

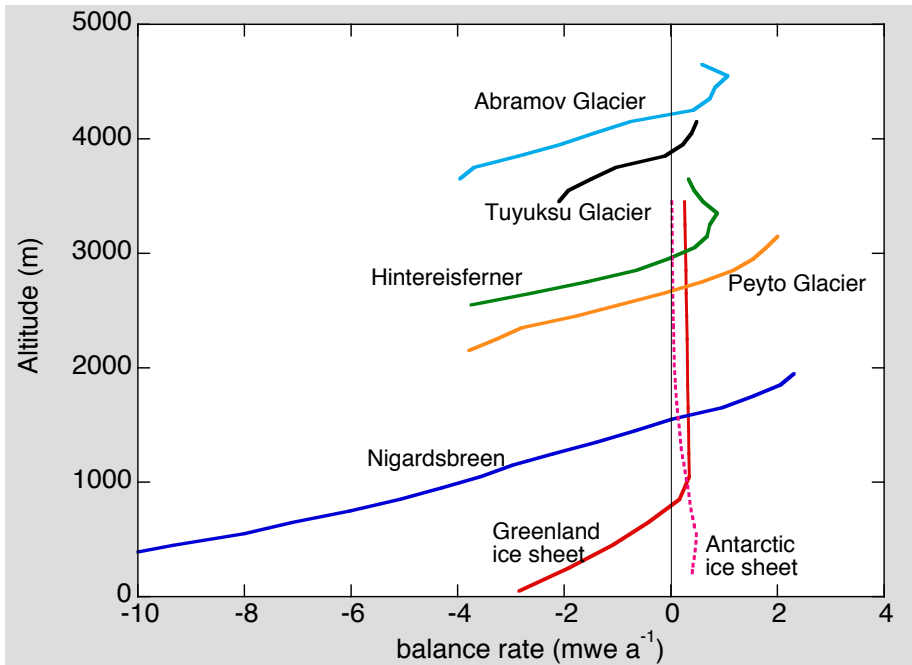


Figure 1.1. Vertical profiles of the balance rate for some glaciers (data from the WGMS, Zürich) and the major ice sheets. The balance profiles for the Greenland and Antarctic ice sheet are schematic.

There are mainly two reasons why \dot{b} increases with altitude. The most obvious reason is the decrease of air temperature with altitude, about 6 to 7 degrees K per km. Lower air temperatures imply a smaller turbulent heat flux to the surface as well as a reduced amount of downwelling longwave radiation from the atmosphere (e.g. Kuhn, 1979; Greuell et al., 1997). Then precipitation generally increases with altitude. In mountain regions the annual precipitation on the higher parts can easily be twice as large as in the valleys.

Altogether it is not surprising that the balance rate increases strongly with altitude. Formally the balance gradient β is defined as

$$\beta = \frac{d\dot{b}}{dz}, \quad (1.3.1)$$

where z is altitude. Typical values of β range from $0.003 \text{ mwe a}^{-1} \text{ m}^{-1}$ on glaciers in a dry (sub)arctic climate to $0.01 \text{ mwe a}^{-1} \text{ m}^{-1}$ on glaciers in an extreme maritime climate [mwe = meters

of water equivalent]. As a consequence, ablation rates on maritime glaciers that push their snouts far down can be quite large. On the lower parts of Vatnajökull (Iceland) and Nigardsbreen (Norway) ice ablation is typically 10 mwe a^{-1} (Kjøllmoen, 2003). On the snout of Franz Josef Glacier, New Zealand, ablation is estimated to be of the order of 20 mwe a^{-1} (Oerlemans, 1997a; Anderson et al., 2006).

Whereas the mass balance conditions on the Greenland Ice Sheet are more similar to those of glaciers and small ice caps, the Antarctic Ice Sheet shows a different picture. Melt and runoff is limited, and once a threshold is passed the balance rate tends to decrease with altitude (Fig. 1.1).

By definition, the accumulation and ablation zones are separated by the equilibrium line, at which $\dot{b} = 0$. The equilibrium-line altitude E ranges from a few hundred of meters above sea level on some arctic islands to over 6000 m in the drier regions of the subtropics. In large parts of the Antarctic continent it drops below sea level, and the concept of the equilibrium line becomes meaningless.

A number of studies have been made to relate the equilibrium-line altitude to meteorological conditions. The pioneering work of Ambach (1963) was based on a consideration of the surface energy balance in the vicinity of the equilibrium line. This work was extended by Kuhn (1989). Another approach, aimed at a more global relation between meteorological quantities and equilibrium-line altitude, was taken by Ohmura et al. (1992). In recent years mass-balance models with spatial resolution have been developed that produce the equilibrium-line altitude as an inherent product of the model simulation (e.g. Klok and Oerlemans, 2002). From these studies it appears that the equilibrium-line altitude typically changes 100 m for a 1 K change of atmospheric temperature. This is less than one would find if the equilibrium line would move up or down with an atmospheric isotherm. In that case the change would be $1/\gamma_a$, where γ_a is the temperature lapse rate in the atmosphere. A typical value for γ_a is 0.0065 K m^{-1} , so the change in equilibrium-line altitude per degree warming would be 154 m. It should also be noted that in the tropics the relation between balance rate and climate is fundamentally different (e.g. Kaser and Osmaston, 2002).

In minimal glacier models simple representations of the mass-balance field have to be used. Three representations are commonly used in simplified models, namely,

(i) a constant positive balance rate:

$$\dot{b} = \dot{a} ; \quad (1.3.2)$$

(ii) a balance rate that varies linearly with altitude z :

$$\dot{b} = \beta(z - E) ; \quad (1.3.3)$$

(iii) a linear balance profile, cut off at a certain altitude:

$$\begin{aligned} \dot{b} &= \beta(z - Z_{ro}) + \dot{a} && \text{for } z < Z_{ro} , \\ \dot{b} &= \dot{a} && \text{for } z \geq Z_{ro} . \end{aligned} \quad (1.3.4)$$

In model (iii) the quantity Z_{ro} is introduced, which can be interpreted as the altitude of an effective runoff line. Note that the use of model (i) implies that there is no direct coupling of the shape of the glacier with the mass-balance field.

1.4 Perfect plasticity

The theory of perfect plasticity was introduced in glaciology a long time ago (Weertman, 1961). It provides a first-order estimate of how the thickness of a glacier varies with its horizontal dimension. When applied to ice sheets or glaciers the theory boils down to the condition that the shear stress at the base of a glacier cannot exceed a certain yield stress τ_0 . When the mass balance conditions are such that stresses are being built up, the result will be that the basal shear stress will always be equal to τ_0 . In a first approximation the shear stress τ at the base can be written as

$$\tau = \rho g H |\nabla h(x,y)| . \quad (1.4.1)$$

Here ρ is ice density, g acceleration of gravity, H ice thickness and h surface elevation. For the one-dimensional case we thus have

$$\rho g H \left| \frac{dh}{dx} \right| = \tau_0 . \quad (1.4.2)$$

The shape of a simple symmetric ice cap resting on a flat bed can now be derived easily. In this case $H = h$, and for the part of the ice cap where $dh/dx > 0$ we have

$$\frac{dh^2}{dx} = \frac{2\tau_0}{\rho g} . \quad (1.4.3)$$

It follows that the profile is parabolic:

$$h^2(x) - h^2(x_0) = \frac{2\tau_0}{\rho g} (x - x_0) . \quad (1.4.4)$$

To construct the solution for an ice cap we have to prescribe its size (L) and the thickness at the boundaries (we take it to be zero). The result is [writing $\sigma = 2\tau_0/(\rho g)$]:

$$h(x) = \sqrt{\sigma x} \quad \text{for } 0 \leq x \leq \frac{L}{2} , \quad (1.4.5)$$

$$h(x) = \sqrt{\sigma(L-x)} \quad \text{for } \frac{L}{2} \leq x \leq L . \quad (1.4.6)$$

The highest point thus is $h_{\max} = \sqrt{\sigma(L/2)}$. Values for the yield stress used in the literature are typically in the 0.5×10^5 to 2×10^5 Pa range, where the smaller values apply to ice caps with low mass turnover and the high values to active valley glaciers. The corresponding range for σ is 10 to 40 m. Figure 1.2 shows the resultant profile. Although it provides a reasonable first approximation to the shape of an ice cap, there are some notable deficiencies. Firstly, the solution is not valid at the ice divide. In reality, here the surface slope is very small and longitudinal stresses are important. Secondly, a property of the perfectly plastic ice sheet is that, given the size, the ice thickness does not depend on the mass balance. This implies that the response to a changing mass-balance field has to operate through a change in L .

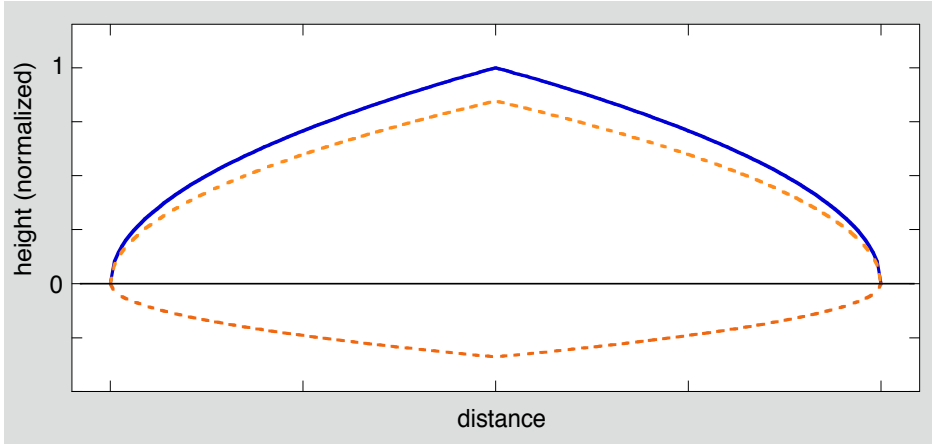


Figure 1.2. The profile of a perfectly plastic ice cap on a flat bed (solid line). The dashed lines show the profile if local isostacy is included.

The perfectly plastic ice-sheet profile can easily be corrected for local isostatic depression. If the bed elevation is denoted by b , isostatic equilibrium requires

$$\rho_i H = -\rho_m b , \quad (1.4.7)$$

where ρ_i is ice density and ρ_m is mantle density. Since $h = b + H$, it follows that

$$b = \frac{\rho_i h}{\rho_i - \rho_m} = -\xi h , \quad (1.4.8)$$

where $\xi = \rho_i / (\rho_m - \rho_i) \approx 0.4$. Therefore the ice thickness can also be written as

$$H = (1 + \xi) h . \quad (1.4.9)$$

This can be substituted in eq. (1.4.2) and apparently the new solution of the ice-sheet profile is (Figure 1.2):

$$h(x) = \sqrt{\frac{\sigma}{(1 + \xi)} x} , \quad (1.4.10)$$

$$H(x) = \sqrt{\sigma(1 + \xi)x} . \quad (1.4.11)$$

An important conclusion can be drawn from this analysis: bedrock sinking makes the mean surface elevation of an ice sheet lower by about 15%, and the ice thickness larger by about 18%.

It should be stressed that the adjustment of the bed to an ice load depends very much on the flexural length scale d_l of the lithosphere. In the case that $L \ll d_l$ there can be no local isostatic balance. For $L \gg d_l$, on the other hand, we expect that a local isostatic balance can be achieved when the ice sheet is in steady state. A typical value for d_l is 100 km. Even the largest glaciers in the Alps are too small to be compensated locally by an adjustment of the bed. Nevertheless, all glaciers in

the Alps together constitute a significant load and will have an effect on the crust on a larger scale. For ice caps like Vatnajökull or Austfonna, we have $L \sim d_l$ and the situation is more complex. By integrating eq. (1.4.5) with respect to x it is easily found that the mean surface elevation is

$$\bar{h} = \frac{\sqrt{2}}{3} \sqrt{\sigma L} . \quad (1.4.12)$$

The mean surface elevation of an ice cap thus varies with the square root of the size. This is an important result, because for mass balance model (ii) it is the mean surface elevation that determines the total mass budget.

Eq. (1.4.2) states that, essentially, ice thickness is small when the slope is large and vice versa. For many mountain glaciers and small ice caps this property has been observed from radar surveys of the distribution of ice thickness. Even when the constraint of perfect plasticity is relaxed and the shear stress is allowed to vary, glacier models strive to a geometry in which the variation in basal shear stress is within a comparatively narrow range. In fact, one can argue that glaciers strive to a geometry in which the driving stress, being proportional to the surface slope and the ice thickness does not vary too much. The associated stress field is not necessarily simple: at some locations shear stresses may dominate, at other places it could be longitudinal stress gradients that are essential in the force balance.



Blåisen, Hardangervidda, Norway

2. Equilibrium states

2.1 The simplest glacier model

The really simple glacier has a uniform width, rests on a bed with a constant slope s , and has a constant balance gradient β (Figure 2.1). The bed $b(x)$ is given by

$$b(x) = b_0 - sx , \quad (2.1.1)$$

and the balance rate by

$$\dot{b} = \beta(h - E) ,$$

where E is the equilibrium-line altitude. (2.1.2)

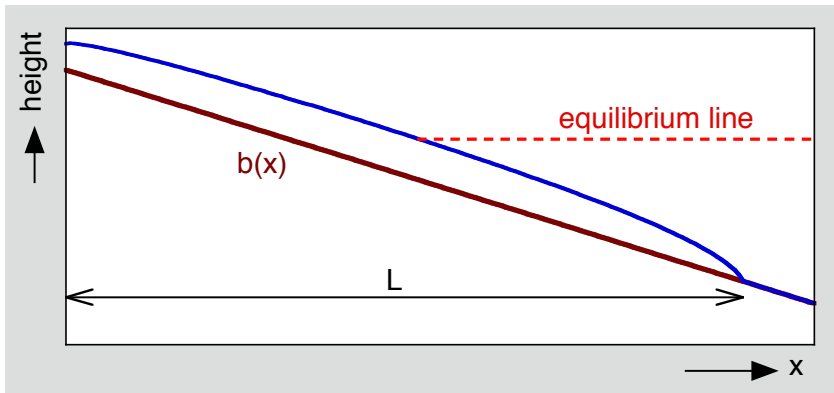


Fig. 2.1. Geometry of the simple glacier model; the slope of the bed is constant and the equilibrium line horizontal.

The total mass budget of the glacier is zero when

$$\int_0^L b dx = \beta \int_0^L (H + b_0 - sx - E) dx = 0 . \quad (2.1.3)$$

Solving for the glacier length L yields:

$$L = \frac{2(H_m + b_0 - E)}{s} . \quad (2.1.4)$$

In eq. (2.1.4) H_m is the mean ice thickness, defined as

$$H_m = \frac{1}{L} \int_0^L H dx . \quad (2.1.5)$$

Note that variations in the surface elevation do not play a role, because the balance profile is linear. It is only the mean surface elevation (equivalent to mean ice thickness when the bed slope is constant) that enters into the solution for L . We also observe that the equilibrium length does not depend on the balance gradient.

H_m can be related to the slope of the bed by assuming perfect plasticity *in a global sense*:

$$\rho g s H_m = \tau_0 . \quad (2.1.6)$$

Eliminating H_m from eqs. (2.1.4)-(2.1.6) then leads to

$$L = \frac{2}{s} \left(\frac{\tau_0}{\rho g s} + b_0 - E \right) . \quad (2.1.7)$$

The solution is illustrated in Figure 2.2. The value of $b_0 - E$ has been set to 500 m, $\tau_0 / (\rho g)$ to 10 m. For reference the solution for constant ice thickness (100 m) is also shown. In the case of the full solution ice thickness increases with decreasing slope, which implies an upward shift of the equilibrium point (intercept of equilibrium line and glacier surface). So the dependence of L on the bed slope now becomes stronger, especially for small values of s . It is clear that there is no solution for a flat bed, unless the equilibrium line is allowed to slope upwards with x . In a more realistic treatment the ice thickness not only depends on the slope, but also on the glacier length itself. This point will be considered later.

The simple model can also be used to make an order-of-magnitude estimate of climate sensitivity. From eq. (2.1.7) we find

$$\frac{dL}{dE} = -2/s . \quad (2.1.8)$$

So glaciers on a bed with a smaller slope are more sensitive in an absolute sense. The fractional change in glacier length is

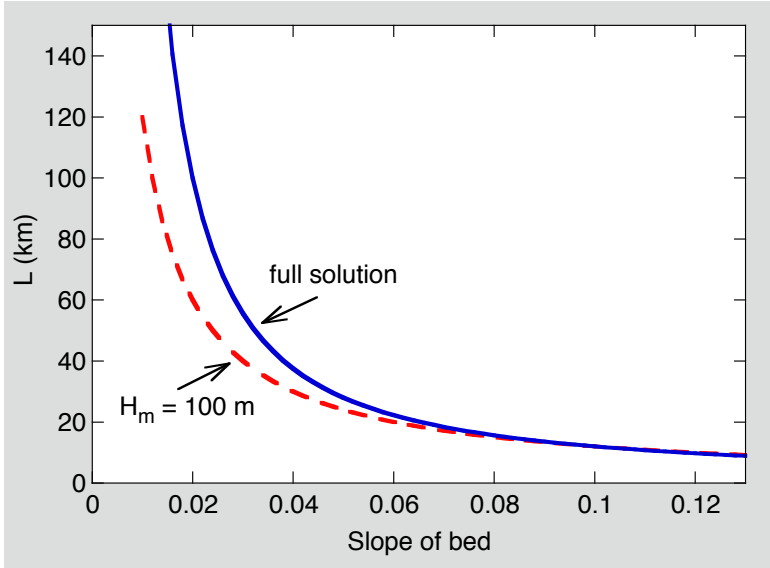


Fig. 2.2. Equilibrium length of a glacier on a bed with a constant slope. The dashed line refers to the case in which the mean ice thickness does not depend on the bed slope.

$$\frac{1}{L} \frac{dL}{dE} = - \left(\frac{\tau_0}{\rho g s} + b_0 - E \right)^{-1} \quad (2.1.9)$$

This quantity actually decreases with decreasing slope.

Now we try to make a first-order estimate of the dependence of glacier length on air temperature. Assuming that the equilibrium line follows an isotherm (which admittedly is only a crude approximation as discussed in Chapter 1), we can write

$$\frac{dE}{dT_{fa}} = -\frac{1}{\gamma_a} , \quad (2.1.10)$$

where T_{fa} is the ambient air (free air) temperature and γ_a is the temperature lapse rate (< 0). Eqs. (2.1.8) and (2.1.10) can be combined to give:

$$\frac{dL}{dT_{fa}} = \frac{2}{\gamma_a s} \quad (2.1.11)$$

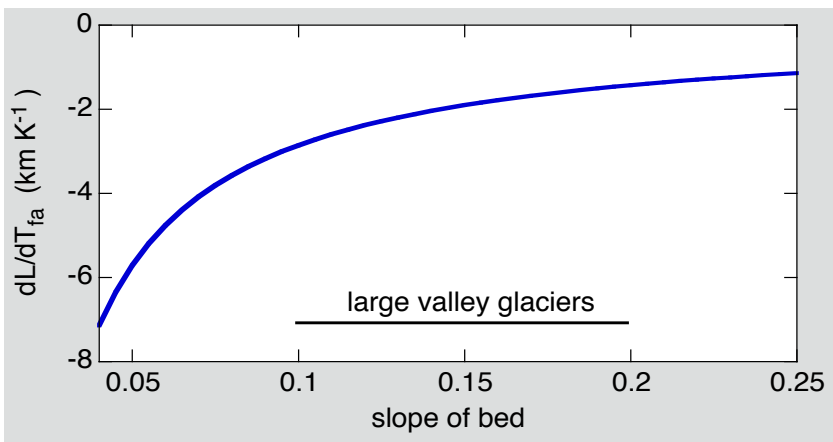


Fig. 2.3. Relation between glacier length and air temperature as a function of the bed slope. The atmospheric temperature lapse rate was set to -7 K/km .

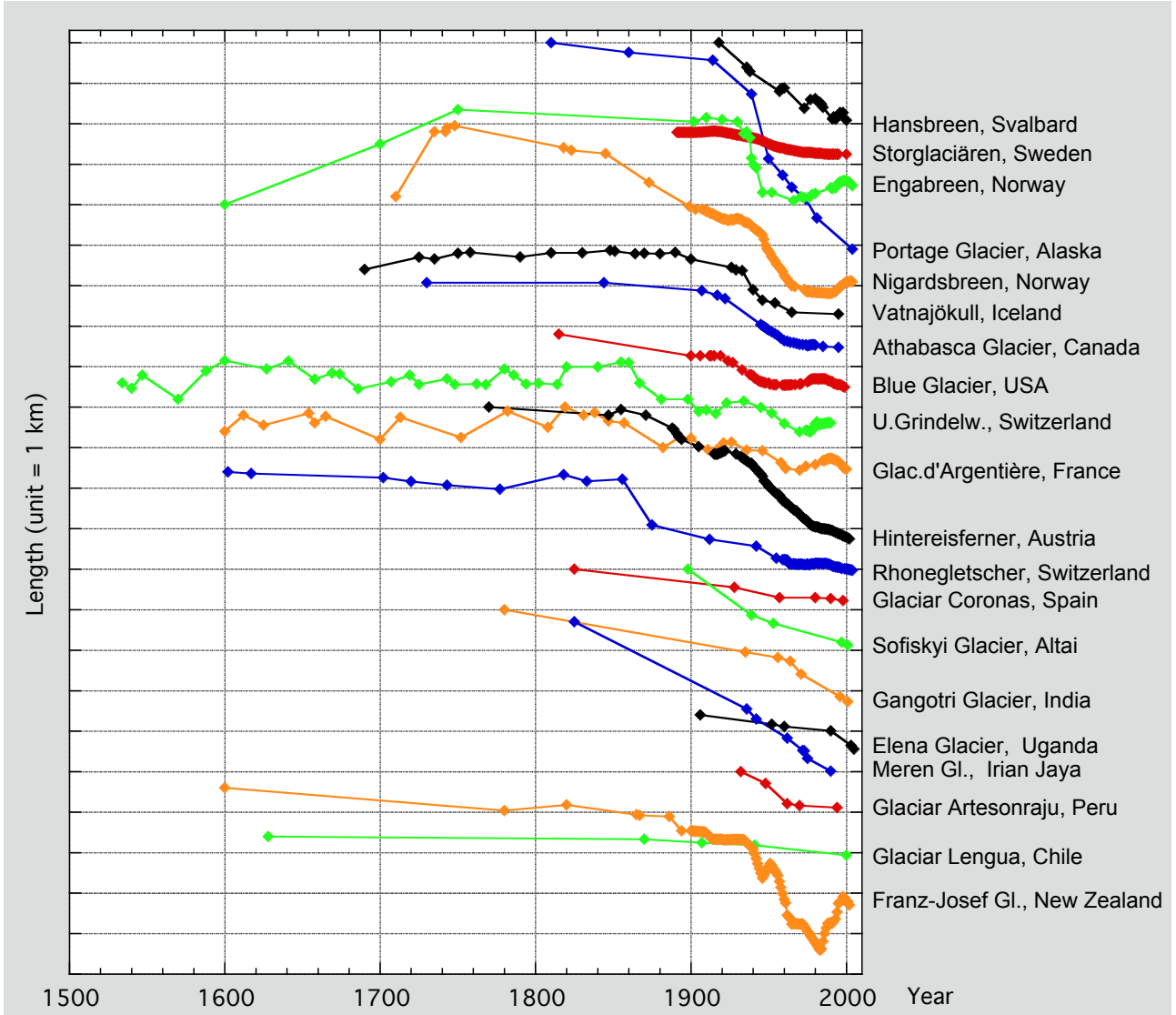


Fig 2.4. A selection of 20 glacier length records. Each symbol represents a data point. The records are ordered according to geographical latitude in a qualitative sense (Oerlemans, 2005).

It is remarkable that the sensitivity of glaciers to temperature change can be estimated by just two parameters: the mean slope and the atmospheric temperature lapse rate. Figure 2.3 shows the result. Larger valley glaciers typically have mean slopes between 0.1 and 0.2, implying that a 1 K temperature rise would lead to a 1 to 3 km decrease in glacier length. This number can be compared with observations of glacier length over the past centuries (Figure 2.4). It appears that since 1850 many larger glaciers have retreated over a distance of typically a few kilometers (e.g. Hintereisferner, Austria; Athabasca Glacier, Canada; Rhonegletscher, Switzerland; Franz-Josef Glacier, New Zealand). According to Figure 2.3 this could have been caused by a temperature rise of 0.5 to 1 K, which is actually what has been observed. We may therefore conclude that the simple glacier model provides an interesting first-order description of the relation between climate change and glacier response.

Some glaciers have shown a retreat that is notably larger, e.g. Nigardsbreen. This is probably related to geometric effects, and we will explore this in the next section.

2.2 More complex geometry

Many glaciers have wider accumulation basins and narrow tongues (Figure 2.5), which will affect the sensitivity of their length to climate change. This can be investigated with two coupled basins of different width.

Figure 2.6 illustrates the idea. A glacier tongue of constant width is nourished by an upper basin of length L_{ub} , also of constant, but different, width. To find the general solution we have to consider two cases, namely $L \leq L_{ub}$ and $L > L_{ub}$.

For $L \leq L_{ub}$ the solution is given by eq. (2.1.4):

$$L = \frac{2(H_m + b_0 - E)}{s} . \quad (2.2.1)$$

When the mass budget of the upper basin is positive, L will be larger than L_{ub} . The length of the glacier is then determined by



Fig. 2.5. Oblique photograph made from the International Space Station (ISS), showing the glaciers of the Bernese Oberland, Switzerland (5 September 2006, NASA). The largest glacier is the Aletschgletscher (≈ 24 km long). It has a wide accumulation basin (three basins, in fact), and a narrow tongue. The lake in the upper left corner is the Brienzer See.

$$\int_0^{L_{ub}} (H + b_0 - sx - E) dx + \xi \int_{L_{ub}}^L (H + b_0 - sx - E) dx = 0 . \quad (2.2.2)$$

In this expression ξ is the width of the glacier tongue scaled with the characteristic width of the upper basin. For most glaciers $\xi < 1$. Evaluating the integrals yields:

$$-\frac{1}{2} \xi s L^2 + \xi (H_m + b_0 - E)L + (1 - \xi)(H_{m,ub} + b_0 - E)L_{ub} - \frac{1}{2} s(1 - \xi)L_{ub}^2 = 0 . \quad (2.2.3)$$

In eq. (2.2.3) H_m and $H_{m,ub}$ are the mean ice thickness of the glacier tongue and the upper basin, respectively. With $H_m = H_{m,ub}$ and $E_r = E - b_0 - H_m$ ($E_r < 0$), the solution is:

$$L = -\frac{1}{s} \left[E_r + \sqrt{E_r^2 - 2s \frac{1-\xi}{\xi} (E_r L_{ub} + \frac{1}{2} s L_{ub}^2)} \right] . \quad (2.2.4)$$

An example is shown in Figure 2.7. L is plotted as a function of E for three different values of ξ . For $\xi = 0.25$, the width of the upper basin is four times that of the glacier tongue, which is not an unusual situation. Clearly, in this case the glacier length increases rapidly when the equilibrium line sinks below 1850 m. In terms of the climate sensitivity dL/dE , a clear maximum exists when the glacier starts to form the tongue. When the equilibrium line sinks still further, dL/dE will approach the value of the original model glacier of uniform width ($\xi = 1$). When the lower part of the glacier is wider than the upper part the opposite is seen. The sensitivity is at a minimum when the budget of the upper basin is just positive. In reality this situation does not occur frequently.

In conclusion we can state that glaciers with a narrow tongue are the ones that are most sensitive to climate change, especially when the glacier front is just below the upper basin.

Finally it should be noted that a similar analysis can be done for a model geometry of more than two basins, for instance a smaller upper basin, a wide basin in the middle, and a narrow tongue.

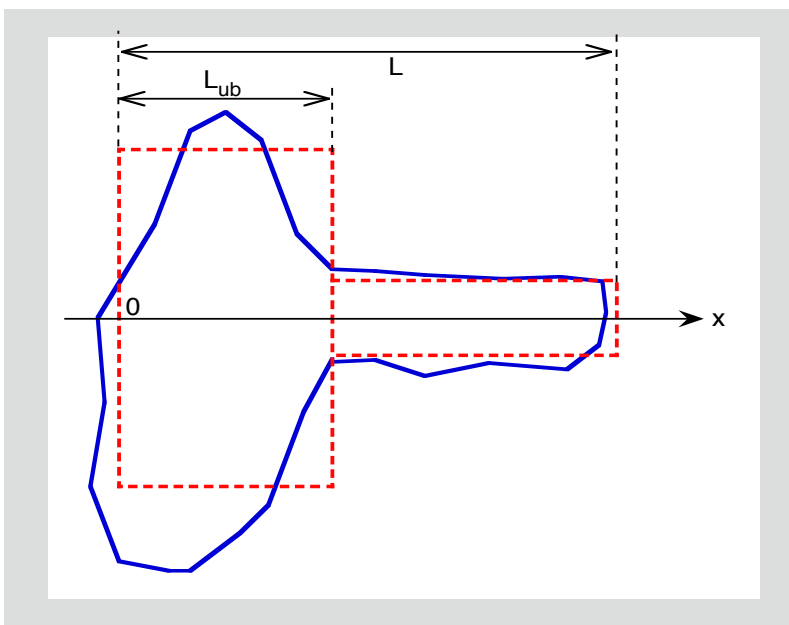


Fig. 2.6. Representing the outline of a real glacier (blue line) by a simple rectangular geometry (red lines), as seen in plan view.

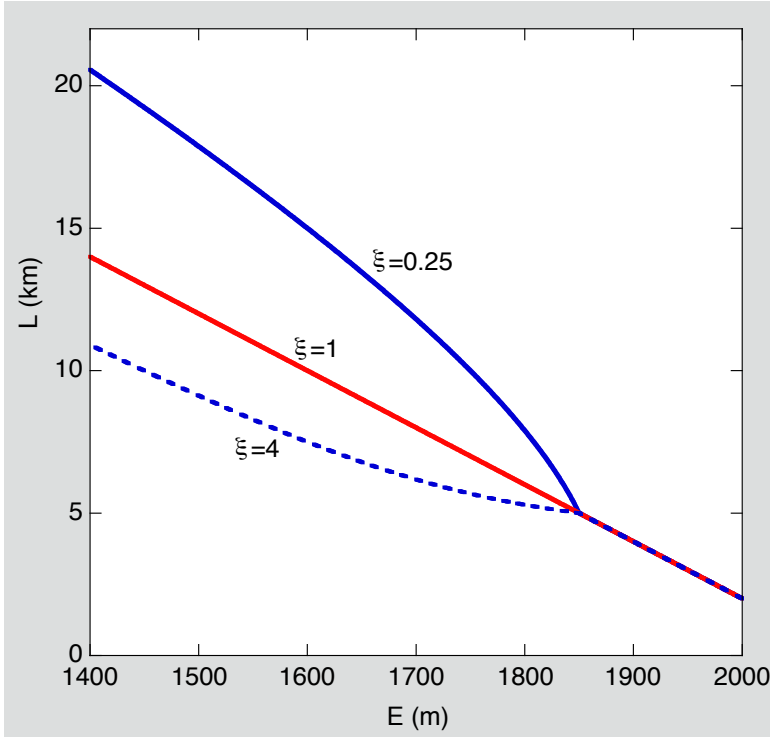


Fig. 2.7. Glacier length as a function of equilibrium-line altitude E , depending on the geometry as prescribed by ξ . Parameter values: $b_0 = 2000$ m, $s = 0.1$, $H_m = 100$ m, $L_{ub} = 5000$ m.

2.3 Including feedback of length on ice thickness (nonlinear model)

In the foregoing analysis the mean ice thickness depended on the average bed slope, but not on the glacier length. It is an obvious next step to include a relation between H_m and L . A meaningful expression for H_m is

$$H_m = \frac{\alpha_m L^{1/2}}{1 + \nu s} . \quad (2.3.1)$$

Here α_m and ν are constants. If the bed slope is set to zero, eq. (2.3.1) reduces to the form of eq. (1.4.12). Eq. (2.3.1) is therefore consistent with the perfectly plastic ice-cap model. Extensive experimentation with numerical glacier models, based on the shallow-ice approximation and Glen's law for simple shear, shows that $H_m \propto L^\kappa$, where κ varies from 0.40 to 0.45, depending on the bed slope (Oerlemans, 2001; p. 69). The larger values of κ are for smaller slopes of the bed. Apparently the exponent 0.5 in eq. (2.3.1) is not a bad choice, or in other words, perfect plasticity provides a workable approximation.

In contrast to eq. (2.1.6), eq. (2.3.1) implies that the characteristic basal shear stress, estimated to be roughly proportional to the ice thickness times the bed slope, increases with glacier length [note that eq. (2.1.6) is not valid for $s \rightarrow 0$].

Substituting eq. (2.3.1) into eq. (2.2.1) yields (now $E_r = E - b_0$):

$$L = \frac{2}{s} \left[\frac{\alpha_m L^{1/2}}{1 + \nu s} - E_r \right] . \quad (2.3.2)$$

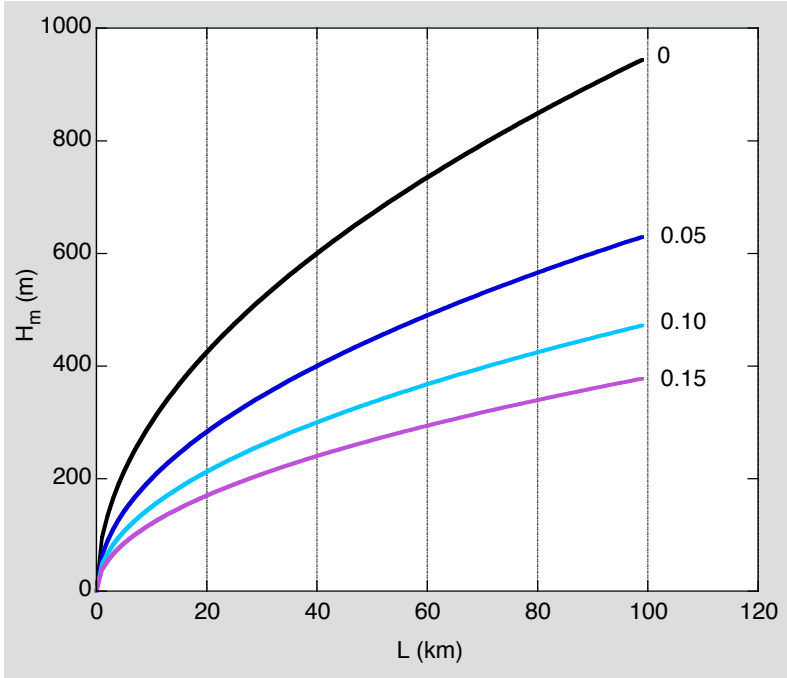


Fig. 2.8. Mean ice thickness as a function of glacier length for different values of the bed slope (labels), as parameterised by eq. (2.3.1). Other parameter values: $\alpha_m = 3 \text{ m}^{1/2}$, $\nu = 10$.

This equation is easily solved by setting $N = L^{1/2}$. It follows that

$$N^2 - \frac{2\alpha_m}{s(1+\nu s)}N + \frac{2E_r}{s} = 0 . \quad (2.3.3)$$

The discriminant of this quadratic equation is

$$Dis = \frac{4\alpha_m^2}{s^2(1+\nu s)^2} - \frac{8E_r}{s} . \quad (2.3.4)$$

Real solution exist only when $Dis \geq 0$. The first term is always positive, which implies that there is a limited range of values of E_r for which real solutions exist. So even when the equilibrium line is above the highest point of the glacier bed but below part of the glacier surface, a steady state is possible.

The solution for L reads

$$L = \frac{1}{2} \left[\frac{2\alpha_m}{s(1+\nu s)} \pm \sqrt{Dis} \right]^2 , \quad (2.3.5)$$

and is illustrated in Figure 2.9. When L is plotted against E_r (note that the solution is invariant for the choice of b_0), two branches appear. The upper branch represents a stable solution, and the lower branch an unstable one. This can be verified by carrying out a linear perturbation analysis, calculating the total mass budget B of a glacier of given size, and analysing the sign of $\partial B / \partial L$.

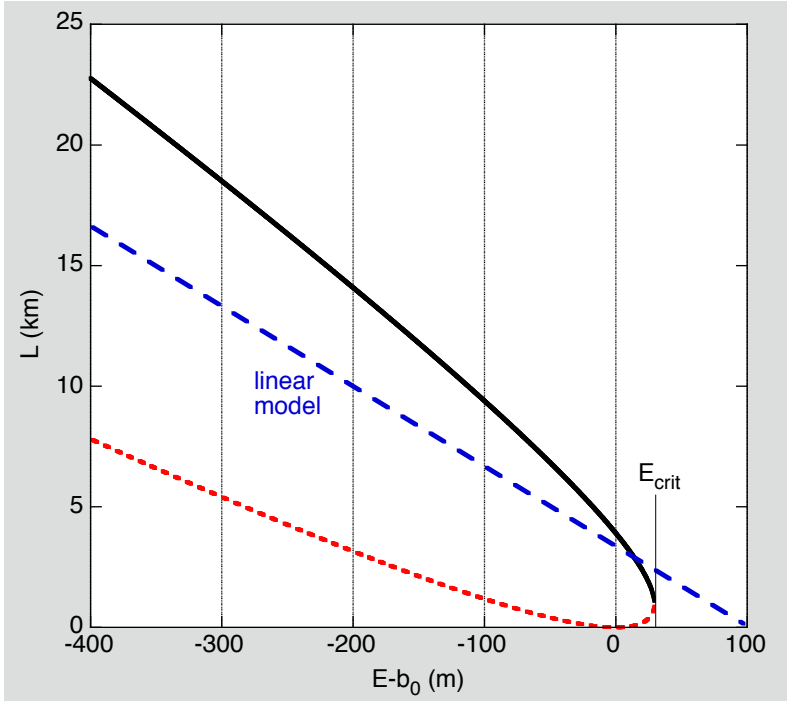


Figure 2.9. Graphic display of eq. (2.3.5). Parameter values: $s = 0.06$, $\alpha_m = 3\text{m}^{1/2}$, $v = 10$, $b_0 = 0$. The result of the linear model, eq. (2.2.1), is shown for the same slope and $H_m = 100 \text{ m}$.

The solution of the linear model derived earlier, eq. (2.2.1) is also shown for comparison. Depending on the choice of the mean ice thickness H_m , the linear solution deviates more or less from the nonlinear solution in a certain range for E_r . Note that the slope of the linear solution equals $-2/s$; a different value of H_m shifts the line up or down.

For $Dis < 0$ there are no real solutions for L , because the equilibrium line is just too high above the highest point of the bed. The critical value of the equilibrium-line altitude, denoted by E_{crit} , is found by setting $Dis = 0$, which yields

$$E_{crit} = \frac{\alpha_m^2}{2s(1+vs)^2} + b_0 . \quad (2.3.6)$$

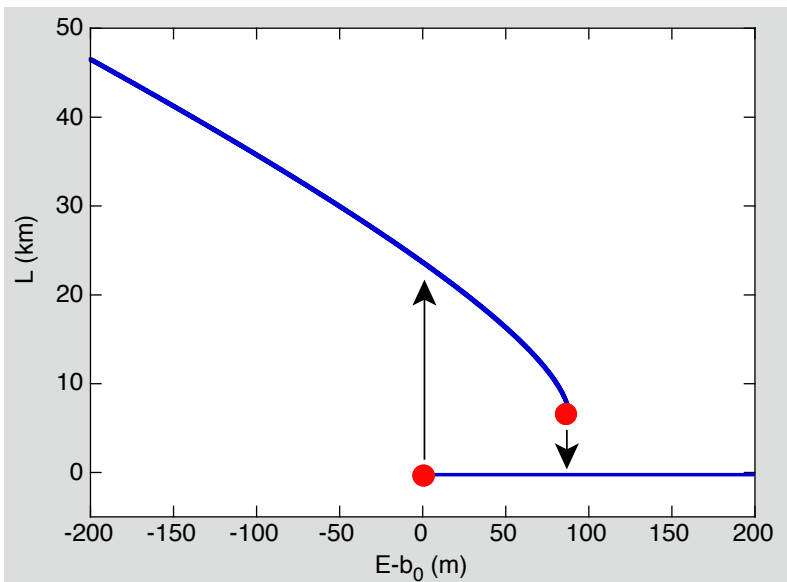


Figure 2.10. Illustration of the hysteresis due to the height-mass balance feedback in the nonlinear model. Parameter values as in Figure 2.9, except for: $s = 0.03$. Now only stable solutions are shown and the bifurcation points are indicated by red dots.

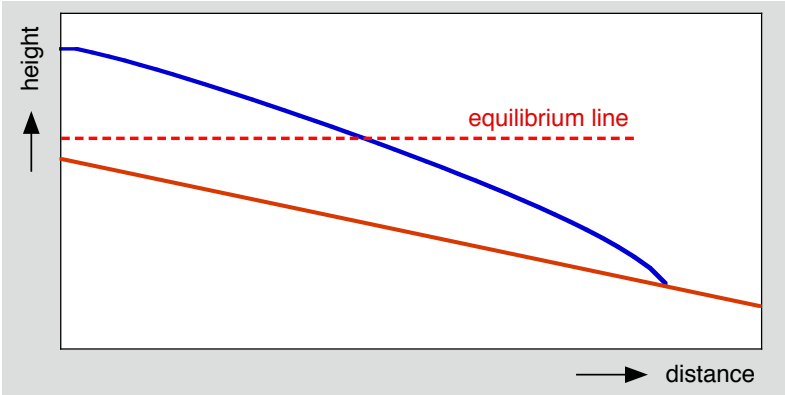


Figure 2.11. A steady state glacier for an equilibrium line which is above the highest point of the bed. If the glacier were to be removed a new one would not form unless the equilibrium line is lowered.

This equation shows that the system becomes more strongly nonlinear when the bed slope becomes smaller. For increasing slope the bifurcation point moves towards the origin and the solution approaches the linear solution for $H_m = 0$. It should be noted that the dynamic properties of this model are quite similar to a set-up in which the bed is horizontal and the equilibrium line slopes upward (Weertman, 1961).

Because $L=0$ is always a stable equilibrium state when $E_r > 0$, the model glacier exhibits hysteresis. This is further illustrated in Figure 2.10, where the solution is drawn for a very small slope of the bed (**Error! Objects cannot be created from editing field codes.**). Stable glaciers with $0 < L < 5.5$ km are not possible. We conclude that there is a range of values for E_r for which two stable steady states are possible, namely

$$0 < E_r < E_{crit} . \quad (2.3.7)$$

The equilibrium line shown in Figure 2.11 is in this range. To create the glacier shown in the figure, the equilibrium line must have been lower once.

One might think that an average bed slope of 0.03 is very small. Indeed, most glaciers in typical alpine terrain are much steeper, but some of the large glaciers in the subpolar regions have very small bed slopes. One example is Vatnajökull in Iceland (Figure 2.12). Drainage basins of this ice cap can be considered as individual glaciers, and those flowing to the west and the north have small slopes. The centre-flowline of Tungnaárljökull, for instance, has an average bed slope of only 0.02 (Björnsson, 1988; marked ‘T’ in Figure 2.11). Brúarjökull is another example (marked ‘B’ in Figure 2.11). On the basis of the theory described above, we may expect that those glaciers are extremely sensitive to changes in the equilibrium-line altitude. Numerical modelling of Vatnajökull has confirmed this (Aðalgeirsdóttir, 2003; Marshall et al., 2005).

It is instructive to write down an explicit expression for dL/dE for the nonlinear model. Differentiating eq. (2.3.5) with respect to E_r yields

$$\frac{dL}{dE} = \frac{-2}{s} \left[1 + \Omega \left(\Omega^2 - \frac{2E_r}{s} \right)^{-1/2} \right] , \quad (2.3.8)$$

$$\text{where } \Omega = \frac{\alpha_m}{s(1 + \nu s)} .$$

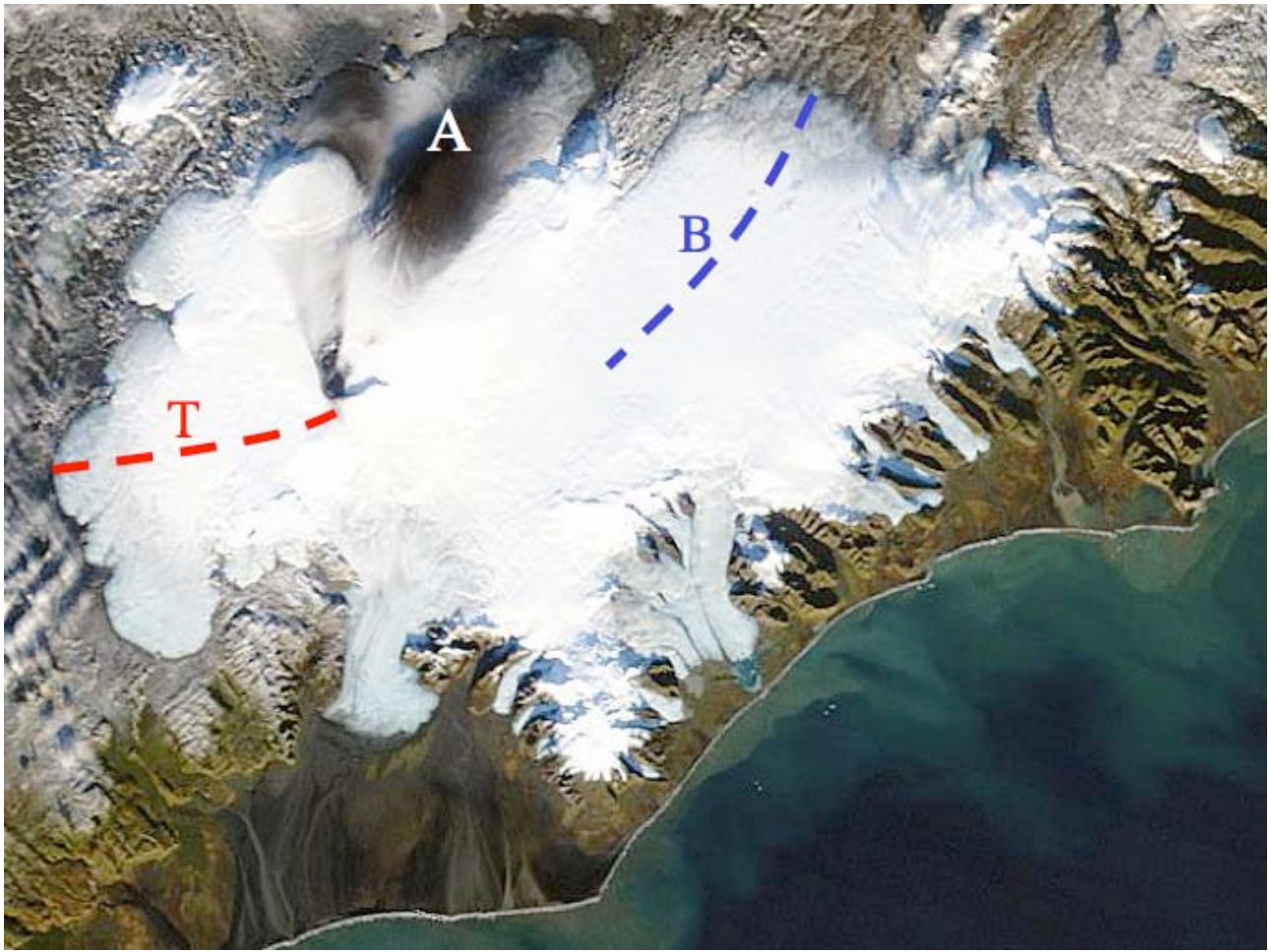


Figure 2.12. Terra/MODIS image (2004) of Vatnajökull, Iceland. Drainage basins in which the ice flows to the west and the north have very small average bedslopes, e.g. Tungnaárjökull (marked ‘T’) and Brúarjökull (marked ‘B’). The dashed lines show approximate flowlines. Note the large amount of volcanic ash deposited on the northern part of the ice cap (marked ‘A’). Courtesy of NASA.

Eq. (2.3.8) shows that dL/dE_r now depends on E_r , which was not the case with the linear model. In fact, the second term between square brackets represents the nonlinear correction to the linear result (-2/s). It is clear that the coupling between ice thickness and glacier length, as included in the nonlinear model, always increases the sensitivity. This is also obvious from Figure 2.9: the slope of the upper branch is always larger than the (constant) slope of the linear solution. For increasing (negative) values of E_r and/or increasing slope of the bed the result approaches the linear case.

In the nonlinear model we only considered a glacier of constant width. However, the relation between ice thickness, slope and glacier length can also be used in the analysis with two basins of different width. This results in a third-order equation for L , which can also be solved relatively easily. The results are similar: making ice thickness a function of L increases the climate sensitivity and creates bifurcation of the equilibrium states.

It should finally be noted that in terms of catastrophe theory (e.g. Gilmore, 1973), eq. (2.3.5) describes a fold. However, because negative values of L are meaningless and we thus ‘add’ $L=0$ as a stable solution, the actual structure as depicted in Figure 2.10 is that of the cusp catastrophe.

2.4 Calving glaciers I (constant accumulation rate)

Many glaciers have their terminus in a lake or in the sea (Figure 2.13) and loose mass because of iceberg calving. Although the details of the calving process are complicated, observations have shown that in general the calving rate is larger in deeper water and also larger in tidal water than in proglacial lakes (e.g. Van der Veen, 1996; Warren, 1999). Several workers have proposed a linear relation between calving rate and water depth (Brown et al., 1982; Pelto and Warren, 1991; Björnsson and others, 2000). Although such a relation is not generally applicable (Van der Veen, 1996), it provides a first-order estimate of mass loss at the calving front.

A very simple model of a calving glacier can be constructed by assuming that the ice thickness at the glacier front is a fixed fraction of the mean ice thickness as defined by eq. (2.3.1). Again, the glacier has a constant width and the bed slope is constant as well ($b(x) = b_0 - sx$), see Figure 2.14.

At first instance, the mass balance is taken as simple as possible. i.e. the accumulation rate \dot{a} is constant. An equilibrium state thus implies that the total accumulation balances the calving flux.

As argued above the calving rate is written as

$$\text{calving rate} = c d , \quad (2.4.1)$$



Figure 2.13. The terminus of Hansbreen, Svalbard. Hansbreen is a well-studied tidewater glacier in Svalbard. Note the increased crevassing towards the glacier front. Courtesy of J. Jania.

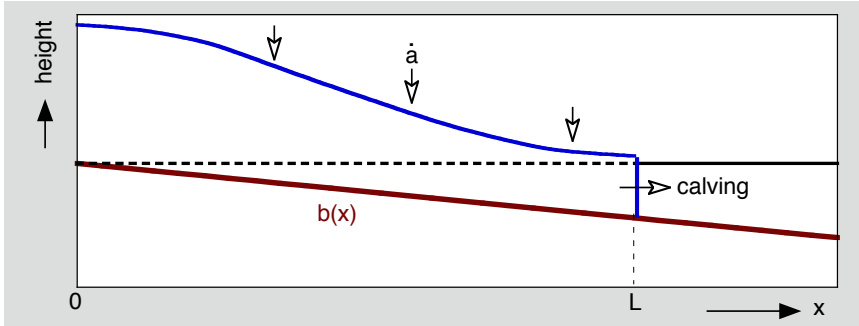


Fig. 2.14. Schematic drawing of a calving glacier. The black line (dashed/solid) represents sea level.

where d is the water depth at the glacier front and c is the calving constant (order of magnitude: 1 m a^{-1} for tidewater glaciers, less for glaciers calving in proglacial lakes). The calving flux F (≤ 0) equals minus the calving rate times the ice thickness at the front (H_f):

$$F = c(b_0 - sL)H_f , \quad (2.4.2)$$

where

$$H_f = \kappa H_m . \quad (2.4.3)$$

Consequently, putting the total mass budget of the glacier to zero yields

$$\dot{a}L + c(b_0 - sL)H_f = 0 . \quad (2.4.4)$$

This equation can only give a meaningful solution if $L > b_0/s$ and if the ice thickness is large enough to keep the glacier away from floating at the front, i.e.

$$H_f > \delta(b_0 - sL) , \quad (2.4.5)$$

where

$$\delta = \frac{\rho_w}{\rho_i} . \quad (2.4.6)$$

Here ρ_w and ρ_i are the densities of sea water and ice, respectively. Now we use eq. (2.3.1) once more to relate the ice thickness to the glacier length. We find

$$\dot{a}L + c(b_0 - sL) \frac{\kappa \alpha_m L^{1/2}}{1 + \nu s} = 0 . \quad (2.4.7)$$

After some rearrangement and substituting $L^{1/2} = N$ we obtain

$$N^2 - \frac{\dot{a}(1 + \nu s)}{c s \kappa \alpha_m} N - \frac{b_0}{s} = 0 . \quad (2.4.8)$$

The discriminant of this quadratic equation is

$$Dis = \frac{\dot{a}^2(1+vs)^2}{c^2 s^2 \kappa^2 \alpha_m^2} + \frac{4b_0}{s}. \quad (2.4.9)$$

Eq. (2.4.9) implies that a real solution exists for $b_0 > b_{0,crit}$, where $b_{0,crit}$ is negative. So when the highest point of the bed is not too far below sea level, a stable glacier is still possible. The solution reads

$$L = \left[\frac{\dot{a}(1+vs)}{2cs\kappa\alpha_m} \pm \sqrt{\frac{\dot{a}^2(1+vs)^2}{4c^2s^2\kappa^2\alpha_m^2} + \frac{b_0}{s}} \right]^2. \quad (2.4.10)$$

In Figure 2.15 the solution is shown for a realistic set of parameters, as a function of the highest point of the bed (b_0) and for two different values of s . The upper branch of the solution is stable, the lower branch is unstable. The close-up in Figure 2.15 shows that the value of $b_{0,crit}$ is quite small, which implies that the hysteresis (similar to that in section 2.3) is over a very small range. For given accumulation rate and calving parameter, the equilibrium glacier length depends strongly on the bed slope. The mechanism behind this is very clear: for a smaller slope it takes a much longer glacier to get in sufficiently deep water and get an appreciable calving rate. As the glacier expands the total accumulation increases as well, because \dot{a} is constant. This will be different for a glacier with a balance rate that depends on altitude (next section).

For the solutions shown in Figure 2.15 it appears that the thickness at the glacier front is always sufficiently large to overcome the flotation criterion (i.e. eq. (2.4.5) is satisfied). However, this is not always the case.

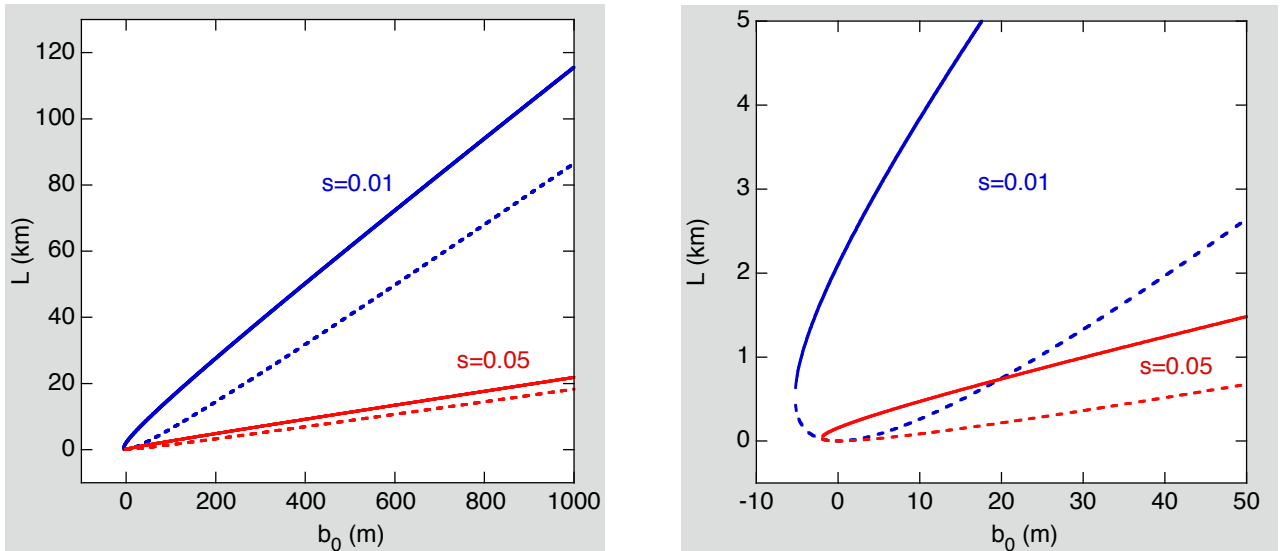


Figure 2.15. Solution of the calving model for varying b_0 and two values of the bed slope s . The picture at right is a close-up. The unstable branch is dashed. Model parameters: $\alpha_m = 3\text{m}^{1/2}$, $v = 10$, $\kappa = 0.4$, $c = 2\text{a}^{-1}$ and $\dot{a} = 1\text{ma}^{-1}$.

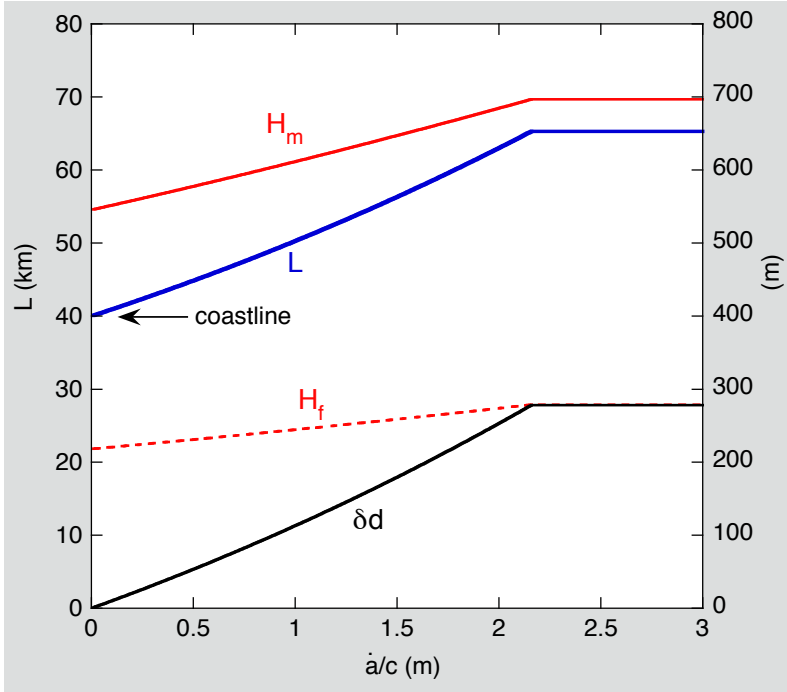


Figure 2.16. Solution of the calving glacier model as a function of \dot{a}/c . Scale for glacier length at left, for mean ice thickness (H_m), thickness at the front (H_f) and flotation thickness (δd) at right. Parameter values: $\alpha_m = 3\text{m}^{1/2}$, $v = 10$, $\kappa = 0.4$, $b_0 = 400\text{ m}$, $s = 0.01$.

In Figure 2.16 the solution is shown as a function of \dot{a}/c . Because the surface balance rate is always positive, a glacier ending on land is not possible. Therefore $L \rightarrow b_0/s$ when $\dot{a} \rightarrow 0$. For the choice of parameter values in Figure 2.16 this implies that the minimum glacier length is 40 km. For increasing glacier length the height of the glacier front approaches the flotation depth. With the parameterizations used this eventually has to happen, because the frontal thickness is proportional to \sqrt{L} and the water depth increases linearly with L . So there is an upper limit to L , in the case shown in Figure 2.16 at about 65 km.

The existence of an upper limit is due to the fact that the glacier thickness does not depend directly on the accumulation rate. This is a property of the perfectly plastic ice cap model. For models based on the shallow-ice approximation and Glen's law for simple shear the glacier size is proportional to $\dot{a}^{1/8}$ (Vialov, 1958), which is still a rather weak dependence.

We should realize that the model of a calving glacier with a constant accumulation rate is not a very good representation of reality. A more or less constant accumulation rate, or at least a mass-balance field that has insignificant melting, is typical for cold Antarctic environments, and under such conditions glaciers entering into the ocean will tend to form floating ice tongues or contribute to the formation of vast ice shelves.

2.5 Calving glaciers II (mass-balance field depending on altitude)

All calving glaciers outside Antarctica have an accumulation and an ablation zone, and the mass-balance field is better represented by the linear balance profile. However, we pay a price: the equation from which the equilibrium solutions have to be calculated is more complex. Nevertheless, insight can be gained without getting explicitly to the full solution.

We formulate the total mass budget (B) as:

$$B = B_s + F ,$$

where

$$B_s = \int_0^L b dx = \beta \int_0^L (H + b_0 - sx - E) dx = -\frac{1}{2} \beta s L^2 + \beta \left(\frac{\alpha_m}{1 + \nu s} L^{1/2} + b_0 - E \right) L , \quad (2.5.1)$$

$$F = \min \left\{ -c(b_0 - sL) H_f = -c(b_0 - sL) \frac{\kappa \alpha_m}{1 + \nu s} L^{1/2}; 0 \right\} . \quad (2.5.2)$$

Again, we have used $H_m = \frac{\alpha_m}{1 + \nu s} L^{1/2}$ and $H_f = \kappa H_m$.

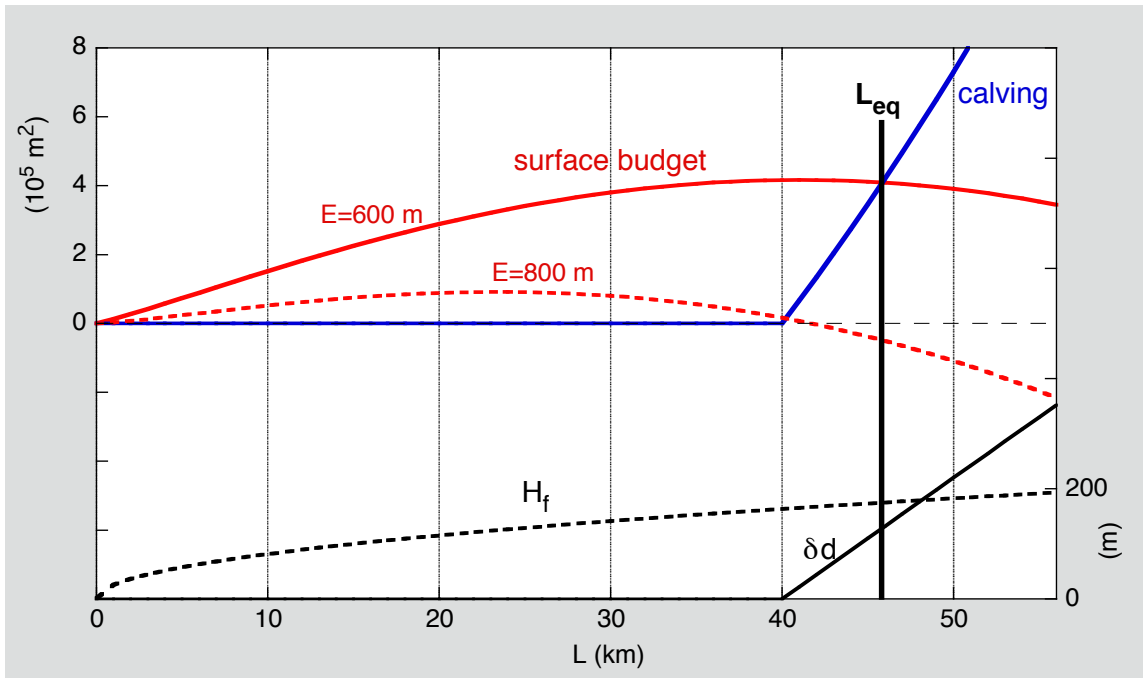


Fig. 2.17. An example of a graphical solution to the calving glacier model with height-dependent balance rate. Parameter values: $\alpha_m = 2.5 \text{ m}^{1/2}$, $\nu = 10$, $b_0 = 800 \text{ m}$, $s = 0.02$, $\beta = 0.005 \text{ m ice a}^{-1} \text{ m}^{-1}$, $c = 2 \text{ a}^{-1}$, and $\kappa = 0.4$. The scale for the mass-budget components is at the left, for ice thickness at the right. The equilibrium glacier length, denoted in the figure by L_{eq} , is given by the intersection of the surface budget curve (red) and the calving flux curve (blue). For $E = 600 \text{ m}$ we have $L \approx 46 \text{ km}$. For $E = 800 \text{ m}$ the glacier front is just at the coast and we have $L \approx 40 \text{ km}$ (dashed red curve).

An example of the mass-budget components for a certain set of parameter values is shown in Figure 2.17. With the highest point of the bed at 800 m, a bed slope of 0.02 and a balance gradient of 0.05, this example could be representative for a typical large tidewater glacier in a maritime climate. Note that the coastline is at a distance of 40 km from the highest point of the bed.

In Figure 2.17, B_s ('surface budget', in red) and $-F$ ('calving', in blue) are plotted as a function of L . Obviously the intersection of the curves determines the equilibrium glacier length for this case. For $E = 600$ m we thus find that $L \approx 46$ km. In Figure 2.17 the ice thickness at the glacier front (H_f) and flotation thickness (δd) are also shown (scale at right). For $L \approx 48$ km we clearly have $H_{fr} > \delta d$, and the solution is therefore 'valid'. Note that for the given bed geometry solutions with $L > 50$ km are not possible.

In Figure 2.17 the mass budget is also shown for a substantially higher equilibrium-line, i.e. $E = 800$ m. We now have $L \approx 40$ km, i.e. the glacier front is just at the coast.



Deep meltwater channel, Vadret da Morteratsch, Switzerland

3. Time-dependent modelling

3.1 Introduction

An analysis of equilibrium states is always useful because it reveals the basic sensitivities of a glacier model. It is also a good check for consistency, at least when one is interested in having models that are valid over a large part of parameter space. In fact, it is the philosophy behind the present text that models can be simple, but should be valid for a wide range of climatic forcings and geometric settings. Valid here means meaningful, not necessarily accurate!

After having explored equilibrium states it is worthwhile to investigate the dynamical aspects of minimal glacier models. It is clear that some dynamic phenomena on glaciers cannot be studied with such models. For instance, the lack of spatial resolution implies that travelling waves cannot be simulated. The dynamics we study here are the ‘slow’ dynamics, in which a glacier gradually adjusts its shape (size) to changing environmental conditions like equilibrium-line altitude, or, perhaps, sea level. The prognostic equation from which the evolution in time should be calculated is the integrated continuity equation.

3.2 The simple dynamic glacier model

We start again with the simple configuration: a glacier of constant width resting on a bed with a constant slope (Figure 2.1). By definition, the glacier volume then V equals the product of the mean ice thickness H_m and the glacier length L . From this it follows immediately that a change in volume can be written as:

$$\frac{dV}{dt} = \frac{d}{dt}(H_m L) = H_m \frac{dL}{dt} + L \frac{dH_m}{dt} . \quad (3.2.1)$$

Using, as before, $H_m = \frac{\alpha_m}{1 + \nu s} L^{1/2}$, we estimate H_m :

$$\frac{dV}{dt} = \frac{3\alpha_m}{2(1 + \nu s)} L^{1/2} \frac{dL}{dt} \quad (3.2.2)$$

Because the change in glacier volume equals the sum of surface balance and calving flux, we thus find

$$\frac{dL}{dt} = \frac{2(1 + \nu s)(B_s + F)}{3\alpha_m} L^{-1/2} . \quad (3.2.3)$$

This equation, and others to be used later, have the form

$$\frac{dL}{dt} = f\{L, P_j\} \quad (3.2.4)$$

Here the P_j is a set of parameters that vary in time and represent the ‘forcing’ of the model glacier, like equilibrium-line altitude, sea level, etc.

Since we work with strongly damped equations, a simple forward or backward Euler method produces an accurate solution (e.g. Hamming, 1987). Higher order schemes can be used, but in view of the character of the equations we use there is little to be gained.

Denoting a time step by Δt and a discrete time variable by t_i , the forward Euler scheme is obtained from

$$\frac{L(t_i + \Delta t) - L(t_i)}{\Delta t} = f\{L(t_i), P_j(t_i)\} , \quad (3.2.5)$$

from which it follows that

$$L(t_i + \Delta t) = L(t_i) + \Delta t f\{L(t_i), P_j(t_i)\} \quad (3.2.6)$$

It is easy to write a code based on eq. (3.2.6). A suitable time step for the applications described in this text is $\Delta t = 1$ a.

We first study land-based glaciers with a linear balance profile, implying that $F = 0$ and B_s is given by:

$$B_s = \beta \int_0^L (H + b_0 - sx - E) dx = -\frac{1}{2} \beta s L^2 + \beta \left(\frac{\alpha_m}{1 + \nu s} L^{1/2} + b_0 - E \right) L \quad (3.2.7)$$

By combining eqs. (3.2.3) and (3.2.7) the model is explicitly formulated in terms of L and can be solved with the Euler method for any prescribed set of model parameters.

In a first calculation we take parameter values that are typical for a large valley glacier in the Alps (for example the Aletschgletscher, see Figure 2.5): $b_0 = 3900$ m, $s = 0.1$, $\beta = 0.007$ m ice $a^{-1} m^{-1}$,

$\alpha_m = 3 \text{ m}^{1/2}$, $\nu = 10$. For $E = 2900 \text{ m}$ the model settles to a steady state in about 300 years, with a glacier length of about 22 km. This is not very different from the actual length of the Aletschgletscher, depending on from which point the length is actually measured. We may wonder why a reasonable value for L is obtained, in spite of the fact that the model assumes a constant glacier width. In fact, it appears that the use of a narrow accumulation area is compensated by the linear balance gradient, which overestimates the balance rate in the highest parts (in reality the accumulation rate tends to level off for the highest parts of a glacier).

A stepwise change of the equilibrium-line altitude causes an immediate reaction of the glacier length. The approach to a new equilibrium state is almost exponentially, and the e-folding time scale for the calculation shown in Figure 3.1 is about 80 a [the e-folding time scale is defined as the time it takes to approach the new equilibrium by a fraction $(1 - e^{-1}) \approx 2/3$]. This value seems very reasonable.

The increase in glacier length for a 100 m drop in E is about 2.1 km. The response is not linear: it can be seen that the decrease in glacier length for a 100 m increase in E is about 2.5 km. The mean balance rate over the glacier is also shown in Figure 3.1. A 100 m change in E generates a change in the mean balance rate of about 0.7 m ice m^{-1} , which then slowly goes down to zero when the new equilibrium state is approached.

In passing we also note that the example shown in Figure 3.1 reveals the danger of using the mean balance rate as a climate signal. The climate signal, E in this case, jumps from one value to another and is then constant for 500 years. In contrast, the balance rate depends on how far the glacier is actually away from the steady state corresponding to the prevailing equilibrium-line altitude (see also Oerlemans, 2001, p. 103-104).

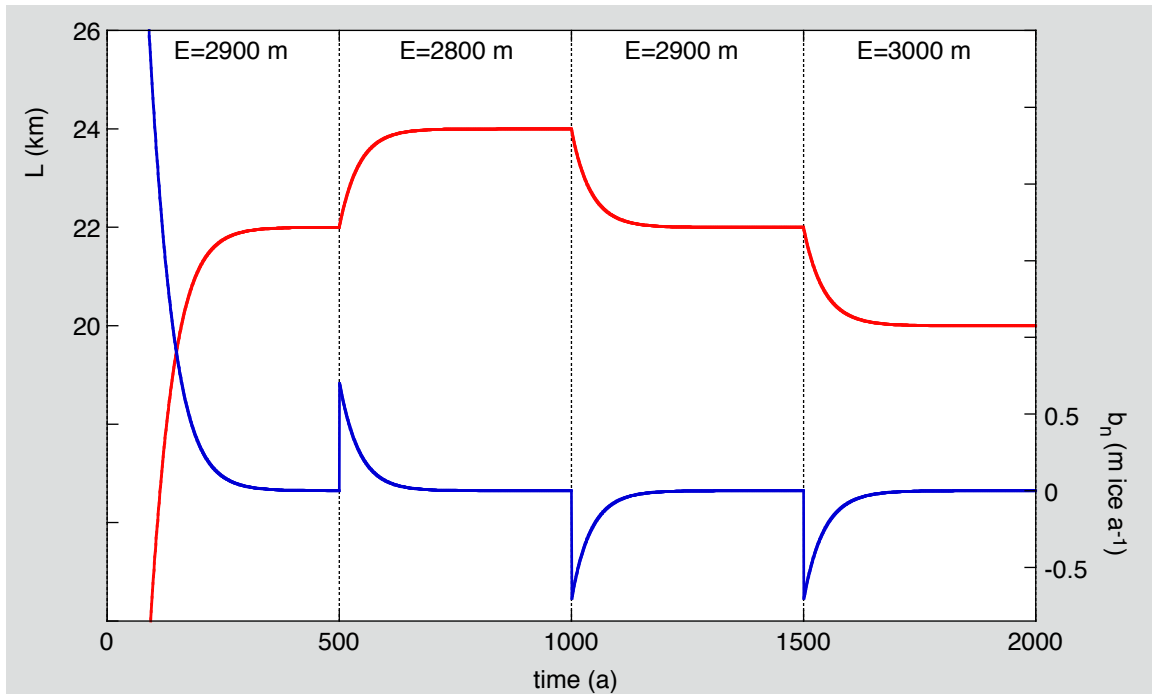


Figure 3.1. Glacier length (red curve, scale at left) and mean balance rate (blue curve, scale at right) for a typical alpine glacier subject to 100 m step changes in the equilibrium-line altitude E . Parameter values (see text) are typical for the Aletschgletscher, Switzerland.

The response of glacier length to changing mass balance conditions is immediate. This is inherent to the type of model developed here, and we may wonder how realistic this is. Numerical models based on the shallow ice approximation (SIA) show an immediate response of glacier volume, and a somewhat delayed response of glacier length. However, this delay depends very much on the grid resolution used. Moreover, higher-order models of glacier flow suggest that the initial response of SIA models is too slow. Even when ice mechanics do not change, in reality an increase in E implies higher ablation rates at the glacier snout and therefore an immediate decrease in glacier length. In view of this we cannot conclude that numerical glacier models with the SIA approximation do a better job than the minimal model discussed here.

It is interesting to repeat the calculation for a steeper glacier ($s = 0.2$), and keep all other parameter values the same. First of all the glacier is much shorter now (about 10.8 km for $E = 2900$ m), and the sensitivity considerably smaller (Figure 3.2). At the same time the e-folding response times is smaller as well, being about 30 a.

The balance gradient β also has a significant effect on the response time. This can be illustrated by repeating the calculation for a much smaller value of β (Figure 3.3). As is obvious from the analysis in Chapter 2, the equilibrium states do not depend on β . However, reducing β from 0.007 to 0.003 m ice $a^{-1} m^{-1}$, a value more typical for high arctic conditions, makes the glacier very slow. As can be seen in Figure 3.3, in this case the glacier does not even reach an equilibrium state within 500 years. The e-folding response time is more than twice as large. So, in summary, a steeper bed and a larger balance gradient make glaciers respond quicker to climate change.

Since the calculations described here are based on a simple equation for volume (mass) conservation, the resulting response times should be interpreted as volume time scales in the terminology of Jóhannesson et al. (1989), even though they apply to glacier length.

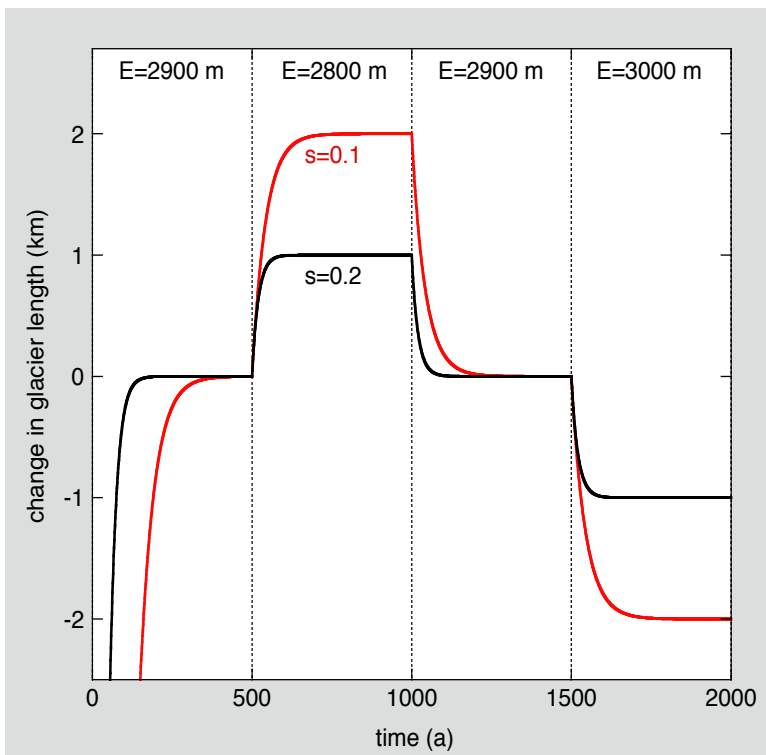


Figure 3.2. Response of the model glacier to stepwise changes in E , for different values of the bed slope. Note that changes in glacier length relative to an equilibrium state are shown.

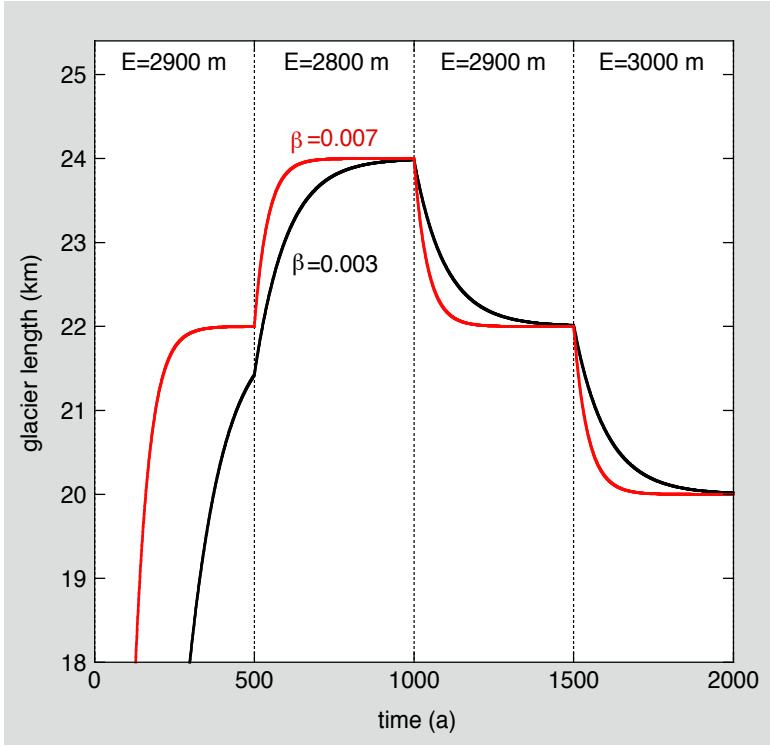


Figure 3.3. Illustrating the effect of the balance gradient β on the response time. The bed slope is 0.1.

The volume time scale proposed by Jóhannesson et al. (1989), denoted by τ_J , can be formulated explicitly in the framework of the present model. Jóhannesson et al. (1989) estimate the volume time scale as the ratio of a characteristic ice thickness (H^*) to the balance rate at the glacier snout ($\dot{b}_{x=L}$):

$$\tau_J = -H^*/\dot{b}_{x=L} . \quad (3.2.8)$$

Using $\dot{b} = \beta(h - E)$ and noting that the altitude at the glacier snout is given by $b_0 - sL$, this then leads to

$$\tau_J = -\frac{H_m}{\beta(b_0 - sL - E)} . \quad (3.2.9)$$

From this equation we see that, although the equilibrium length does not depend on β , the response time is inversely proportional to β . This is in line with the result of Figure 3.3. To investigate the dependence of the response time on the bed slope s we eliminate H_m and L from eq. (3.2.9). We thus find that τ_J can be expressed as

$$\tau_J \approx -\frac{H_m}{\beta(b_0 - sL - E)} \approx \frac{\alpha_m L^{1/2}}{\beta(E - b_0)(1 + vs)} \approx \frac{\sqrt{2}\alpha_m}{\beta(E - b_0)^{1/2}(1 + vs)s^{1/2}} , \quad (3.2.10)$$

where we have used $H_m = \frac{\alpha_m}{1 + vs} L^{1/2}$ and $L \approx 2(b_0 - E)/s$.

Eq. (3.2.10) clearly shows that τ_J decreases with increasing bed slope, again in agreement with the calculation with the minimal model (Figure 3.2).

3.3 Model for a glacier of varying width

We will now develop a more general model in which the constraint of a constant width is relaxed. Starting again with the continuity equation we have

$$\frac{dV}{dt} = H_m \frac{dA}{dt} + A \frac{dH_m}{dt} = B_s + F , \quad (3.3.1)$$

where A is the glacier area and H_m the mean ice thickness. Then there are various ways to proceed. Because we will use a simple geometry in which the glacier width is a prescribed function of the x -coordinate, denoted by $W(x)$, it makes sense to define a mean glacier width W_m .

$$\frac{dA}{dt} = L \frac{dW_m}{dt} + W_m \frac{dL}{dt} . \quad (3.3.2)$$

So using eq. (2.3.1) once more, the time rate of change of glacier volume can now be expressed as:

$$\begin{aligned} \frac{dV}{dt} &= \frac{\alpha_m}{1+vs} L^{1/2} \left[L \frac{dW_m}{dt} + W_m \frac{dL}{dt} \right] + \frac{\alpha_m}{2(1+vs)} L^{1/2} W_m \frac{dL}{dt} = \\ &= \frac{3\alpha_m}{2(1+vs)} L^{1/2} W_m \frac{dL}{dt} + \frac{\alpha_m}{1+vs} L^{3/2} \frac{dW_m}{dt} . \end{aligned} \quad (3.3.3)$$

Note that for a constant glacier width eq. (3.3.3) takes the same form as eq. (3.2.2).

At this point $W(x)$ has to be specified and a relation between H_m and L has to be derived. Many alpine glaciers have a wide accumulation basin and a narrow tongue, and a suitable formulation describing such a geometry is

$$W(x) = w_0 + w_1 x e^{-ax} . \quad (3.3.4)$$

The parameter w_0 determines the width of the glacier snout, the other two parameters the shape of the glacier. Note that the maximum width is found at $x = a^{-1}$. Although the basic glacier shape is determined by eq. (3.3.4), different glaciers can be ‘mapped’ on this shape by selecting the best values for w_0 , w_1 and a . An example is shown (in plan view) in Figure 3.4.

Using (from standard calculus)

$$\int x e^{-ax} dx = -\frac{e^{-ax}}{a^2} (ax + 1) , \quad (3.3.5)$$

the mean glacier width can be found:

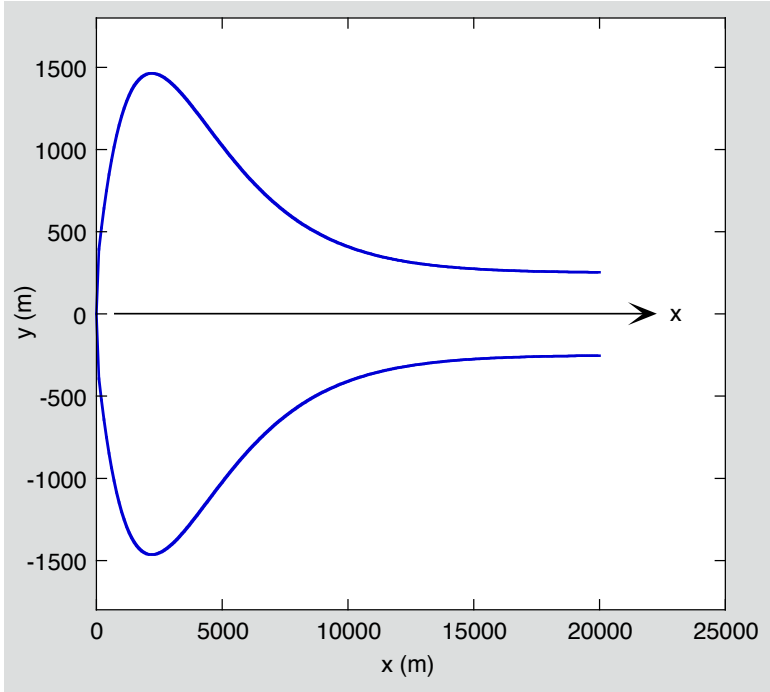


Figure 3.4. Plan view of a glacier with a width prescribed by eq. (3.3.4). Parameter values: $w_0 = 500$ m, $w_1 = 3$, $a = 0.00045 \text{ m}^{-1}$.

$$W_m = \frac{1}{L} \int_0^L w(x) dx = w_0 + \frac{w_1}{L} \int_0^L xe^{-ax} dx . \quad (3.3.6)$$

Evaluating the integral yields

$$W_m = w_0 + w_1 a^{-2} \left\{ L^{-1} - ae^{-aL} - L^{-1}e^{-aL} \right\} . \quad (3.3.7)$$

It also follows that

$$\frac{dW_m}{dt} = w_1 \left[-a^{-2}L^{-2} + e^{-aL} + a^{-2}L^{-2}e^{-aL} + a^{-1}L^{-1}e^{-aL} \right] \frac{dL}{dt} . \quad (3.3.8)$$

Now eqs. (3.3.3), (3.3.7) and (3.3.8) can be combined to yield

$$\begin{aligned} \frac{dV}{dt} &= \frac{3\alpha_m}{2(1+vs)} L^{1/2} \left[w_0 + a^{-2} \left\{ L^{-1} - ae^{-aL} - L^{-1}e^{-aL} \right\} \right] \frac{dL}{dt} + \\ &+ \frac{\alpha_m}{1+vs} L^{3/2} \left\{ -a^{-2}L^{-2} + e^{-aL} + a^{-2}L^{-2}e^{-aL} + a^{-1}L^{-1}e^{-aL} \right\} \frac{dL}{dt} = B_s + F \end{aligned} \quad (3.3.9)$$

Or, in short,

$$\frac{dV}{dt} = \Psi(L) \frac{dL}{dt} . \quad (3.3.10)$$

The model can thus be solved by integrating

$$\frac{dL}{dt} = \Psi^{-1}(B_s + F) \quad (3.3.11)$$

Ψ is a fairly complicated function of L , but still requires not more than a few lines of code.

The final step is to evaluate the surface balance B_s . To keep the algebra manageable the ice thickness is taken constant over the entire glacier (in fact, we set $H = H_m$, which only depends on L) and the bed elevation is not allowed to vary across the glacier. Assuming a linear balance field and a linear bed profile we have

$$B_s = \int_0^L w(x) \dot{b}(x) dx = \beta \int_0^L w(x) \{h(x) - E\} dx = \beta \int_0^L w(x) \{b_0 - sx - E + H_m\} dx . \quad (3.3.12)$$

This can be rewritten as

$$B_s = \beta w_0 \left[(b_0 - E + H_m)L - \frac{s}{2}L^2 \right] + \beta w_1 \int_0^L (b_0 - sx - E + H_m) x e^{-ax} dx , \quad (3.3.13)$$

or

$$B_s = \beta w_0 \left[(b_0 - E + H_m)L - \frac{s}{2}L^2 \right] + \beta w_1 (b_0 - E + H_m) \int_0^L x e^{-ax} dx - \beta w_1 s \int_0^L x^2 e^{-ax} dx . \quad (3.3.14)$$

For convenience we write

$$\int_0^L x e^{-ax} dx = a^{-2} (1 - aL e^{-aL} - e^{-aL}) = \Lambda_L , \quad (3.3.15)$$

and we note that (e.g. Carmichael and Smith, 1962)

$$\int_0^L x^2 e^{-ax} dx = -a^{-1} L^2 e^{-aL} + 2a^{-1} \Lambda_L . \quad (3.3.16)$$

The surface mass budget can thus be written as

$$B_s = \beta w_0 \left[(b_0 - E + H_m)L - \frac{s}{2}L^2 \right] + \beta w_1 (b_0 - E + H_m) \Lambda_L - \beta w_1 s \left\{ -a^{-1} L^2 e^{-aL} + 2a^{-1} \Lambda_L \right\} . \quad (3.3.17)$$

The model is complete now because all quantities have been expressed in terms of the glacier length L . Before we consider solutions of eq. (3.3.7) we first study the nature of eq. (3.3.17), i.e. we investigate how B_s varies with L for a given equilibrium-line altitude.

Figure 3.5 shows B_s for the glacier geometry of Figure 3.4. The equilibrium-line altitude is 250 m below the highest point of the bed. At the equilibrium length we have $B_s = 0$, of course. This implies that $L \approx 20.4$ km. Note that this solution is stable because $\partial B_s / \partial L < 0$. For comparison the

case of a glacier of constant width (i.e. $w_1 = 0$) is also shown. As expected, the equilibrium length is much smaller now, because the glacier does not have the wide accumulation basin. These results are very plausible, and we conclude that the parameterisation of glacier geometry given by eq. (3.3.4) provides a workable approach. It represents only one class of glacier geometry, of course, but perhaps the most common one.

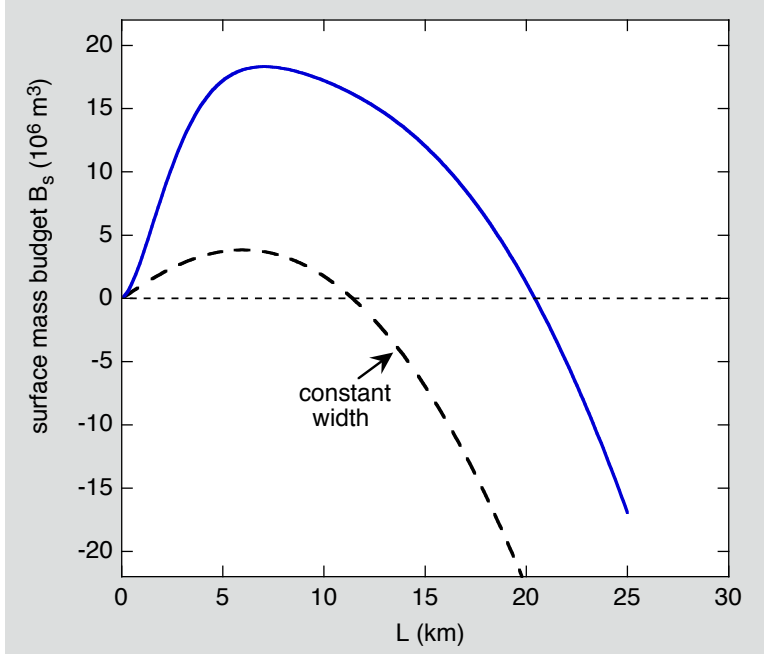


Figure 3.5. Mass budget of the glacier shown in Figure 3.4, for a fixed value of the equilibrium-line altitude and varying length. The case of constant width is shown for comparison.

Parameter values:

$$\begin{aligned} b_0 &= 3000 \text{ m}, \\ s &= 0.1, \\ v &= 10, \\ \alpha_m &= 3 \text{ m}^{1/2}, \\ E &= 2750 \text{ m}, \\ \beta &= 0.007 \text{ m ice a}^{-1} \text{ m}^{-1}. \end{aligned}$$

Next we consider time-dependent solutions of the model as described by eq. (3.3.11). We impose a periodic forcing according to

$$E(t) = 2750 + 200 \sin(2\pi t/1000) , \quad (3.3.18)$$

where t is in years. So with a period of 1000 years the forcing can be considered as rather slow. The stationary periodic response is shown in Figure 3.6. It turns out that the phase difference between forcing and response is about 60 years.

For comparison the result of a calculation for a glacier with constant width is also shown. The glacier with constant width is shorter on average, and its response is considerably slower (now the phase difference is about 100 years). This example illustrates that the response time is not only determined by quantities like the balance gradient and the characteristic ice thickness, but also by the geometry.

The response of the model to stepwise forcing is shown in Figure 3.7. Every 500 years the equilibrium-line altitude is instantaneously changed by 150 m. The e-folding response time is about 75 years, and it is noteworthy that the response time does not increase when the glacier gets larger for lower equilibrium altitudes. This once more illustrates that larger glaciers are not necessarily slower in their reaction to climate change. In practice, however, large glaciers have typically lower bed slopes and thus a stronger height-mass balance feedback, which increases the response time (Oerlemans, 2001).

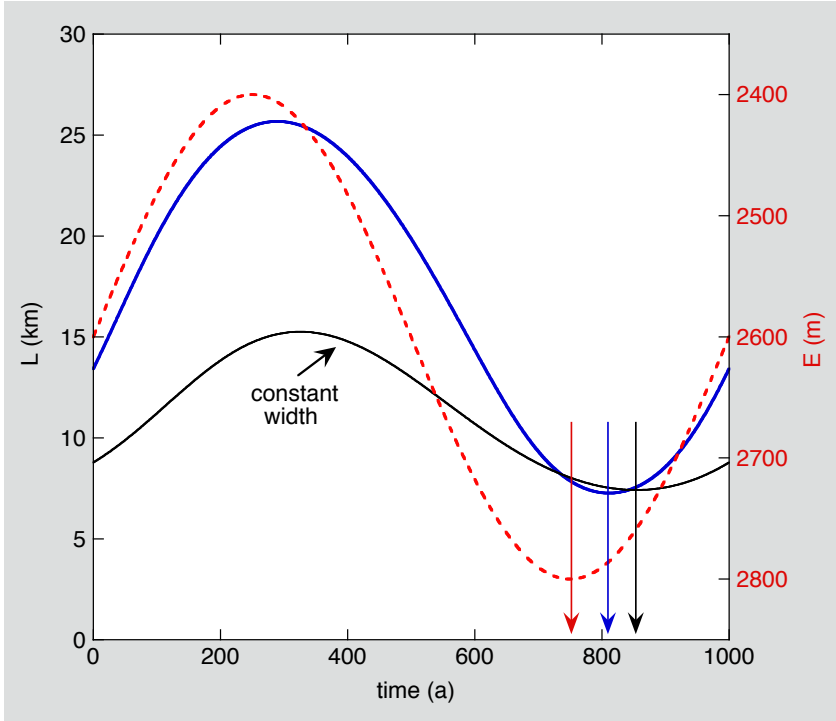


Figure 3.6. The response of the glacier model to periodic forcing with a period of 1000 a. Note that the scale for E is reversed. Arrows mark minima in the curves to illustrate the phase differences. Parameter values as in Figure 3.5.

Another feature seen in Figure 3.7 is the fact that the climate sensitivity $\partial L / \partial E$ is not constant, but exhibits a maximum. This is in line with the earlier result for a glacier with two basins, of which the upper one is wider than the lower one (see Figure 2.7). We investigate this a bit further.

It is easy to calculate equilibrium states for any given value of E . In Figure 3.8, equilibrium glacier length and volume are plotted as a function of E . The (E,L) -curve has the same shape as in Figure 2.7, but it is smoother because the transition from a wide basin to a narrower tongue is more gentle. The climate sensitivity has a maximum around $E \approx 2700$ m.

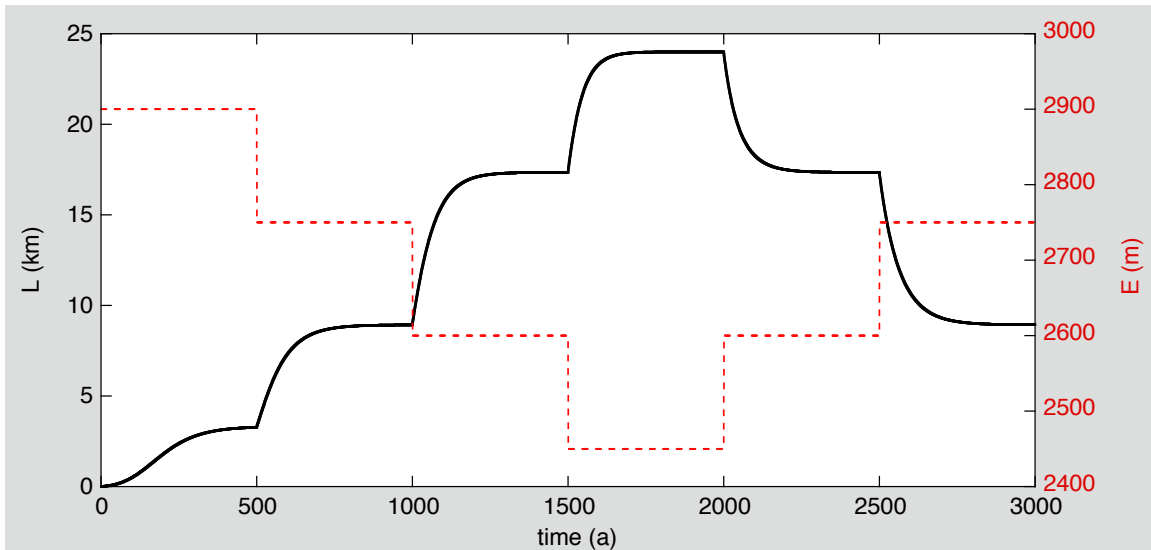


Figure 3.7. The response of the model to stepwise forcing. The steps in E are 150 m. Parameter values as in Figure 3.5.

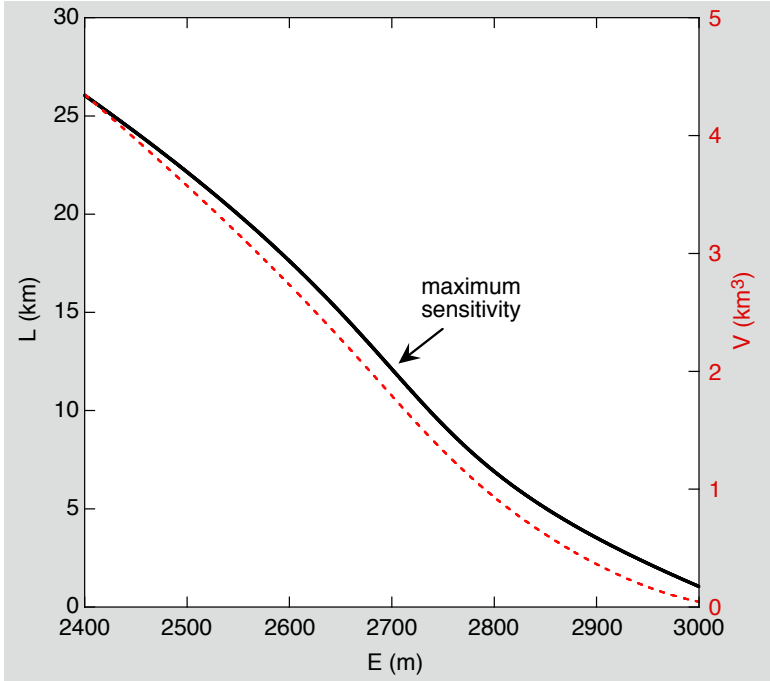


Figure 3.8. Equilibrium glacier length and volume plotted as a function of E . Parameter values as in Figure 3.5.

The glacier volume is also shown. The volume curve is slightly steeper than the length curve because the ice thickness H_m increases with L .

3.4 Climate change experiments

In the preceding sections schematic calculations were discussed for an idealised climate forcing. In principle the glacier model can also be used to study the response to observed climate change, or to climate change scenarios for the future.

In recent years a large amount of research has been undertaken to understand the microclimate of glaciers, and to develop mass-balance models that generate the specific balance from meteorological input data (e.g. Oerlemans, 1992; Klok and Oerlemans, 2002). This has revealed that maritime glaciers are more sensitive than continental glaciers, for instance, and also how meteorological factors other than air temperature determine the balance rate. Nevertheless, in spite of the complexity of the relation between specific balance and climate, we use a very simple scheme in which the fluctuations in E are the result of temperature fluctuations only (note that this does not imply that other factors are irrelevant; they are considered to be constant).

Energy balance modelling has been used by several authors to determine values of $\partial E / \partial T_a$ (here T_a is the annual mean atmospheric temperature at some reference level). Kuhn (1989) finds a value of 65 m/K for the Hintereisferner. Excluding very maritime or very continental glaciers, Oerlemans (2001; p. 50) found a value of typically 80 m/K for a set of alpine glaciers. Note that these values are substantially smaller than the value one would get if the ELA would follow an atmospheric isotherm: in that case x would be equal to 1 over the atmospheric temperature lapse rate, i.e. about 130 m/K. In the following we will consider typical conditions for the Alps and therefore use $\partial E / \partial T_a = 80$ m/K.

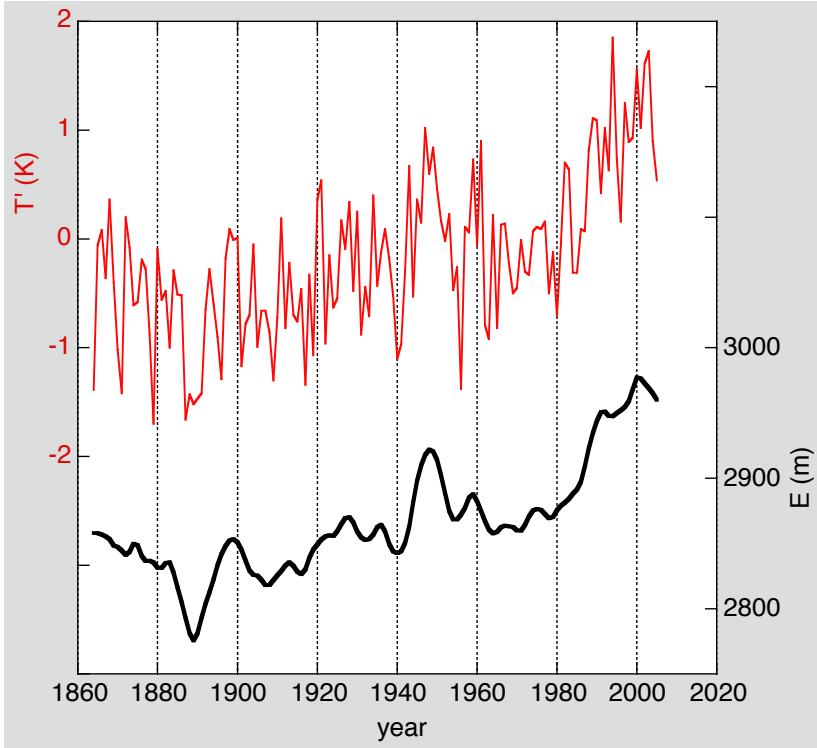


Figure 3.9. Mean temperature anomaly (annual) for Switzerland (data from MeteoSwiss) and inferred smoothed (low pass) equilibrium-line altitude.

For a set of four glacier geometries we will now look at the response to temperature fluctuations as observed over Switzerland since 1865. Although one may argue that it is more appropriate to use a local climatic series to force local glaciers, practice has shown that this is not as straightforward as it seems. All meteorological series have their peculiarities, and for a schematic study it is better to work with an areal mean temperature series.

In Figure 3.9 the forcing $E(t)$ is shown. We use a smoothed curve, because the glacier model cannot respond in a physical way to very fast fluctuations. This is due to the nature of the model, in which L and H_m are fully coupled. For instance, in reality a sharp rise of the equilibrium line from one year to another would reduce the ice thickness immediately over a large part of the glacier without affecting the length very much. However, in the model this would immediately lead to a strong reduction of the glacier length, because that is the only way to accommodate the smaller value of H_m . Although forcing of the glacier model with a noisy record does not blow up the integration, the output has too much variation on the smallest time scales. It is thus advisable to apply a low pass filter (with a filter width of 10 or 15 years) to a series of equilibrium-line altitudes with annual resolution.

From Figure 3.9 it is clear that the climate has warmed significantly over the past 140 years - much more than the global mean temperature (e.g. Luterbacher et al., 2004). The estimated rise in the equilibrium-line altitude over the 20th century is about 150 m, with half of this rise after 1985.

The glacier shapes to be considered are defined in the table below and illustrated in Figure 3.10. In all cases $w_0 = 500$ m, $v = 10$ and $\alpha_m = 3 \text{ m}^{-1/2}$. Glacier 1 is a large glacier (30.4 km in the reference state, defined as the equilibrium state for $E = 2750$ m) with a small slope and a wide accumulation basin, and a modest balance gradient. Glacier 2 is steeper and has a less pronounced tongue, whereas the balance gradient is somewhat larger. Glacier 3 is steep, but nevertheless fairly long. This is achieved by choosing a larger value for b_0 . Glacier 4 is a small glacier with a small slope, with b_0 just above the reference equilibrium line.

	w_1	$a (\text{m}^{-1})$	$\beta (\text{m ice m}^{-1})$	$b_0 (\text{m})$	s	$L (\text{km}) \text{ in 1850}$
Glacier 1	4	0.00045	0.005	3400	0.10	30.4
Glacier 2	3	0.00045	0.007	3400	0.20	8.2
Glacier 3	3	0.0008	0.007	4000	0.25	11.0
Glacier 4	0		0.007	2775	0.10	1.8

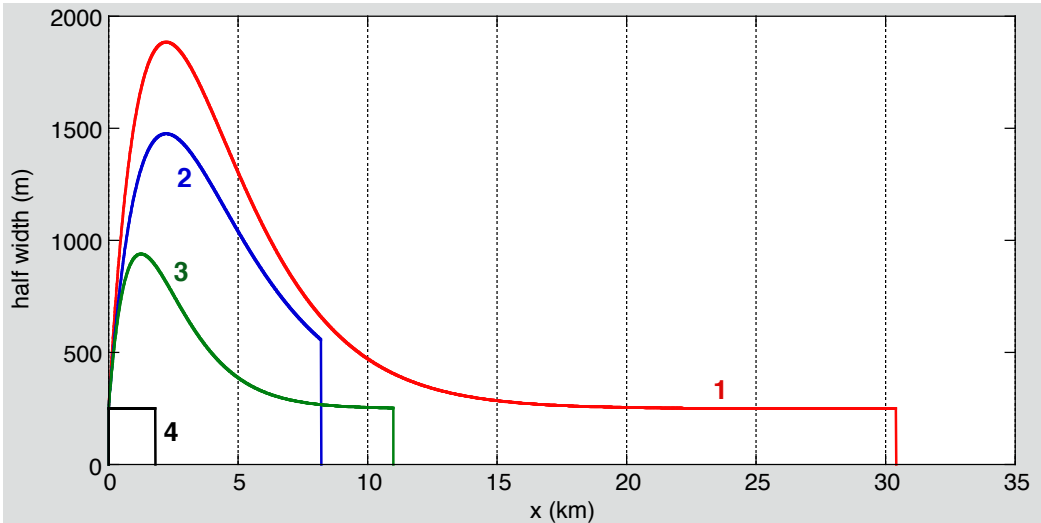


Figure 3.10. Shapes of the four glaciers for which climate change experiments are carried out. The glaciers are shown in plan view - note that they have different slopes as well (see table). The length is for the reference state, which is the equilibrium state corresponding to an equilibrium-line altitude of 2750 m.

All model glaciers were first integrated with $E = 2750$ m until a steady state was reached. Then from 1864 onwards $E(t)$ as shown in Figure 3.9 was imposed as forcing. It should be noted that this does not reflect a realistic situation, because in 1864 the glaciers in the Alps were certainly not in balance with the prevailing climate. However, we do not worry too much about this because the purpose of the calculation is mainly to see the effects of different geometries.

The calculated length relative to the length in 1864 is shown in Figure 3.11. All glaciers show net retreat, of course, but the differences are very large. Glacier 1 shows a large and steady retreat over more than 5 km, and at no time there is a significant advance. Glacier 2, which is steeper and has a larger balance gradient, apparently has a shorter response time. There are some periods of slow advance (1950-1975), while at the same time glacier 1 is retreating, albeit at a lower pace. The behaviour of glacier 3 is very similar to that of glacier 2. Glacier 3 is steeper and the front slightly wider with respect to the maximum width. The climate sensitivity of this glacier is therefore smaller than that of glacier 2.

Glacier 4 shows a very different behaviour. The total retreat is less than 1 km, and the rate of retreat is almost constant. The reason for this is the very large response time. Glacier 4 is in a state not so far from the bifurcation point (see Figures 2.9 and 2.10), because in the reference state $b_0 - E$ is only 25 meters (theoretically, the response time goes to infinity when the bifurcation point is approached). So glacier 4 is an example of a flat and small glacier that steadily melts away. This example demonstrates that small glaciers do not necessarily respond fast to climate change.

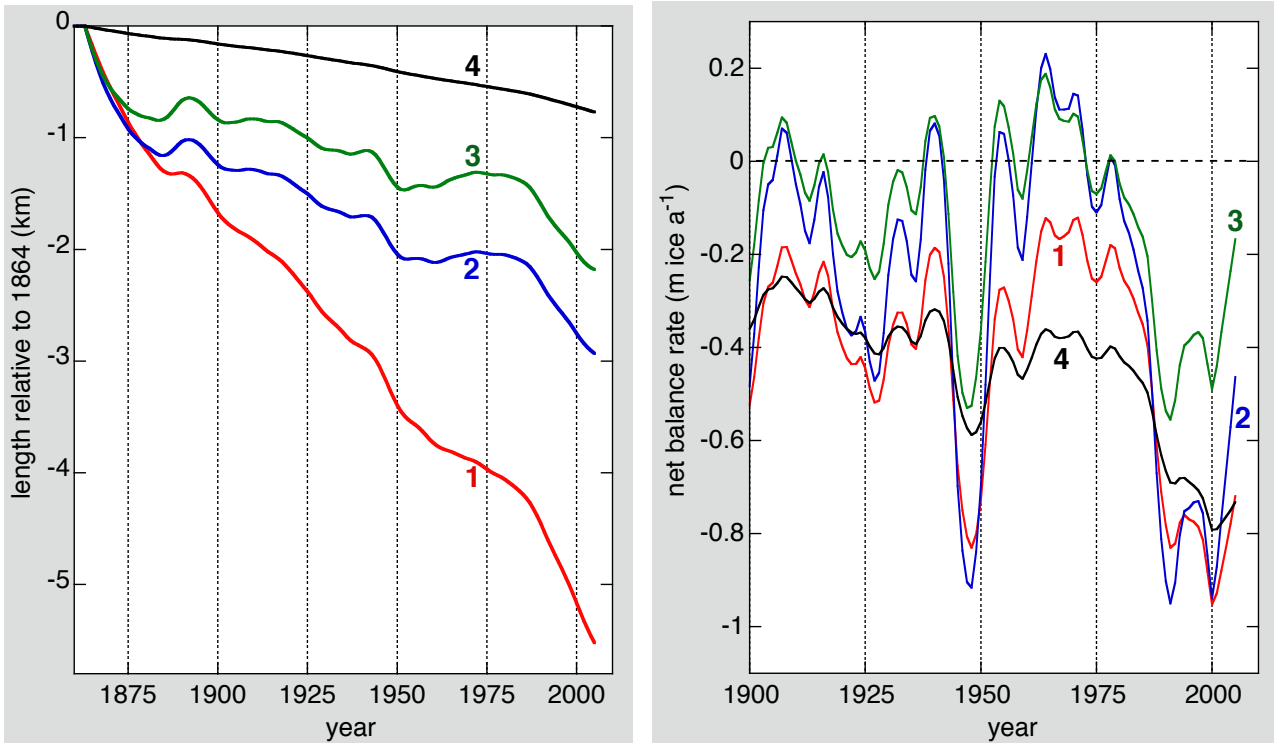


Figure 3.11. Response of the four glaciers subject to the forcing of Figure 3.9. The labels correspond to the glacier numbers as listed in the table. Glacier length (left) shown is relative to the equilibrium glacier length in 1964. The net balance rate (right) is shown from 1900 onwards.

It is instructive to see how the net balance curves for the glaciers differ (Figure 3.11). For the present glacier model the net balance and glacier length are uniquely related, implying that the net balance is positive when $dL/dt > 0$ and negative when $dL/dt < 0$. This may appear as a trivial result, but it stresses once more that glaciers with different geometries can have substantially different net balance histories even when the climate forcing is identical!

3.5 Application to Nordenskiöldbreen, Svalbard

As another application we apply the model to a calving glacier. We consider Nordenskiöldbreen in northern Spitsbergen, Svalbard (Figure 3.12). This glacier is about 24 km long and used to be a calving glacier. In recent years the glacier front has been retreating from the fjord and calving has become insignificant. The geometry of the glacier is not too complex and the surface slope is relatively constant.

Nordenskiöldbreen has been studied in some detail by Kuipers Munneke (2005), who constructed a one-dimensional flowline model for this glacier. Although the overall simulation of the shape of the glacier was successful, a proper formulation of the calving process at the front appeared to be a difficult point. It is thus interesting to find out how far we can get with the simple model developed here. The geometry of Nordenskiöldbreen can only be handled in a schematic way, of course, but it should be possible to capture the main characteristics.

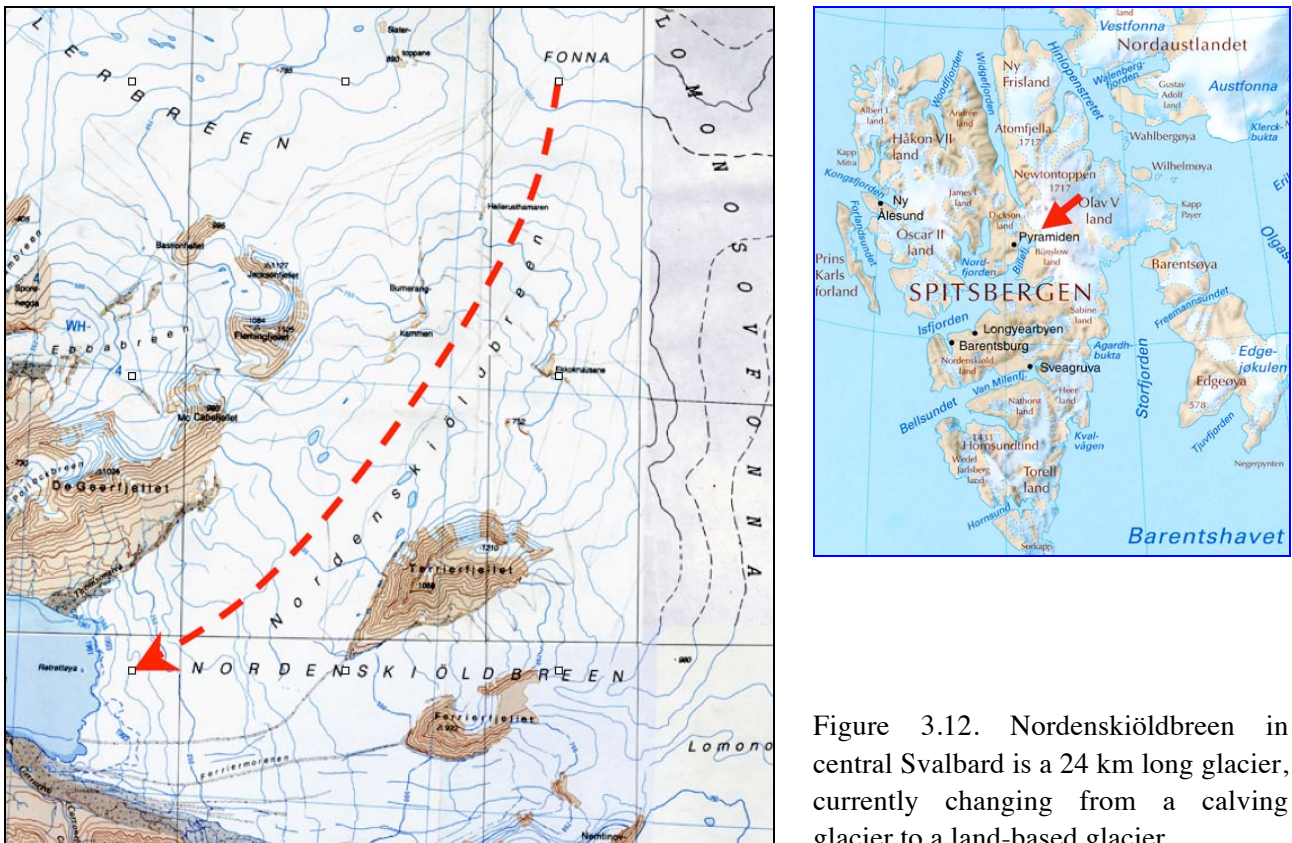


Figure 3.12. Nordenskiöldbreen in central Svalbard is a 24 km long glacier, currently changing from a calving glacier to a land-based glacier.

For the mass balance we use a linear profile again, in line with the (very scarce) measurements. In reality the accumulation levels off in the higher regions (Kuipers Munneke, 2005). In the model a constant glacier width is used, although a varying width could be accommodated along the lines discussed in the previous section. However, it is not so obvious how glacier width should be defined. It is clear that in the accumulation region the glacier is wider (Figure 3.12). Therefore the overestimation of accumulation due to the linear balance profile will be counteracted by the underestimation of the size of the accumulation area.

Like many glaciers in Svalbard, Nordenskiöldbreen reached its maximum neoglacial extent towards the end of the 19th century, and retreated during the 20th century over a distance of about 2 km (Plassen et al., 2003; Kuipers Munneke, 2005; Figure 3.13). A significant part of this retreat must have been due to the widespread warming that occurred over Svalbard during the first half of the 20th century. It is tempting to see if the simple model can simulate the retreat when temperature forcing is used as input. For this purpose a smoothed version of the temperature record reconstructed by Kuipers Munneke (2005) is used. In this record instrumental observations have been combined with temperatures inferred from oxygen isotope measurements from an ice core drilled on the plateau from which Nordenskiöldbreen originates (Isaksson et al., 2003).

To simulate the behaviour of Nordenskiöldbreen the following parameters are used: $b_0 = 1050$ m, $s = 0.044$, $w_0 = 3500$ m, $\beta = 0.006 \text{ m ice } a^{-1} \text{ m}^{-1}$, $\nu = 10$, $\alpha_m = 2.5 \text{ m}^{1/2}$, $\kappa = 0.4$. Note that the slope is small compared to the glacier geometries used in earlier examples. With the values of b_0 and s the coastline is at 23.86 km from the glacier head.

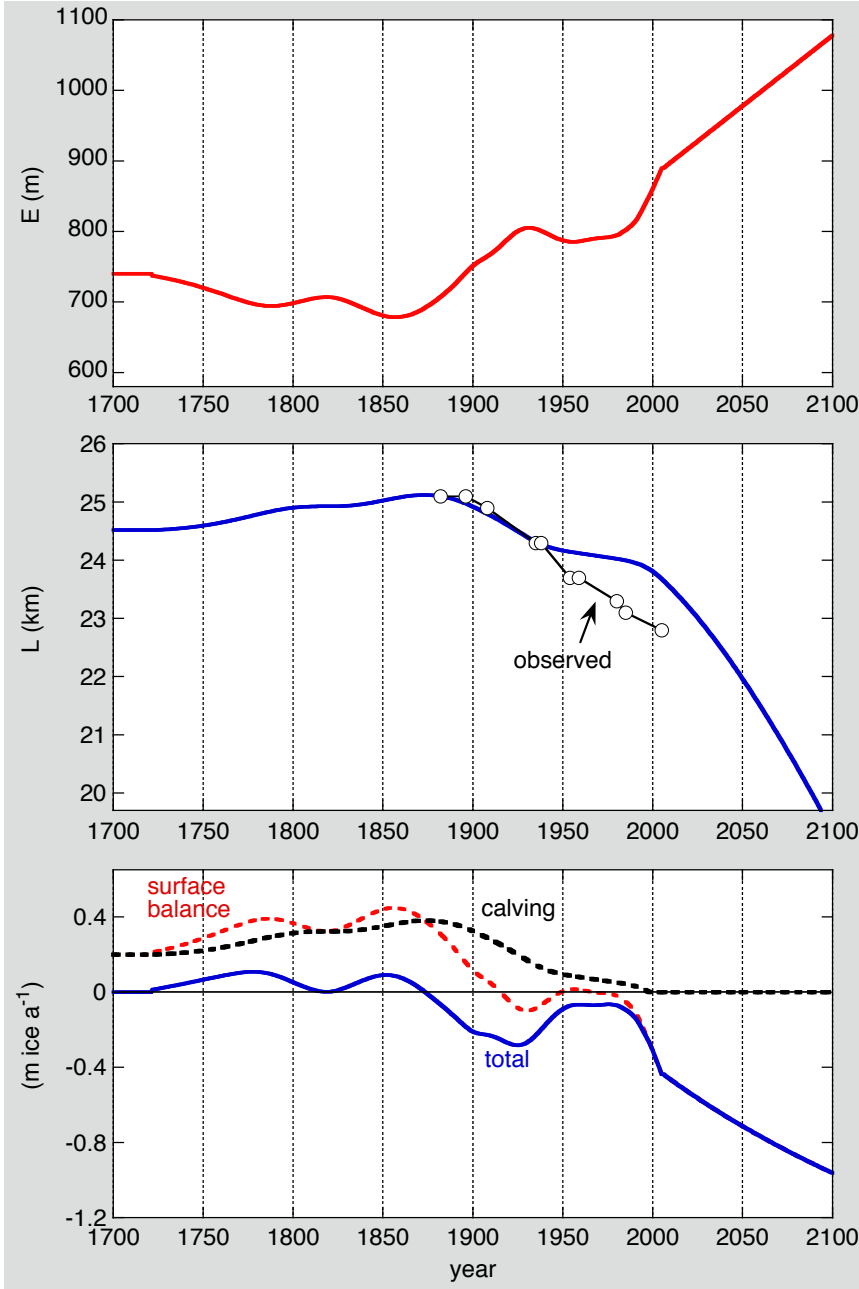


Figure 3.13. Model simulation of the evolution of Norden-skiöldbreen. The upper panel shows the forcing (equilibrium-line altitude). In the middle calculated glacier length is compared with observations (as compiled by Kuipers Munneke, 2005).

The components of the mass budget are shown in the lower plot. Note that the calving flux becomes zero around the year 2000.

The forcing is prescribed as

$$E(t) = E_0 + E'(t) , \quad (3.5.1)$$

where E is a reference value of the equilibrium-line altitude and $E'(t)$ a time-dependent perturbation. For the period 1722-2005 $E'(t)$ is based on the temperature reconstruction described above. From 2005 until 2100 the equilibrium line is assumed to rise at a constant rate of 2 m a^{-1} . This is meant to reflect the implication of global warming in the Arctic. For $E_0 = 725 \text{ m}$, the resulting forcing $E(t)$ is shown in the upper panel of Figure 3.13. In fact, the value of E_0 has been chosen in such a way that the glacier front is at the coastline in the year 2000.

A comparison between calculated and observed glacier length reveals that the simulation is reasonable, but underestimates the rate of retreat in the 20th century (Note: the observed glacier

length has been translated slightly to put the first data point from 1882 exactly on the simulated length curve for a better comparison). The timing of the maximum glacier stand is fine.

The components of the mass budget are shown in the lower panel of Figure 3.13. The calving flux has been divided by the total glacier area. This gives a number which is comparable to the mean surface budget. The calving flux reaches its largest value when the glacier has its maximum length. The mass loss from iceberg calving is then equivalent to a net balance of $-0.4 \text{ m ice a}^{-1}$. After 1916, the glacier is definitely in a mode of retreat: the surface balance never becomes positive again. As expected the further rise of the equilibrium line will cause the glacier to retreat by another 4 km. This depends very much on the prescribed rate at which E increases.

It is interesting that the study with a flowline model, in which variations in bed geometry and glacier width are taken into account (Kuipers Munneke, 2005), does not yield a better result. Again, the rate of retreat during the 20th century is not captured by the model. The cause for the discrepancy between observations and simulation is apparently common to both models. Likely, the raise of the equilibrium line starting around 1860 was larger than assumed here. Alternatively, ice-mechanical processes acting at the glacier front, like increased crevassing and calving, could have been responsible for the stronger retreat.

Finally, a calculation with a stepwise forcing revealed that the e-folding response of Nordenskiöldbreen is about 230 a, which is in good agreement with the result from the flowline model (200 ± 30 a; Kuipers Munneke, 2005). Compared to the Aletschgletscher, which has about the same length, the response is slow. The main reason for the difference is the much smaller average slope of Nordenskiöldbreen.



Variegated Glacier, Alaska, during the 1982/83 surge. Photo by J. Alean

4. Surging glaciers

4.1 Introduction

Surging of glaciers is a very intriguing phenomenon that has drawn the attention of many researchers. In spite of two decades of dedicated research, the mechanics of surging are not yet fully understood (Raymond, 1987; Sharp, 1988; Murray et al., 2003; Milana, 2007). For (almost) temperate glaciers it has become clear that changes in the hydraulic system play a crucial role in the initiation and propagation of a surge. However, many cold or polythermal glaciers also surge (e.g. Dowdeswell and Williams, 1997), and then the interaction of mechanics and the thermal field seems to be crucial (e.g. Murray et al., 2000).

The first attempt to model the behaviour of a glacier through a full surge cycle was made by Budd (1975). After that more refined theories of the mechanism behind a surge have been developed (e.g. Kamb et al., 1987; Fowler, 1987). In most of these studies the discussion focusses on the relation between sliding, basal drag and hydraulics.

A question of a more general nature is concerned with the role of surges in the long-term mass budget of a glacier. Although the character of surges may vary greatly with respect to the dynamical aspects, there is also a clear common element: *mass is transferred to lower elevations where melt rates are higher*. As a consequence, shortly after a surge a glacier will be subject to an increased loss of mass and a very negative net balance. It has to be expected that the long-term mean length of a glacier will be smaller if regular surges occur. Recent numerical modelling studies on the dynamics of Vatnajökull (Adalgeirsdóttir et al., 2005) have suggested that without surging this ice cap would grow to a much larger size, covering a substantial part of Iceland.

In spite of the fact that the modelling of surging as a problem in ice mechanics is difficult, it may be possible to estimate the integrated effects of regular surging by a consideration of the total mass budget. In such an approach surging is then simply imposed to a minimal glacier model.

4.2 Describing a surge in the minimal glacier model

The model glacier has a constant width, rests on a bed with a constant slope and is subject to a linear balance profile. As before, the mean thickness of the glacier is determined by its length L and the bed slope s , i.e.

$$H_m = S \frac{\alpha_m}{1 + \nu s} L^{1/2}, \quad (4.2.1)$$

A ‘surge parameter’ S has now been added. In the ‘normal mode’ $S = 1$. A surge is imitated by suddenly decreasing the value of S . This is a very crude representation of what actually happens during a surge, because it does not take into account a redistribution of ice thickness but merely reduces the ice thickness everywhere. However, since mass conservation then requires an increase in glacier length, and consequently an increase in H_m by virtue of eq. (4.2.1), the lower part of the glacier may still have an appreciable thickness after the surge (Figure 4.1; linear surface profiles have been drawn, but this is not necessary for the model formulation).

The volume of the glacier is

$$V = \int_0^L H(x) dx = \frac{\alpha_m}{1 + \nu s} S L^{3/2}. \quad (4.2.2)$$

Conservation of mass thus requires

$$\frac{dV}{dt} = \frac{\alpha_m}{1 + \nu s} \left\{ L^{3/2} \frac{dS}{dt} + \frac{3}{2} S L^{1/2} \frac{dL}{dt} \right\} = B_s. \quad (4.2.3)$$

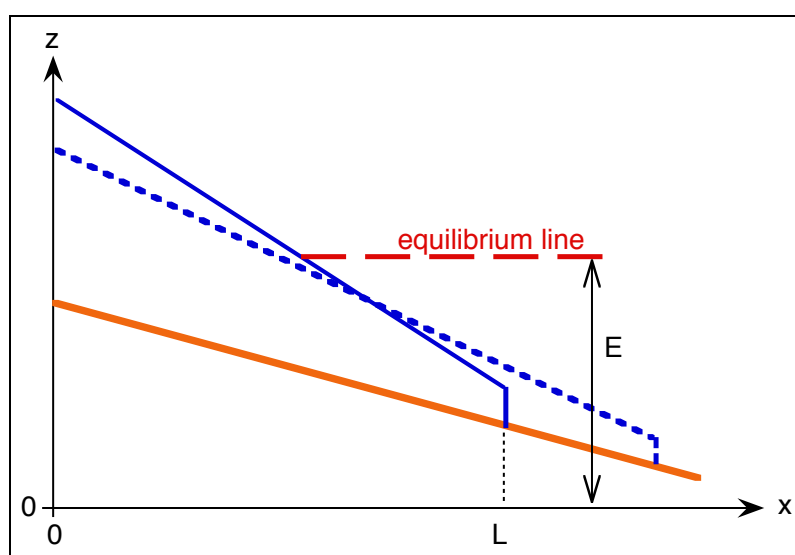


Figure 4.1. Possible geometry of the model. The solid blue line shows the surface profile before a surge, the dashed line after the surge. The glacier volume has not changed.

Rearranging then yields the prognostic equation for the length of the glacier:

$$\frac{dL}{dt} = \frac{2(1+\nu s)}{3\alpha_m} B_s S^{-1} L^{-1/2} - \frac{2}{3} S^{-1} L \frac{dS}{dt} . \quad (4.2.4)$$

From this equation it is clear that a sufficiently rapid decrease of S ($dS/dt \ll 0$) leads to a strong increase in L (but not in V).

The calculation of the surface mass budget B_s is similar to that in section 3.2, i.e.

$$B_s = \beta \int_0^L (H + b_0 - sx - E) dx = -\frac{1}{2} \beta s L^2 + \beta \left(\frac{\alpha_m}{1+\nu s} S L^{1/2} + b_0 - E \right) L . \quad (4.2.5)$$

When $S(t)$, the surge function, is prescribed, eqs. (4.2.4)-(4.2.5) can easily be integrated in time.

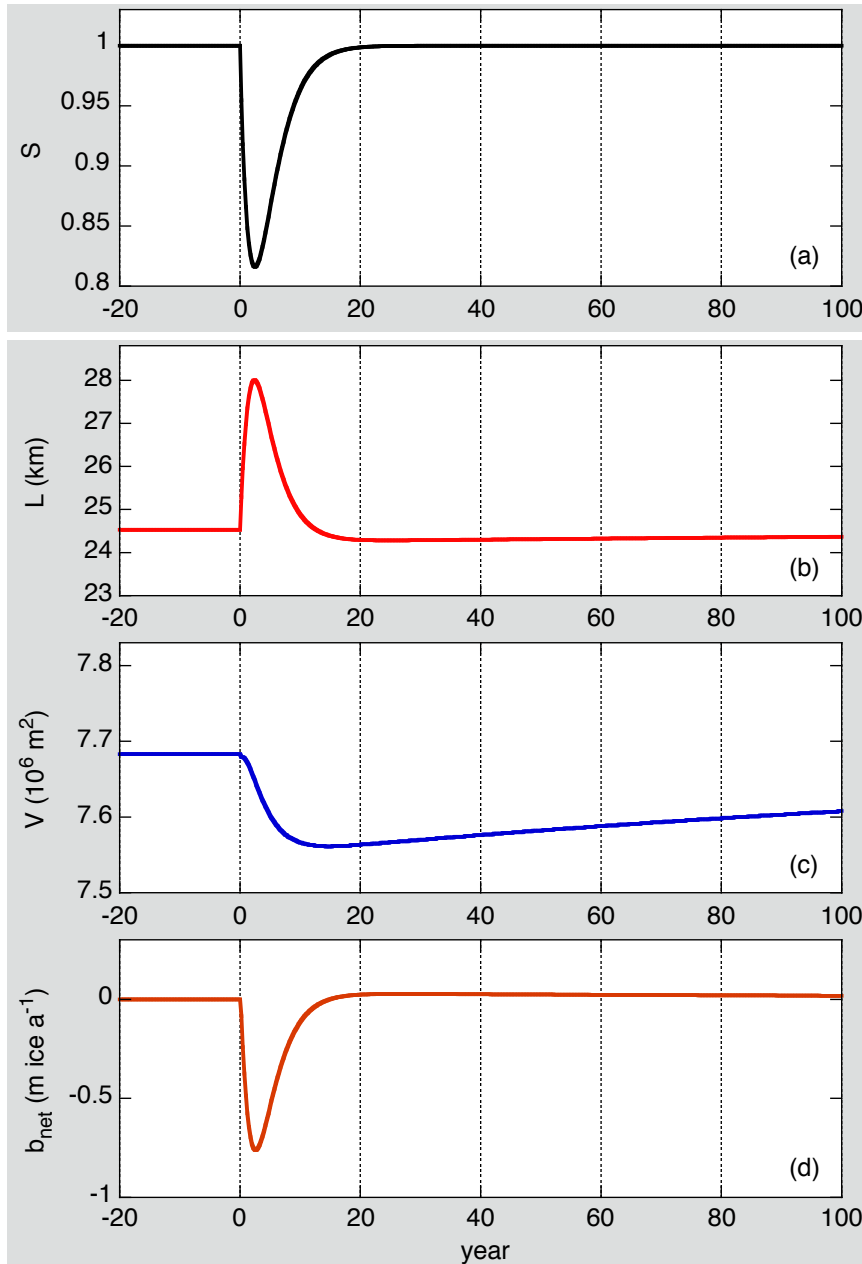


Figure 4.2. Diagnosis of a simulated surge. S represents the forcing and is plotted in (a). The glacier response is shown in terms of length (b), volume (c) and net balance rate (d).

A surge is imposed to the model by prescribing

$$S(t) = 1 - S_0(t - t_0)e^{-(t-t_0)/t_s} . \quad (4.2.6)$$

The surge starts at $t = t_0$ and S_0 determines by how much the thickness of the glacier is reduced. The characteristic time scale of the surge is denoted by t_s .

An example is shown in Figure 4.2 (with $t_0 = 0$). First the model is integrated until a steady state has been reached (parameter value used: $b_0 - E = 300$ m, $s = 0.05$, $\nu = 10$, $\alpha_m = 3 \text{ m}^{1/2}$). The equilibrium glacier length is about 24.5 km. The imposed surge implies that S drops from 1 to 0.82 in a few years ($t_s = 2.5$ a, $S_0 = 0.2 \text{ a}^{-1}$). The glacier responds by advancing over a distance of 3.5 km. Since the mean surface elevation starts to decrease immediately, the surface mass budget becomes negative and the glacier volume decreases. The minimum in the net balance is already reached after a couple of years and amounts to $-0.78 \text{ m ice a}^{-1}$. The volume decreases for a considerable time and reaches a minimum 14 years after the initiation of the surge. The relative changes in the volume are small, however.

It is tempting to use the model to investigate the effect of regular surging on the long-term stability of glaciers. As mentioned in the Introduction, Vatnajökull seems to be a typical example of a glacier that cannot grow further because regular surging drains the ice to lower regions and lowers the surface. For the calculation we therefore chose parameter values that could characterize a lobe of Vatnajökull, Iceland (Figure 4.3). Several parts of this ice cap surge regularly (Björnsson et al., 2003). Apart from a few distinct high outcrops, the major part of the bed of Vatnajökull is well below the equilibrium line, which, in the terminology of the minimal model, implies that $b_0 - E$ is quite small.

The following parameter values are used: $b_0 - E = 50$ m, $\beta = 0.01 \text{ m ice a}^{-1} \text{ m}^{-1}$, $s = 0.025$, $t_s = 5$ a, $S_0 = 0.15 \text{ a}^{-1}$. These values are not meant to represent a particular part of Vatnajokull or any other ice cap - merely the order of magnitude matters.

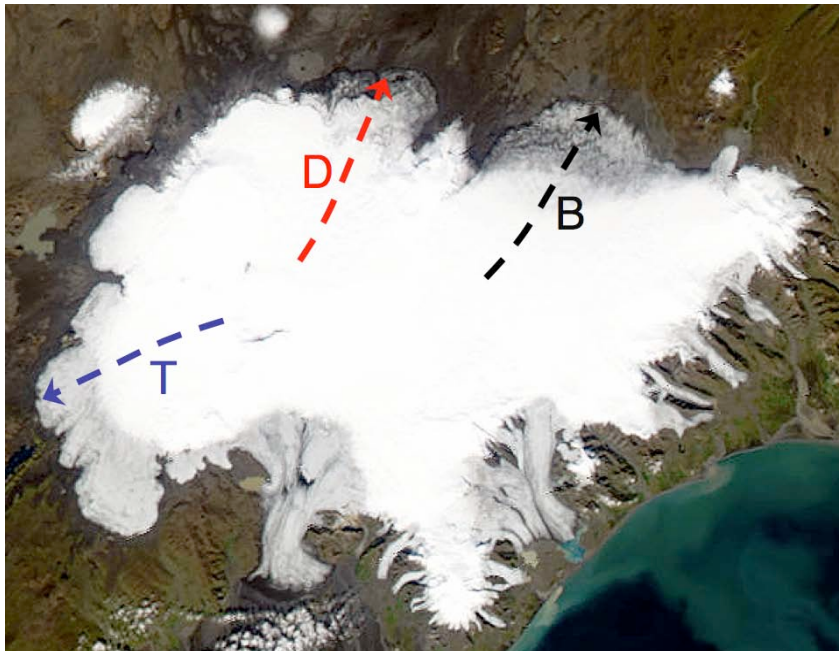


Figure 4.3. MODIS-image of Vatnajökull, Iceland, 9th September 2002 (courtesy of NASA). The width of the image is approximately 150 km.
Brúarjökull (B) surged in 1963–1964, Tungaárjökull (T) in 1994–1995, and Dyngjujökull (D) in 1998–2000.

Starting without ice the model is first integrated until a steady state is reached. Because the equilibrium line is just under the highest point of the bed and the slope of the bed is small, this takes more than 2000 years (Figure 4.4). At $t = 2500$ a the surge mechanism is switched on. There is a surge every 50 years. With the parameter values given above, S drops to 0.82 at the peak of the surge.

The effect of the surges on the long-term behaviour of the glacier turns out to be significant. The mean volume is only 65% of the steady state volume in case of no surges. During a surge the glacier length increases by 8 km, i.e. ~20% (note: Brúarjökull advanced over about 8 km when it was surging in 1963/64). In the model the magnitude of the surge can easily be changed by using a different value for S_0 .

Altogether, we conclude that a minimal glacier model is able to simulate an important aspect of the long-term behaviour of surging glaciers. The main effect of a surge, i.e. the increase of the ablation area and the lowering of the surface, is captured. Since the surge mechanism is imposed, we learn little about the surge mechanism itself. Nevertheless, the model is consistent in terms of mass budgets and the feedback between balance rate and mean surface elevation, and can therefore be used to quantify the statistical impact of regular surges on the size of a glacier.

There is ample room for exploring the parameter space here, but this is left to the interested reader. It should also be possible to apply the model to a particular glacier by optimising/calibrating the parameter set.

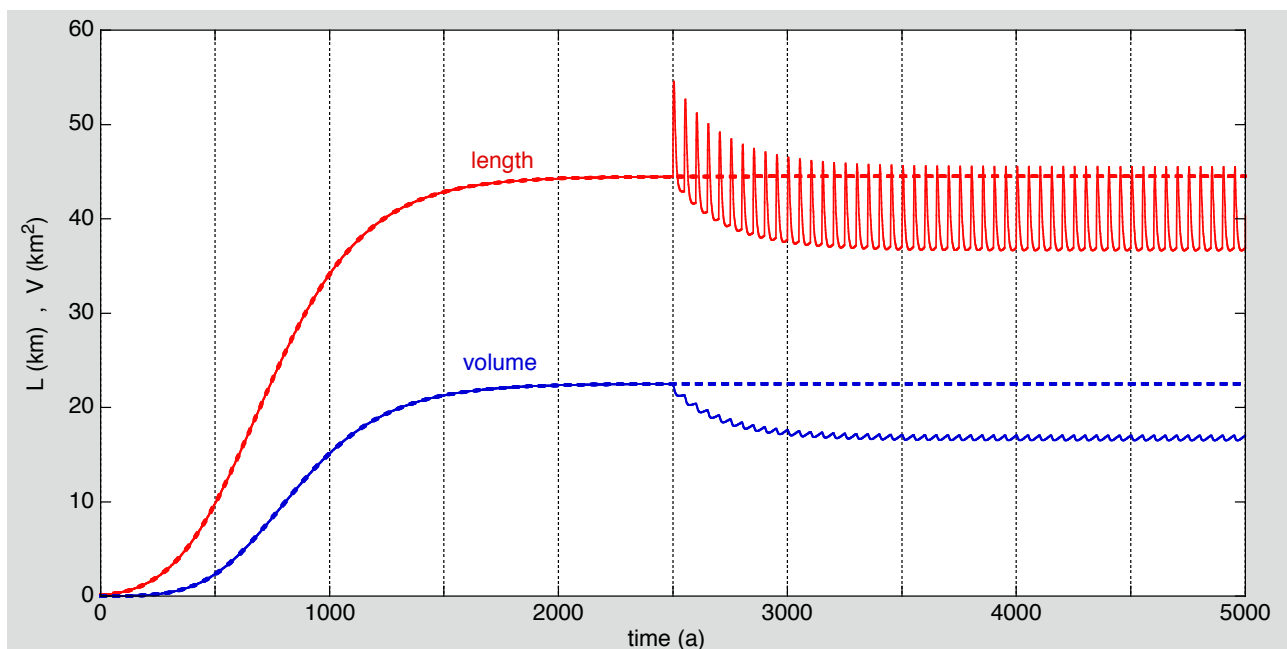


Figure 4.3. The effect of regular surging (every 100 years) on the long-term size of a large glacier. The surging mechanism is switched on after 2500 years of integration. The dashed curves refer to the case without surging. The volume is ‘per unit width’, and therefore in km^2 .



Piz Bernina (4049 m), Switzerland

5. Varying bed slope

5.1 Introduction

In all models discussed in the previous chapters the bed has been assumed to have a constant slope. For many glaciers this is not a very good approximation, of course. It is therefore tempting to find out if an analysis can also be done for a bed with a variable slope. To be compatible with the approach of the minimal glacier model this then implies that the mean ice thickness is related to the mean bed slope \bar{s} . To obtain a feeling for the effect of a varying mean bed slope we consider the bed profile of Nigardsbreen (Figure 5.1).

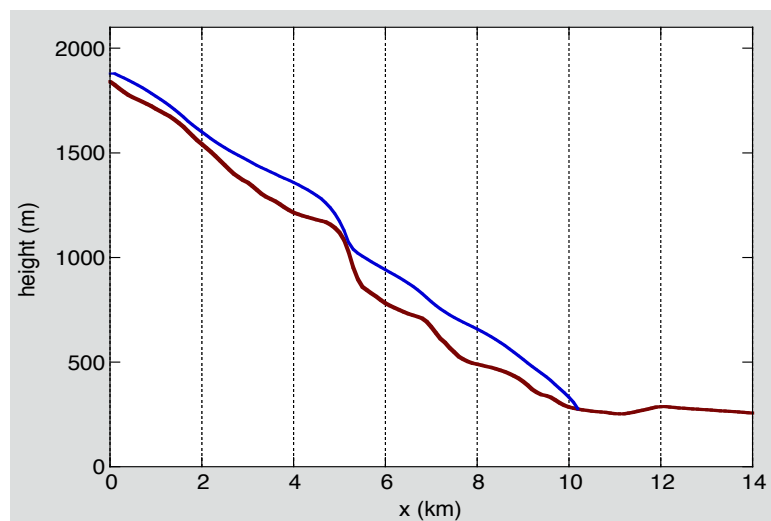


Figure 5.1. Profile along the flowline of Nigardsbreen, 1988 (from Oerlemans, 1997b). The bed is drawn in brown, the glacier surface in blue.

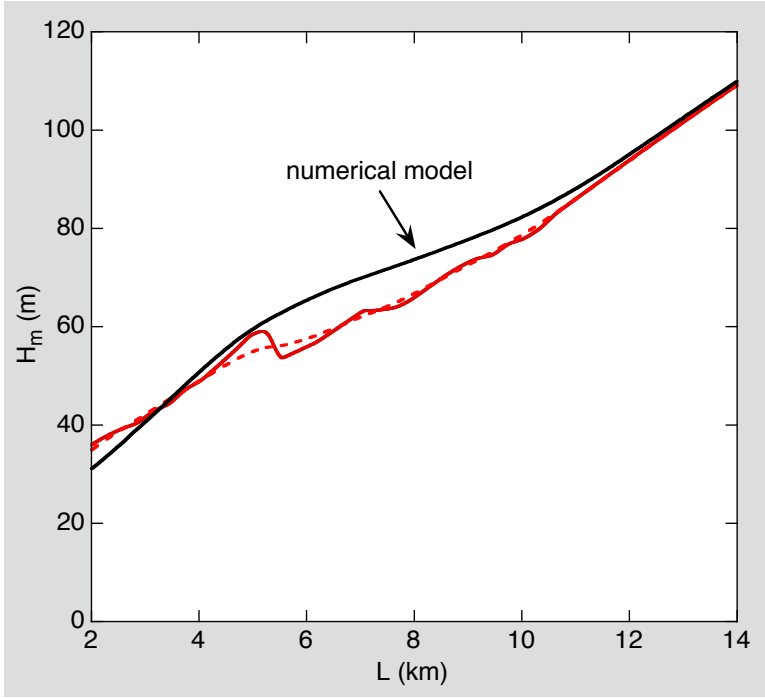


Figure 5.2. The dependence of the mean ice thickness on glacier length according to the minimal model (red) and the numerical model (black).

The bed is characterized by a steeper part (icefall) around $x = 5$ km and a transition to a much smaller slope at $x \approx 10$ km. For the minimal model the mean ice thickness is obtained from

$$H_m = \frac{\alpha_m}{1 + \nu \bar{s}} L^{1/2} , \quad (5.1.1)$$

in which \bar{s} is the mean bed slope for the given glacier length. The result for the bed profile of Figure 5.1 is shown in Figure 5.2 (solid red line; $\alpha_m = 2 \text{ m}^{1/2}$; $\nu = 10$). Note that the mean thickness decreases for increasing glacier length just after the icefall. A calculation with a numerical ice flow model (shallow ice approximation) does not show this feature (black line in Figure 5.2). This may be due to smoothing inherent to the finite difference approach in the numerical model, but it is probably also related to the physical properties of the shallow ice approximation.

In any case, the variation of H_m predicted by eq. (5.1.1) when the glacier snout passes the steep part of the bed is too large. This becomes evident when the volume is considered as a function of length. For $5.2 < x < 5.8$ km the volume (mean thickness times length) does not increase with L , which is not realistic. When $H_m(L)$ is smoothed, an acceptable relation between thickness and length is obtained.

Broadly speaking, the relation between thickness and length as emerging in Figure 5.2 is fairly linear. Here additive effects are evident: when L increases \bar{s} decreases at the same time, and these changes both imply a larger ice thickness. Since a concave glacier bed is the rule rather than the exception, for many glaciers the effective dependence of thickness on length may be somewhat stronger than $\propto \sqrt{L}$.

So the conclusion from this exercise is that the use of eq. (5.1) is justified when the bed is smooth and changes in the slope are gradual.

5.2 Modifying the continuity equation

A bed slope changing in time implies that the continuity equation has to be revised. As before, we take as starting point

$$\frac{dV}{dt} = \frac{d}{dt}(H_m L) = H_m \frac{dL}{dt} + L \frac{dH_m}{dt} . \quad (5.2.1)$$

From eq. (5.1.1) it follows that

$$\frac{dH_m}{dt} = \frac{\alpha_m}{2(1+\nu\bar{s})} L^{-1/2} \frac{dL}{dt} - \frac{\alpha_m \nu}{(1+\nu\bar{s})^2} L^{1/2} \frac{\partial \bar{s}}{\partial L} \frac{dL}{dt} . \quad (5.2.2)$$

Combining eqs. (5.2.1) and (5.2.2) yields

$$\frac{dV}{dt} = \left\{ \frac{3\alpha_m}{2(1+\nu\bar{s})} L^{1/2} - \frac{\alpha_m \nu}{(1+\nu\bar{s})^2} L^{3/2} \frac{\partial \bar{s}}{\partial L} \right\} \frac{dL}{dt} . \quad (5.2.3)$$

The evolution of the glacier length can thus be calculated from

$$\frac{dL}{dt} = \left\{ \frac{3\alpha_m}{2(1+\nu\bar{s})} L^{1/2} - \frac{\alpha_m \nu}{(1+\nu\bar{s})^2} L^{3/2} \frac{\partial \bar{s}}{\partial L} \right\}^{-1} B_s , \quad (5.2.4)$$

where, as before, B_s is the total surface budget.

In the case of a linear balance profile the calculation of B_s is straightforward, because

$$B_s = \beta \int_0^L (H(x) + b(x) - E) dx = \beta(H_m + \bar{b} - E)L , \quad (5.2.5)$$

where \bar{b} is the mean bed elevation over the glacier length.

5.3 A simple concave bed

For most glaciers the bed slope tends to decrease when going downglacier. It is thus natural to study the case with

$$b(x) = b_0 e^{-x/x_l} . \quad (5.3.1)$$

Here x_l is just the length scale that determines how quickly the height of the bed decreases. For a given glacier length, the mean bed slope is

$$\bar{s} = \frac{b_0(1 - e^{-L/x_l})}{L} . \quad (5.3.2)$$

The mean bed elevation is given by

$$\bar{b} = \frac{b_0}{L} \int_0^L e^{-x/x_l} dx = \frac{x_l b_0}{L} (1 - e^{-L/x_l}) . \quad (5.3.3)$$

And finally

$$\frac{\partial \bar{s}}{\partial L} = -\frac{b_0(1 - e^{-L/x_l})}{L^2} + \frac{b_0 x_l^{-1} e^{-L/x_l}}{L} . \quad (5.3.4)$$

With eqs. (5.2.5), (5.3.2) and (5.3.4), eq. (5.2.4) can now be integrated in time. As an example we consider the response of the model glacier to stepwise changes in the equilibrium-line altitude (Figure 5.3). The parameter values are: $b_0 = 2000$ m, $x_l = 5000$ m, $\beta = 0.008$ m ice a^{-1} m^{-1} , $\nu = 10$, $\alpha_m = 3$ $m^{1/2}$ (see Figure 5.4 for the bed profile).

The effect of the changing bed slope is evident. E is changed in equal steps of 200 m, yet the change in L is much larger for a longer glacier. It will be clear from the earlier analysis that this is a consequence of the smaller mean bed slope, not of the larger glacier length in itself. Because the bed profile as described by eq. (5.3.1) goes asymptotically to zero, and \bar{s} as well, the glacier will grow to infinity for a sufficiently low value of E (about 600 m in this case).

Figure 5.4 shows the position of the glacier front for the various values of E . The front positions refer to the equilibrium states. The length of the vertical bar is a measure of the *mean* ice thickness. Once more we should realise that the analysis only requests a parameterisation of the mean ice thickness, and not of the thickness profile along x .

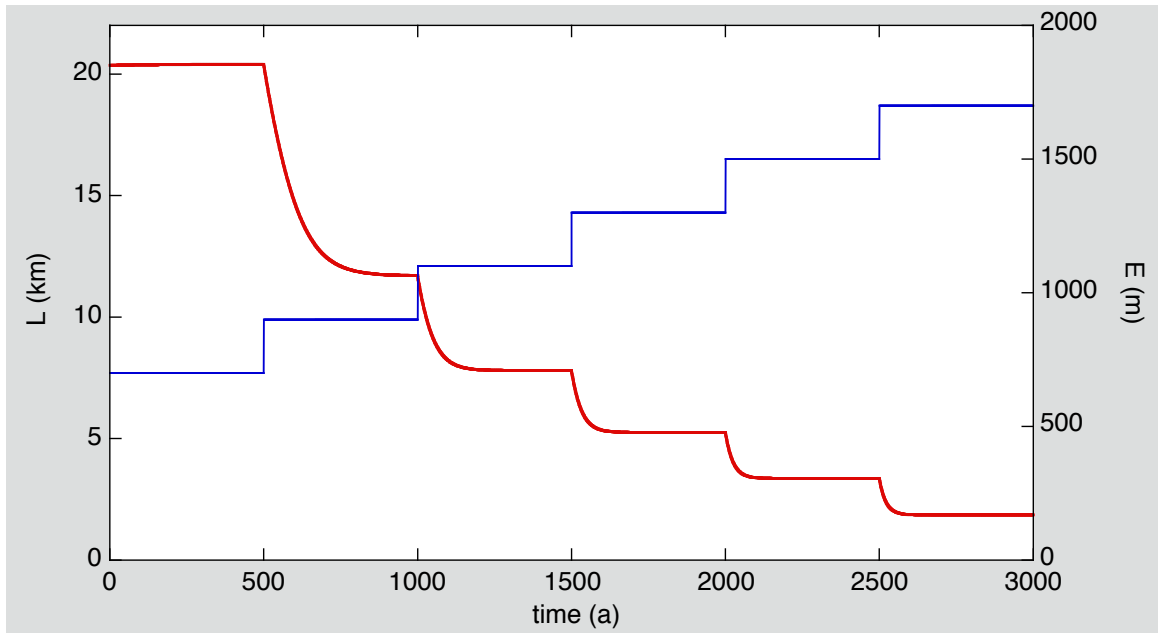


Figure 5.3. Glacier length L (red) as a response to stepwise forcing through the equilibrium-line altitude E (blue).

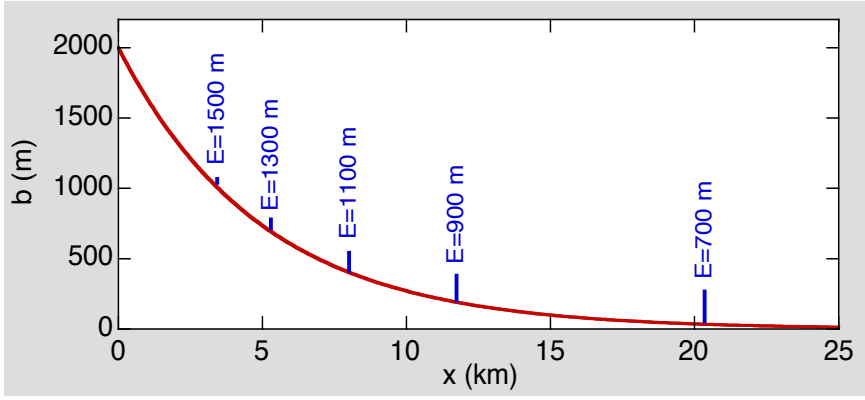


Figure 5.4 Front positions for equilibrium states. Mean ice thickness is indicated by blue bars (scale at left).

5.4 Overdeepening

A large number of glaciers have a bed with a reversed slope over a certain distance along the flowline. In many cases this is due to the action of the glacier itself, i.e. erosion in the middle of the glacier and deposition of debris towards the glacier front. It is obvious that the feedback of glacier action on the shape of the bed may create interesting dynamic behaviour (e.g. Van der Veen, 1997). In this chapter we discuss the implications of an overdeepened bed profile that does not change in time.

A simple representation of a bed with a reversed slope is obtained by superposing a Gaussian bump on a linearly sloping bed:

$$b(x) = b_0 - sx + b_1 e^{-\{(x-x_0)/x_l\}^2}. \quad (5.4.1)$$

The amplitude of the bump is determined by b_1 , its location along the bed profile by x_0 and its width by x_l . An example is shown in Figure 5.5. In analogy with the approach described in the previous section, the mean bed slope for a given glacier length is easily obtained. The mean bed elevation is calculated as

$$\bar{b} = \frac{1}{L} \int_0^L b(x) dx = b_0 - \frac{sL}{2} + \frac{b_1}{L} \int_0^L e^{-\{(x-x_0)/x_l\}^2} dx. \quad (5.4.2)$$

With $x' = (x - x_0)/x_l$ the last integral in eq. (5.4.2) can be written as

$$\int_0^L e^{-\{(x-x_0)/x_l\}^2} dx = x_l \int_{-x_0/x_l}^{(L-x_0)/x_l} e^{-x'^2} dx' = x_l \left[\int_0^{(L-x_0)/x_l} e^{-x'^2} dx' - \int_0^{-x_0/x_l} e^{-x'^2} dx' \right]. \quad (5.4.3)$$

We have thus written the integral as the sum of two values of the error function $\int_0^p e^{-p'^2} dp'$, for which standard approximations exist (e.g. Hamming, 1987). The error function is also an intrinsic function in most programming languages (however, note that sometimes a scaling factor $2/\sqrt{\pi}$ is used, sometimes not).

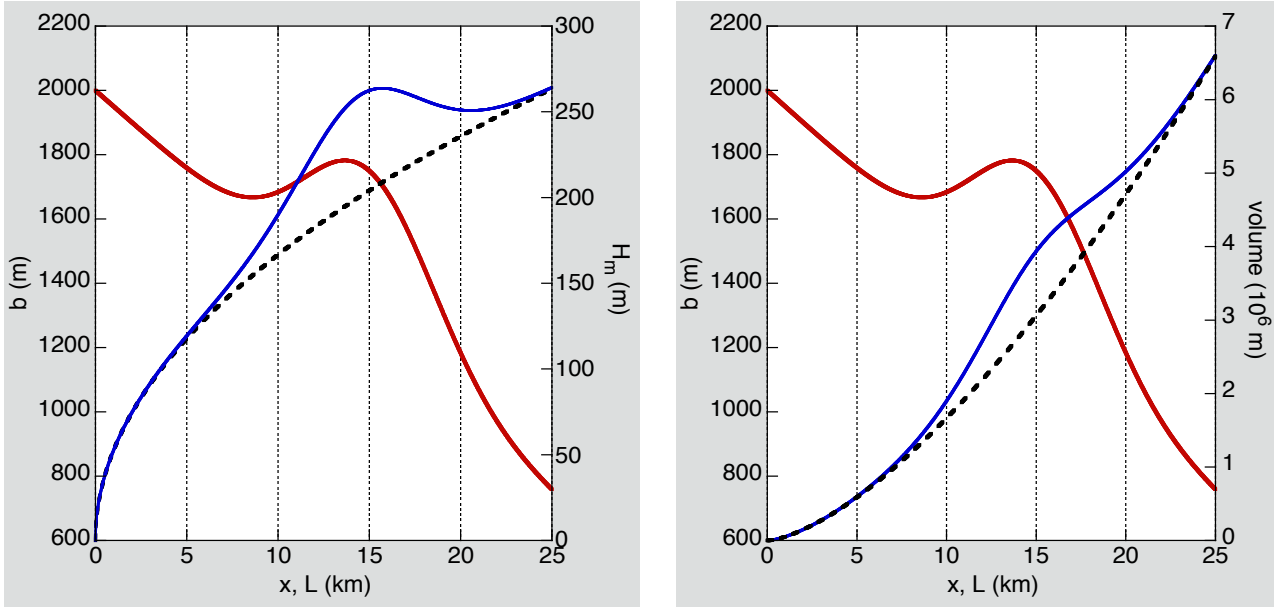


Figure 5.5. The effect of an overdeepened bed (red curve) on the mean ice thickness (left) and the ‘volume’ (mean ice thickness times length). The dashed black curves show ice thickness and ice volume for the case with a constant slope (no Gaussian bump).

Parameter values: $b_0 = 2000 \text{ m}$, $s = 0.05$, $b_1 = 400 \text{ m}$, $x_0 = 15000 \text{ m}$, $x_l = 5000 \text{ m}$, $\alpha_m = 2.5 \text{ m}^{1/2}$, $\nu = 10$.

Finally, after a bit of manipulation an expression for $\partial \bar{s} / \partial L$ is obtained (note that \bar{s} is counted positive when the bed slopes down in the x -direction):

$$\frac{\partial \bar{s}}{\partial L} = -\frac{b_1}{L^2} \left\{ e^{-(x_0/x_l)^2} - e^{-[(L-x_0)/x_l]^2} \right\} + \frac{b_1}{L} \frac{2(L-x_0)}{x_l^2} e^{-[(L-x_0)/x_l]^2}. \quad (5.4.4)$$

The model formulation is complete now and eq. (5.2.4) can be integrated in time.

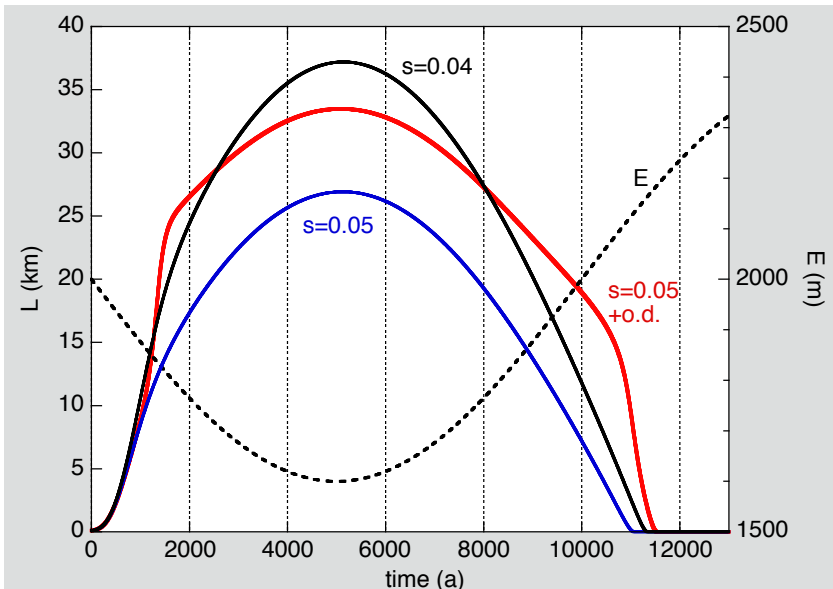


Figure 5.6. Calculated glacier length for very slow variation of E (dashed line). The red curve is for the bed with overdeepening as shown in Figure 5.5, the other curves for a bed with constant slope as indicated.

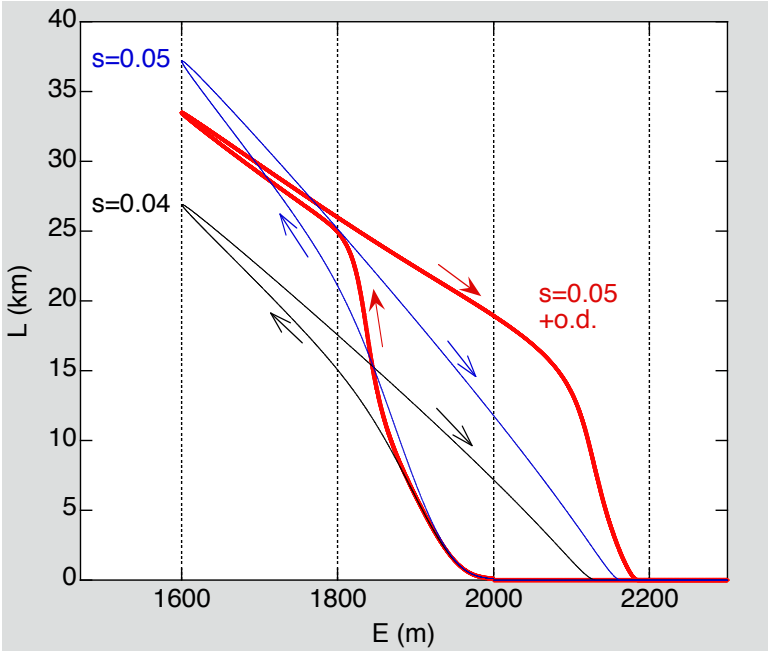


Figure 5.7. Illustrating the nonlinear effect of the height-mass balance feedback. Hysteresis is evident in all cases, notably for the overdeepened bed (red curve). Glacier length follows the path indicated by the arrows.

We now investigate the effect of the bed profile on glacier length for a slow sinusoidal variation of the equilibrium line (dashed line in Figure 5.6). In the beginning of the integration the equilibrium line is at the highest point of the bed (2000 m) and is then lowered slowly to reach a value of 1600 m after 5000 years. Then it rises until the glacier has disappeared. The red curve in Figure 5.6 is for the bed profile with the overdeepening as shown in Figure 5.5. For comparison, two calculations were also done for beds with constant slopes. Just removing the Gaussian bump leads to a significantly smaller glacier, and therefore a calculation with a smaller slope (0.04 instead of 0.05) was also done.

It is evident that the overdeepening leads to a strongly nonlinear response. Because the forcing is very slow, the glacier length is close to equilibrium most of the time. When the glacier front is located on the reversed bed slope, the sensitivity to changes in E is particularly large. Also during the phase of retreat the effect of the Gaussian bump is evident.

Another view is given in Figure 5.7. It is a kind of phase diagram, showing the path of the glacier in the E, L -plane. The hysteresis due to the height mass-balance feedback is obvious in all cases, but it is most pronounced for the case with overdeepening. On ‘the way back’, coming from a lower value of E , the glacier length for $E = 2000$ m is about 19 km. However, this value is roughly halved when the bump is removed.

It is clear that the parameterisation of the mean ice thickness given by eq. (5.1.1) can only be a rather crude approximation. Intuitively, the main weakness is that for larger L the mean ice thickness does not depend on the depth of the overdeepening for a fixed height of the bump. Therefore, at this point it seems useful to compare a solution of the minimal model with one obtained with a numerical flowline model in which the glacier profile is calculated explicitly. Using a flowline model (based on the shallow-ice approximation) with a 200 m grid resolution and identical geometry and forcing yields the solution shown in Figure 5.8 (blue curve). The similarity of the solutions is remarkable.

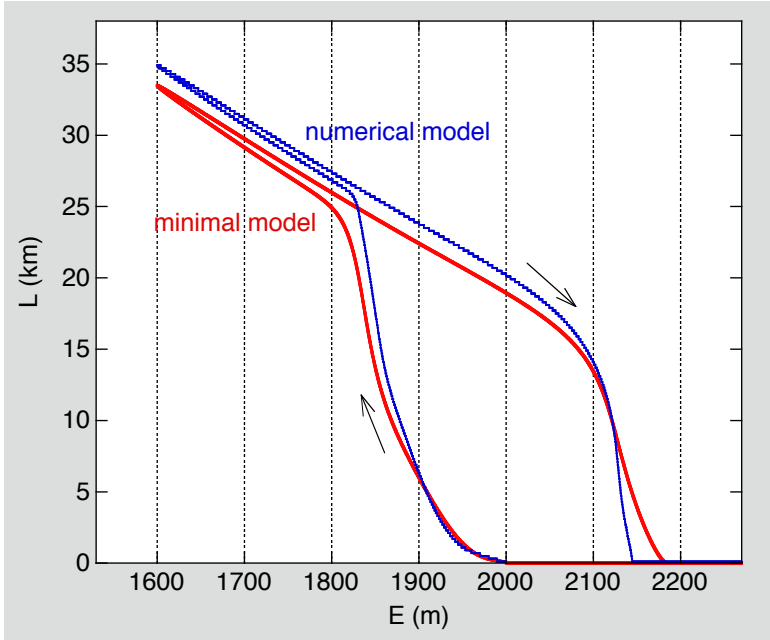


Figure 5.8. A comparison of models for the case with the overdeepened bed. The climate forcing is identical to that in Figure 5.6.

In conclusion, it appears that the minimal model is able to simulate the effect of an overdeepening on the state of a glacier. The effective mechanism is the dependence of the mean ice thickness on the mean bed slope, having a direct impact on the mass budget. In the example shown above a small slope of the bed was used, because this brings out the nonlinear respons more sharply. With steeper beds and smaller amplitudes of the overdeepening the effects will be smaller, of course.



Jökulsárlón, Iceland

6. Calving glaciers

6.1 Introduction

In Chapter 2, sections 2.4 and 2.5, equilibrium states of calving glaciers were considered for a glacier bed with a constant slope. In such a situation the process of calving always tends to stabilise the glacier, because a decreasing length implies a smaller calving rate and an increasing length implies a larger calving rate (at least when the calving rate increases monotonically with water depth). In this chapter we will do a more elaborate analysis, in which a reversed slope of the sea floor is included and the transient response to climatic forcing is considered. However, the width of the model glacier is kept constant. The analysis follows to a large extent the paper by Oerlemans and Nick (2005).

With respect to the climatic forcing we will consider two cases. In the first case the balance rate is assumed to be constant in space (corresponding to model (i) in section 1.3), and is denoted by \dot{a} . Note that in this case the surface mass budget does not depend on the shape of the glacier, but only on its size L . In the second case the balance rate is allowed to vary with altitude, in a way similar to model (ii) in section (1.3).

The case with a constant balance rate is perhaps not very realistic, because such a situation is more typical for very cold climates in which glaciers flowing into the sea would produce floating ice tongues (the Drygalski ice tongue, flowing into the Ross Sea, Antarctica, provides a fine example). However, when we consider glaciers with a very small surface slope, i.e. spanning a limited altitudinal range, the approximation may be reasonable. Anyway, the case with constant balance rate first of all serves to delineate the effect of a reversed bed slope on the global dynamics of a calving glacier without complicated mass-balance feedbacks.

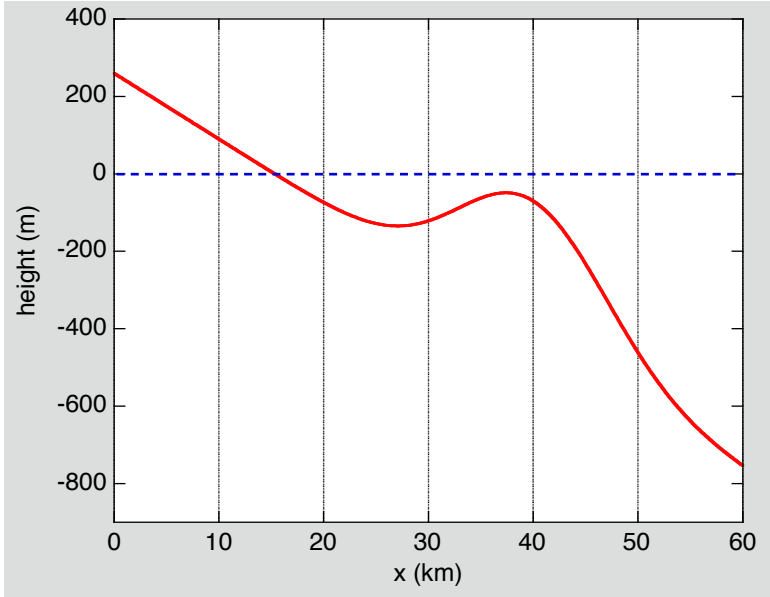


Figure 6.1. Bed profile used to study the effect of a reversed slope on the dynamics of a calving glacier.

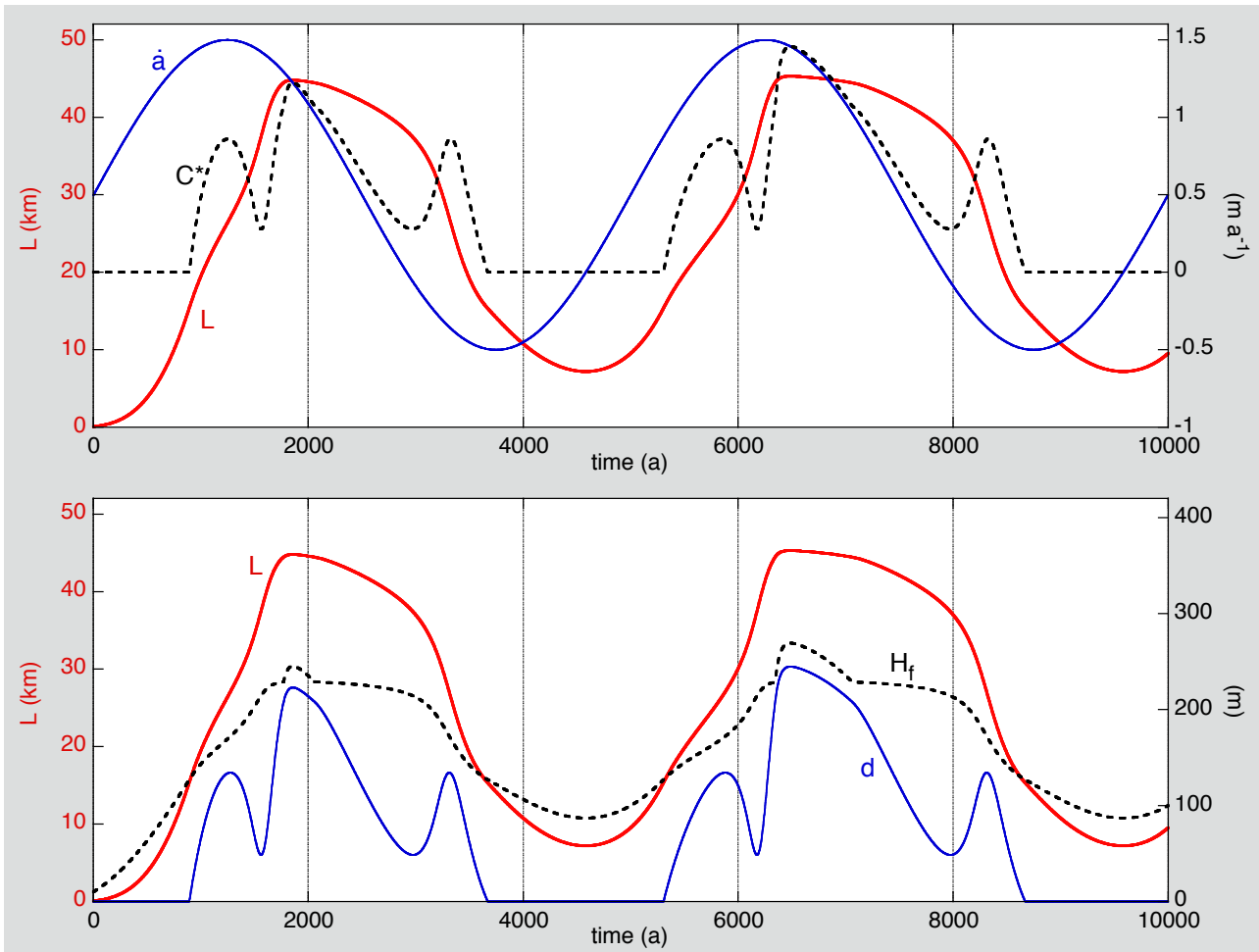


Figure 6.2. Response of the model glacier to periodic forcing. Upper panel: glacier length (red), balance rate (blue) and calving flux (dashed). The calving flux is a ‘specific flux’, i.e. the loss of mass has been divided by the glacier length. Lower panel: glacier length (red), water depth at the glacier front (blue) and height of the glacier front (dashed).

Following Oerlemans and Nick (2005), we now parameterise the ice thickness at the glacier front as

$$H_f = \max\{\kappa H_m; \varepsilon \delta d\} . \quad (6.1.1)$$

Here d is the water depth at the glacier front and δ is the ratio of water density to ice density. So δd is the ice thickness at which the ice just starts to float. A parameter ε is included to specify to what extent the frontal thickness is above buoyancy. The use of eq. (6.1.1) allows a smooth transition from a glacier with the terminus on land to a calving glacier.

6.2 Constant balance rate

The shape of the bed to be used is shown in Figure 6.1. As before, it is a linearly sloping bed combined with a Gaussian bump, see eq. (5.4.1). The parameters have been chosen such that the highest point of the bump is about 50 m below sea level [$b_0 = 260$ m, $b_1 = 350$ m, $x_0 = 40000$ m, $x_1 = 10000$ m, $s = 0.017$]. Note that the slope s has been given a fairly small value, in order to highlight the effect of the reversed slope.

We first consider the following periodic forcing:

$$\dot{a} = 0.5 + \sin\left(\frac{2\pi t}{5000}\right) \text{ m ice a}^{-1} . \quad (6.2.1)$$

Here time t is in a. Although \dot{a} also takes negative values, we prefer to use this symbol instead of \dot{b} to remind us that the balance rate is constant across the glacier.

The result of a 10 ka integration is shown in Figure 6.2. Starting with no ice, the glacier steadily grows and reaches the coastline after about 850 years. Then the calving slows down the growth, until the slope of the bed reverses and leads to an acceleration again. After about 1800 years a fairly stable state is reached with the glacier front in relatively deep water. At this time the balance rate is decreasing fast, but because the calving rate now depends strongly on the glacier length (large slope of the bed, i.e. a large value of $|\partial F / \partial L|$, only a small reduction of the length is needed to make the mass budget neutral again. Nevertheless, after about 3100 years a critical point is passed (the glacier snout is on the bedrock sill) and rapid retreat sets in. The calving flux divided by glacier length is shown in Figure 6.2, and can be compared directly to \dot{a} . Note that the second cycle differs from the first one because the ‘initial state’ is different.

The second panel in Figure 6.2 shows the water depth at the front and the ice thickness at the glacier front. Apparently, the thickness is always larger than the flotation thickness, except for the largest extent of the glacier. However, this is a direct consequence of the rather arbitrary choice of κ . For $\kappa = 0.3$, for instance, the frontal thickness is equal to the flotation thickness more frequently, but this hardly affects $L(t)$, because the calving flux changes in a modest way only.

Next equilibrium states can be calculated for the same geometry. Since the balance rate is constant in space, equilibrium solutions with the terminus on land are not possible. Once the terminus is in the sea and calving can balance the accumulation, an equilibrium state is possible (Figure 6.3). Evidently, for a smaller calving parameter c , as defined in eq. (2.4.1), the water depth has to be larger and therefore the glacier longer to produce the same calving flux. For $\sim 27 \text{ km} < L < \sim 37 \text{ km}$ stable equilibria are not possible, because $\partial F / \partial L < 0$. The locations of the bifurcation points shown

in Figure 6.3 approximately coincide with the depression and sill in the bed. Once the terminus gets into deeper water the sensitivity of glacier length to the balance rate becomes small. Since here the slope of the bed is large, only a small adjustment in glacier length is needed to change the calving flux substantially.

The nonlinear behaviour seen here is that of the canonical cusp catastrophe (e.g. Gilmore, 1981). The bifurcation or critical points in Figure 6.3 are connected by an unstable equilibrium solution (dotted). The range of \dot{a} for which three equilibria exists depends on the value of c and the amplitude of the overdeepening. The nonlinearity is stronger when the calving parameter is larger or the overdeepening more pronounced. The essential control parameter therefore is $c b_1$.

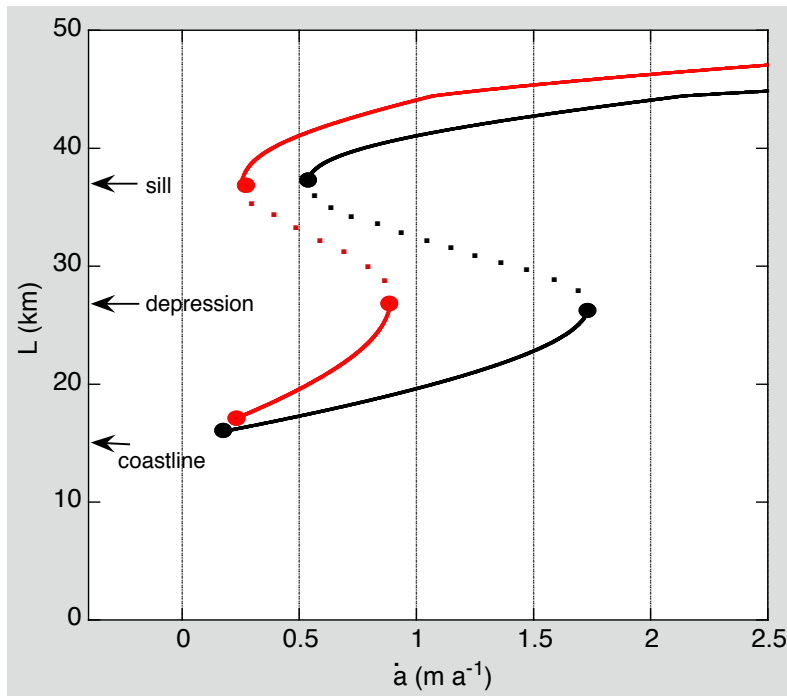


Figure 6.3. Equilibrium states of a calving glacier with a constant balance rate, for two values of the calving parameter c . Features of the bed (see Figure 6.1) are indicated by arrows. In red: $c = 1\ a^{-1}$; in black: $c = 2\ a^{-1}$. The dots represent the unstable equilibrium branch.

6.3 Balance rate depending on altitude

Having analysed the simplest case to isolate the nonlinear effects of an undulating bed, we now turn to the more realistic case with a balance rate depending on altitude. The feedback between glacier length, mean surface elevation and net balance rate thus becomes effective. In Figure 6.4, results are shown for periodic forcing of the equilibrium line, a balance gradient of $0.005\ m\ ice\ m^{-1}$ and a calving parameter of $2\ m\ a^{-1}$. All other parameters are the same as before (bed profile, etc.). In a qualitative sense the solution is very similar to the solution for a constant balance rate (Figure 6.2). Only one cycle is shown because now the glacier totally disappears.

One thing to note is that the retreat of the glacier front after 3300 years is relatively fast now. The retreat is about 14 km in 200 years. Although this is still slow compared to the catastrophic break-up of for instance Columbia Glacier, it is an appreciable change. The cause for this is that an increased calving flux comes with a negative net surface balance, as illustrated in the lower panel of Figure 6.4. Similarly, an advance can be very rapid when the equilibrium line is low and the glacier front is on the reversed part of the bed.

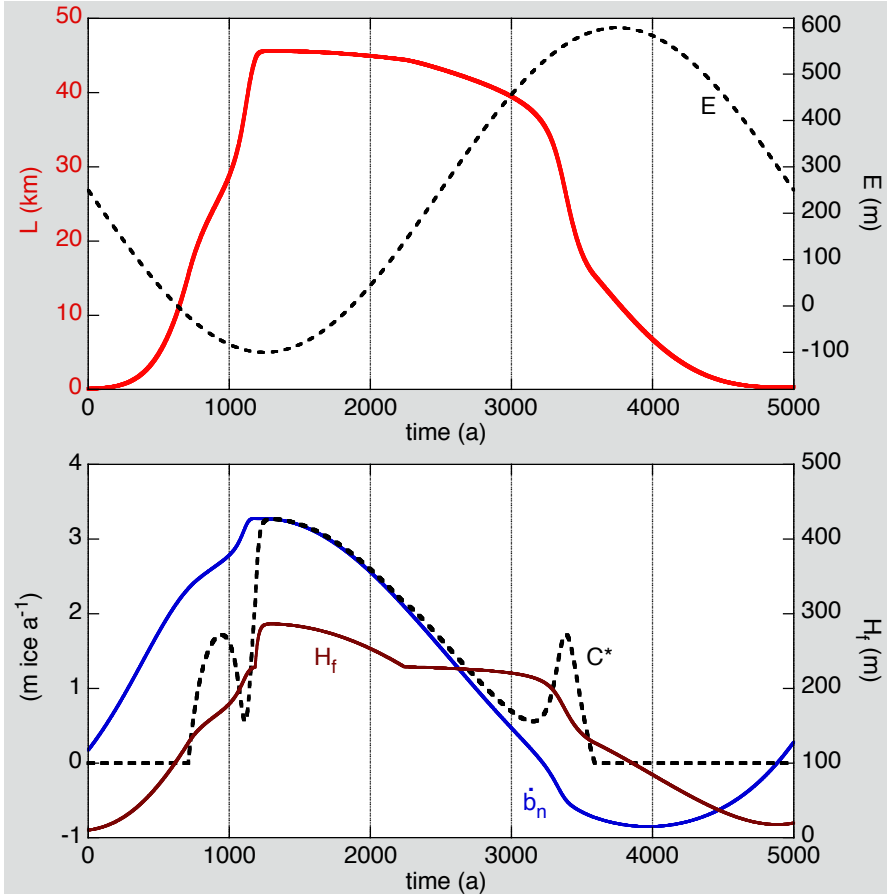


Figure 6.4. Response of the model glacier with a height-dependent balance rate to periodic forcing.

Upper panel: glacier length (red) and equilibrium-line altitude (dashed)

Lower panel: mass budget components (blue: net balance rate, dashed: specific calving flux) and ice thickness at the glacier front (brown).

By looking at the mass budget components we can also understand why the glacier is so stable once it is in an advanced position beyond the sill in the bed. After 1200 years the equilibrium line rises strongly, but the glacier length hardly reacts. Because the slope of the bed is large, only a minor adjustment of the position of the front is needed to reduce the calving flux and match the reduced net surface balance (blue curve in Figure 6.4). Although the glacier length thus varies little between 1100 a and 3000 a, the throughput of mass certainly does!

Equilibrium states can be found by varying E and starting from different initial conditions. Because the system is highly nonlinear now, this has to be done with some care. There are two processes that may lead to branching of the equilibrium solutions: (i) the dependence of the calving rate on water depth, and therefore on L , and (ii) the height mass-balance feedback discussed extensively before. For the parameter values used the solution diagram was calculated and is shown in Figure 6.5.

There appear to be three branches of stable equilibria. First of all, $L=0$ represents a stable equilibrium state for $E \geq 260$ m, because in this case the equilibrium line is above the highest point of the bed (260 m). Then we have a stable branch between critical points 2 and 3, representing a glacier with a moderate calving rate. It should be noted that for the chosen geometry a stable state with glacier terminating on land is not possible. However, this would change if the bed slope were to be increased: in that case critical point 2 moves towards critical point 1 (Chapter 2; see also Oerlemans and Nick, 2005). As before, a stable equilibrium solution with the front on the reversed bed slope is not possible. Critical points 3 and 4 are very close to the location of the bed depression and sill, but not exactly.

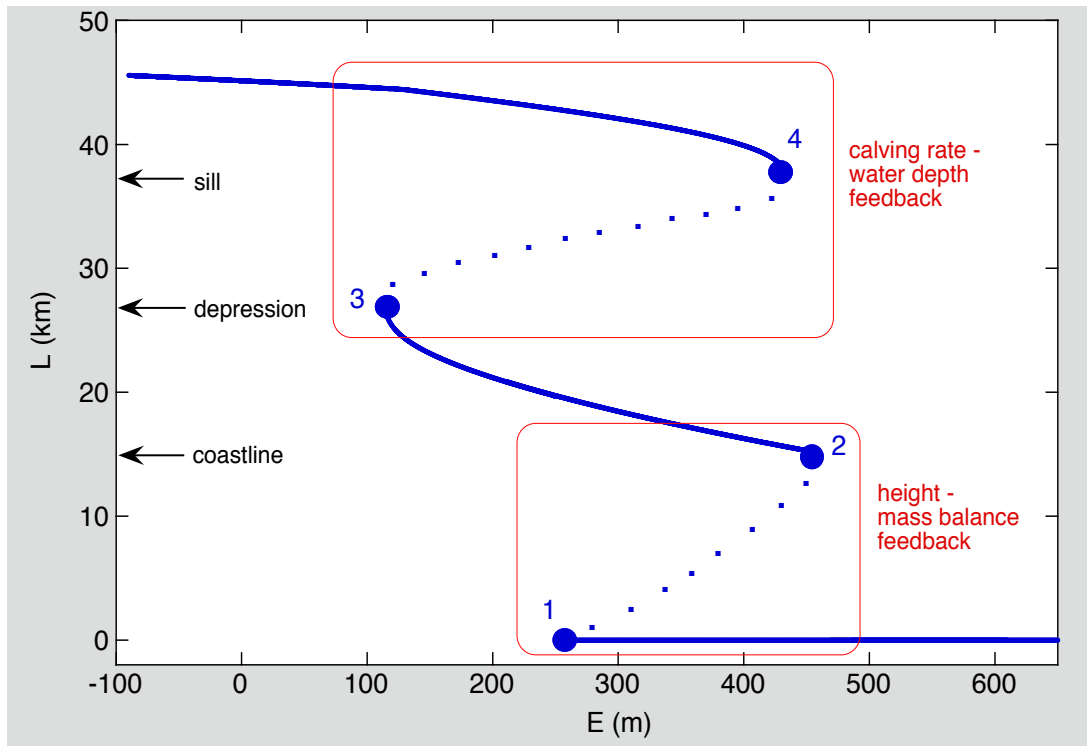


Figure 6.5. Solution diagram for the case with a height-dependent balance rate. Solid lines represent stable equilibrium states. The unstable branches are indicated by dots. Critical points are numbered to facilitate the discussion (see text).

Altogether, the nonlinearities induced by the coupling of calving rate and water depth on one hand, and by the dependence of the balance rate on mean ice thickness on the other hand, lead to a fairly complex solution diagram. For an equilibrium line altitude between 260 and 430 m, there are three possible stable equilibrium states: $L = 0, \sim 17, \sim 34$ km. No need to say that the response to climate change can be complex. Another implication of the nonlinear processes is the widely varying response time. The response time increases strongly when critical points are approached (in theory it goes to infinity).

Finally it should be noted that the characteristics of the solution are very similar to those obtained with a flowline model based on the shallow-ice approximation (Nick and Oerlemans, 2006). Unfortunately, for the higher-order flow model of Vieli et al. (2001) solution diagrams have never been published and therefore a comparison cannot be made.

6.4 Application to Hansbreen, Svalbard

It is tempting to apply the theory developed for an over-deepened bed to a real calving glacier. An obvious candidate is Hansbreen, southern Svalbard, because it has a fairly regular geometry and the bed has an over-deepening with a not too large amplitude. Hansbreen has been the object of many glaciological studies, notably by Polish scientists (e.g. Jania et al., 1996). A few modelling studies have also been attempted, focussing on understanding the recent retreat (Vieli et al., 2001; Smorenburg, 2007).

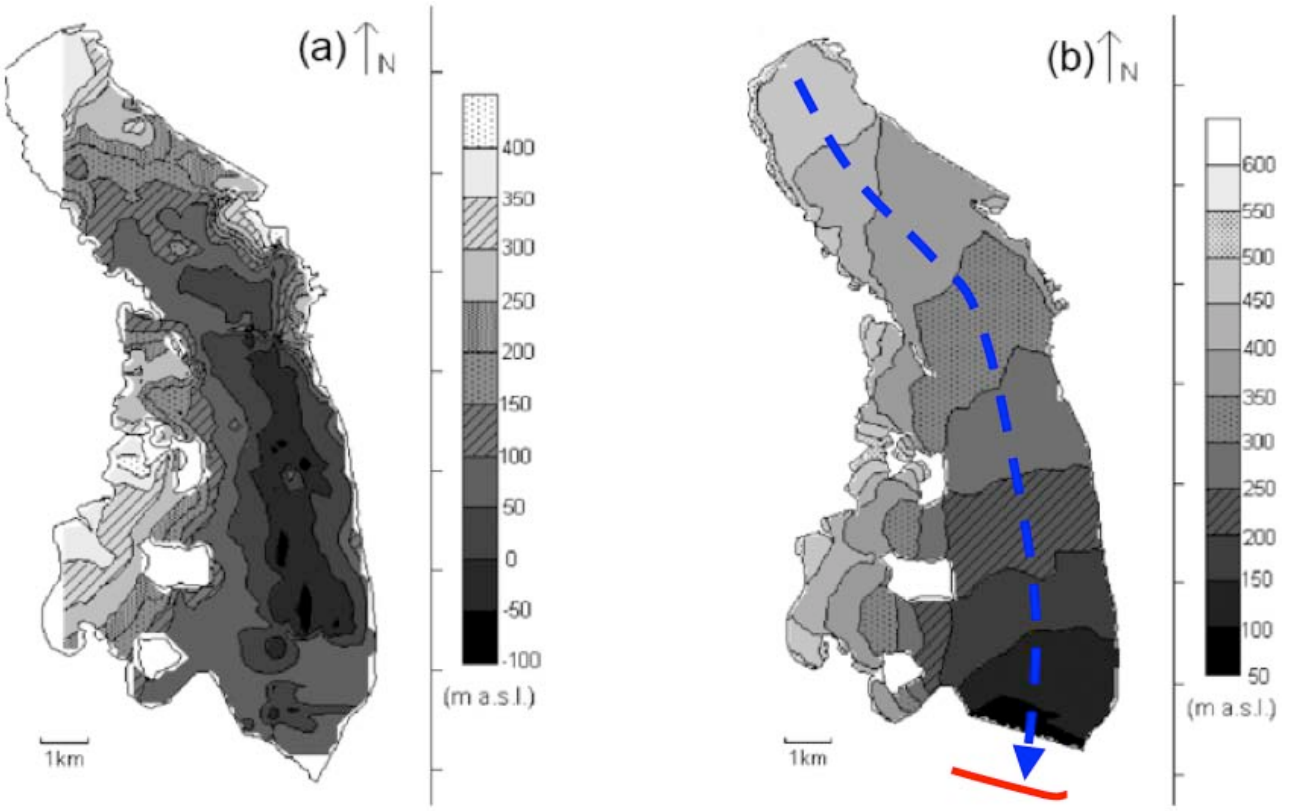


Figure 6.6. Geometry of the bed (a) and surface elevation (b) of Hansbreen, taken from Pälli et al. (2003). The blue dashed line shows a schematic flowline, and the present-day approximate position of the calving front is indicated by the red bar.

The schematic geometry adopted here is based on maps of the bed and surface geometry as published by Pälli et al. (2003), see Figures 6.6 and 6.7. The over-deepening is not very large: at a few spots the bed is about 100 m below sea level. The calving front is currently in fairly shallow water and slowly retreating. The front positions along the flowline for the years 1900 and 2000 are indicated in Figure 6.7.

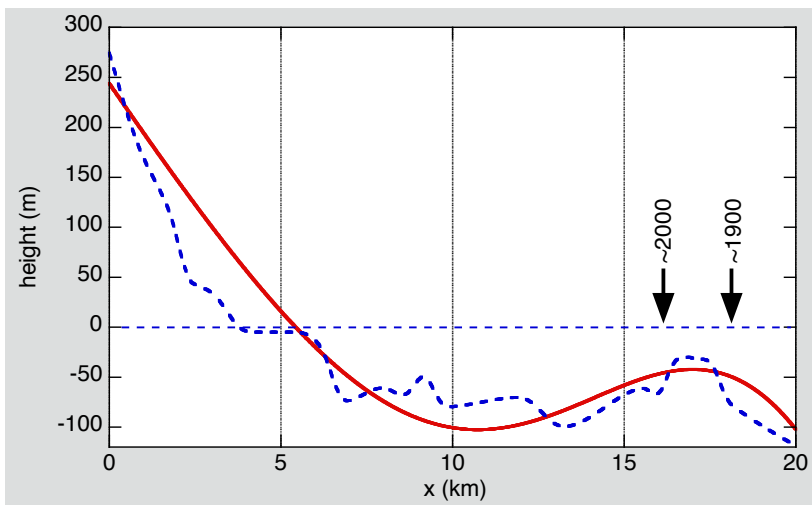


Figure 6.7. The schematic bed profile of Hansbreen used in the model calculation (red curve, dashed). The blue curve shows the bed profile as derived by Smorenburg (2007) on the basis of the 2-d bed geometry (Figure 6.6).

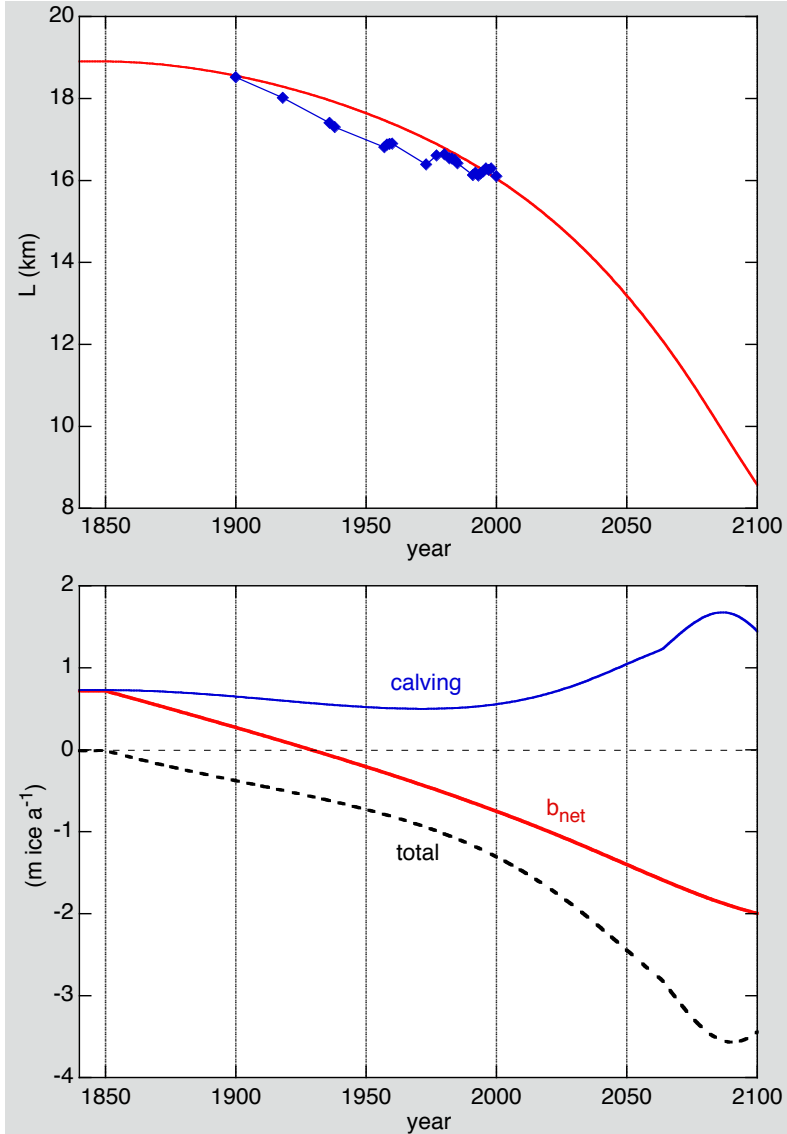


Figure 6.8. Results of a model calculation for Hansbreen. The upper panel shows simulated and observed glacier length. The components of the mass budget are plotted in the lower panel.

Like many other calving glaciers in Svalbard, Hansbreen has been retreating steadily. The record of observed front positions (J. Jania, personal communication) is shown in Figure 6.8. During the past 100 years the glacier front has moved from a position seaward of the current moraine shoal to a position behind the moraine shoal. The glacier front is currently positioned on a part of the bed with a ‘negative slope’. In view of the theory developed earlier the glacier is unlikely to be close to a steady state. In contrast, it can be expected that the glacier front will retreat for a wide range of climate change scenario’s, unless the net surface balance would become much more positive.

The bed profile is described by eq. (5.4.1) with the following parameters: $b_0 = 240 \text{ m}$, $s = 0.052$, $b_1 = 700 \text{ m}$, $x_0 = 20500 \text{ m}$, $x_l = 9000 \text{ m}$. Values of the other model parameters are $\alpha_m = 3 \text{ m}^{1/2}$, $v = 10$, $\kappa = 0.4$, $c = 1.5 \text{ a}^{-1}$, $\beta = 0.006 \text{ m ice a}^{-1} \text{ m}^{-1}$. The model is forced by prescribing the equilibrium-line altitude according to (t is time):

$$\begin{aligned} t < 1850 \text{ a: } E &= 220 \text{ m ,} \\ t \geq 1850 \text{ a: } E &= 220 + 1.45(t - 1850) \text{ m .} \end{aligned} \tag{6.4.1}$$

This implies that from 1850 onwards the equilibrium line rose by 1.45 m per year. The numbers in eq. (6.4.1) have been chosen in such a way that the calculated glacier length matches the observed length in the years 1900 and 2000. It is clear that a further rise of the equilibrium line as prescribed by eq. (6.4.1) will lead to an accelerating retreat of Hansbreen. As illustrated in the lower panel of Figure 6.8, the net surface balance becomes more and more negative, and the calving flux increases because the glacier front retreats into deeper water. The model predicts a retreat of about 8 km until the year 2100. However, this depends very much on the imposed climate change scenario, of course.

It should be noted that different tuning options exist. For the example shown above the calving parameter c was set to 1.5 a^{-1} . If the value of this parameter is reduced, a similar tuning to the 1900- and 2000- glacier lengths can be achieved by raising the equilibrium line.

6.5 A note on more complicated bed profiles

The bed profiles used so far have been quite simple. More complicated profiles can still be used in the framework of the minimal model, but the function describing the bed should be integrable to evaluate the mean bed elevation for any given value of L . (Special) polynomials are clearly suitable for this.

Special problems arise when the bed is not fixed but changes its shape in time due to erosion or lodging of sediments (or, when larger spatial scales are considered, due to lithospheric flexure). It is not so easy to describe the evolution and movement of a moraine shoal by a simple polynomial function. Oerlemans and Nick (2006) studied the advance-retreat cycle of a tidewater glacier with a minimal model including sediment dynamics. However, in this approach some concessions had to be done: the evolving bed profile was calculated on a grid, and mass conservation is only approximated - not exact as in the models discussed in this book.



Medial moraine disappearing in the Vadret Pers, Switzerland

7. Linear modelling

7.1 Introduction

The models discussed so far were simple, but not linear. We looked at the response of glaciers to large-amplitude forcing. However, for smaller changes in climate it might well be that a linear (or linearised) approach is useful.

Broadly speaking glacier systems are highly damped systems. Only surging glaciers do show quasi-periodic behaviour which may be classified as self-sustaining relaxation oscillations (although mass needs to be added to the glacier all the time to keep the oscillation going). If we want to describe the response of a non-surging glacier to relatively *small* changes in climate, a first-order linear differential equation is a natural choice.

When we observe a glacier as a scholar two questions evolve naturally: (i) How sensitive is this glacier to climate change?, and (ii) How fast does it adjust its shape to such a change? It is of some importance to realize that sensitivity and response time are fundamentally different quantities. In the literature on glacier fluctuations there is a certain ‘nonchalance’ with regard to the description of the reaction of a glacier to climate change. For example, a glacier increasing its length very quickly after a drop of the equilibrium-line over one or two decades can do so because its response time is short, but also because its has a large climate sensitivity. The ‘reaction time’, as it is used sometimes to indicate how long it takes before a glacier starts to advance after a marked climatic deterioration, is even more troublesome. It does not reflect a physical property of the glacier system, but depends on the history (e.g. if the glacier was in a mode of retreat when the climate started to deteriorate, the reaction time will be longer). Related to this is the misleading idea that there can be something like a constant phase shift between climate forcing and glacier response.

A first-order linear model is the best tool to sort out these things. It is the simplest model that can deal with lag effects and differences in climate sensitivity. A linear model also has the advantage that it can easily be inverted, i.e. the (unknown) forcing can easily be derived from the (observed) response. The price to pay is that only relatively small changes can be considered.

Writing

$$L(t) = L_0 + L'(t) , \quad (7.1.1)$$

where L_0 is a reference glacier length, a linear theory is applicable when

$$\sigma_{L'} \ll L_0 . \quad (7.1.2)$$

Here $\sigma_{L'}$ is the standard deviation of the glacier length fluctuations. Typically, one would like to have $\sigma_{L'}$ an order of magnitude smaller than L_0 . Figure 7.1 shows four glacier length records for which the quantity $\sigma_{L'}/L_0$ has been calculated. The values are 0.081 for Nigardsbreen, 0.035 for Glacier de Bosson, 0.050 for Brikdalsbreen and 0.19 for South Cascade Glacier. Obviously, care has to be taken when a linear theory is used to study the fluctuations of South Cascade Glacier over this period. For the other glaciers the condition (7.1.2) is well met.

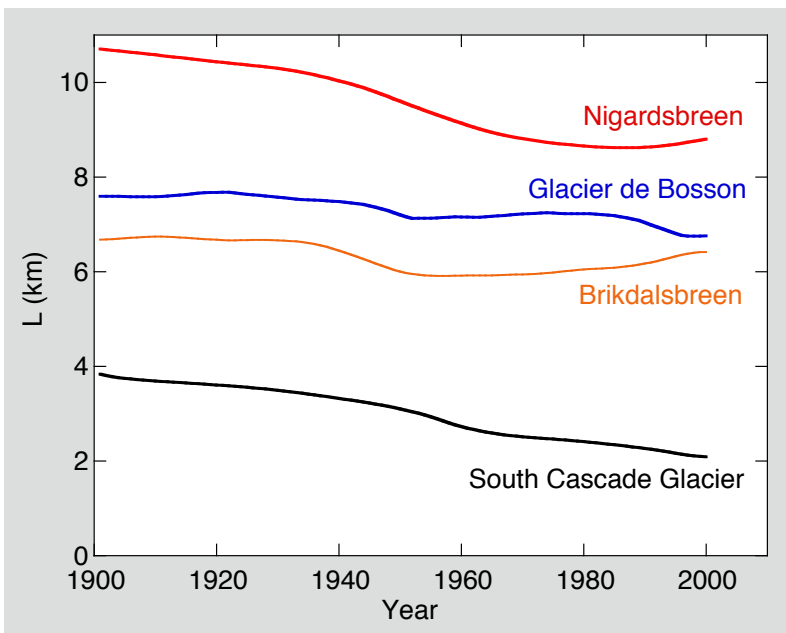


Figure 7.1. The length records of four glaciers during the 20th century. The records have been smoothed and data gaps have been filled with Stineman interpolation.

7.2 A first-order linear model for glacier length

A first-order linear response equation is a basic equation from calculus, and its properties and solutions have been studied extensively and can be found in almost any textbook on differential equations. Here the equation is written as

$$\frac{dL'}{dt} = \frac{1}{\tau} (k E' - L') . \quad (7.2.1)$$

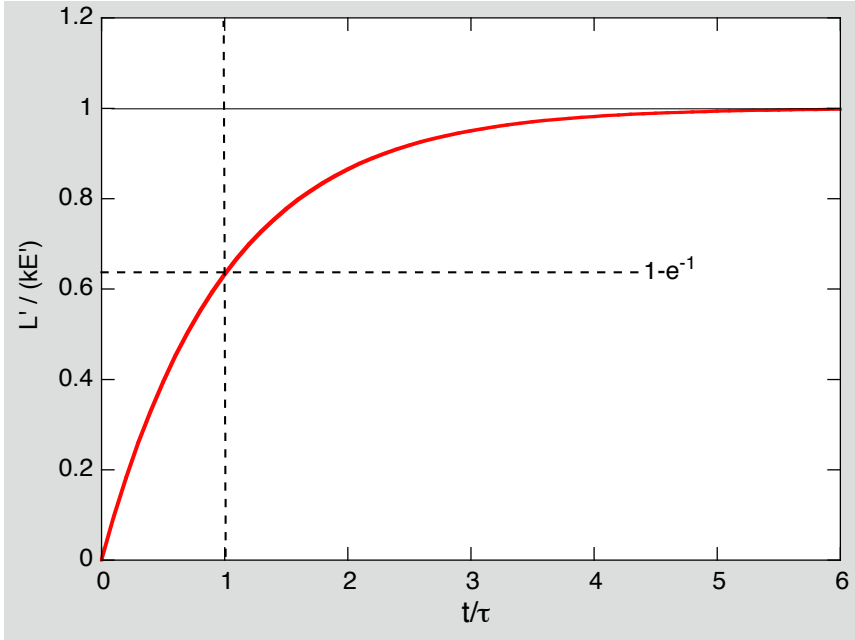


Figure 7.2. The solution of the linear response equation for a step change in the equilibrium line altitude (plotted here in nondimensional form).

L' and E' are glacier length and equilibrium-line altitude relative to reference values, k is the climate sensitivity (< 0), and τ is the response time. Note that in the case of equilibrium $L' = kE'$, implying that the equilibrium-line altitude is relative to the value E_0 that corresponds to L_0 . For an initial condition $L'(t = 0) = 0$ and E' is constant the solution reads

$$L'(t) = (1 - e^{-t/\tau}) kE' . \quad (7.2.2)$$

This implies that at $t = \tau$ about 2/3 of the response has been accomplished (Figure 7.2). Therefore it takes typically 2τ before the new equilibrium is really approached.

Next we consider the heterogeneous equation with periodic forcing

$$\frac{dL'}{dt} = -\frac{L'}{\tau} + \frac{k}{\tau} E_A \sin \omega t , \quad (7.2.3)$$

where E_A is the amplitude of the forcing and ω is the frequency. There are several methods to solve this equation. We do not consider transient effects related to a particular initial state and simply substitute $L'(t) = A \sin \omega t + B \cos \omega t$ in eq. (7.2.3). This yields

$$A\omega \cos \omega t - B\omega \sin \omega t = -\frac{A}{\tau} \sin \omega t - \frac{B}{\tau} \cos \omega t + \frac{k E_A}{\tau} \sin \omega t . \quad (7.2.4)$$

A and B are now found by equating the coefficients of the cosine and the sine terms. It follows that

$$A = \frac{k E_A}{1 + \omega^2 \tau^2} , \quad B = \frac{-\omega \tau k E_A}{1 + \omega^2 \tau^2} . \quad (7.2.5)$$

Alternatively, the solution can be formulated as

$$L'(t) = D \sin(\omega t - \phi) , \quad (7.2.6)$$

where the amplitude and phase are given by

$$D = k E_A \sqrt{\frac{1}{1 + \omega^2 \tau^2}} , \quad \phi = \arctan(\omega \tau) . \quad (7.2.7)$$

In terms of the period of the forcing $P (= 2\pi/\omega)$, the solution can also be written as

$$D = k E_A \sqrt{\frac{1}{1 + 4\pi^2(\tau/P)^2}} , \quad \phi = \arctan\left(\frac{2\pi\tau}{P}\right) . \quad (7.2.8)$$

The relevant quantity to consider is the period of the forcing relative to the response time, i.e. P/τ . Eq. (7.2.8) shows that the amplitude of the solution decreases with a decreasing value of P/τ : the glacier length hardly reacts when the period of the forcing is very small compared to the response time τ . On the other hand, for very slow forcing ($P/\tau \rightarrow \infty$) the glacier is always close to equilibrium ($D = k E_A$). Of particular interest is the phase difference between the forcing and the response, given by $\omega^{-1} \arctan(\omega \tau)$.

The amplitude and phase of the solution are plotted in Figure 7.3. Note that the maximum phase difference between forcing and response is 90° . The amplitude shown actually is the normalized glacier length $L'/(kE_A)$. It is also instructive to look at an example in which $L'(t)$ is plotted. In Figure 7.4 the response of glacier length to forcing with a period of 100 a is shown (this actually implies a characteristic time scale of 50 years for variations in the equilibrium line altitude). The response is plotted for glacier response times of 20, 50 and 100 a. For a response time of 20 a the lag with respect to the forcing is about 14 years. For response times of 50 a and 100 a it is about 20 and 22 years, respectively. It is also clear that the amplitude of the response decreases strongly when the response time approaches the period of the forcing.

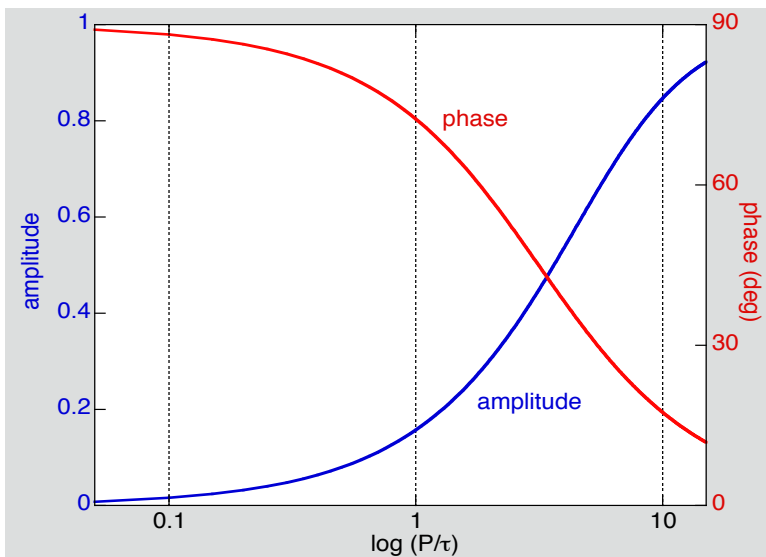


Figure 7.3. Amplitude and phase of glacier length for periodic forcing of the equilibrium line with period P .

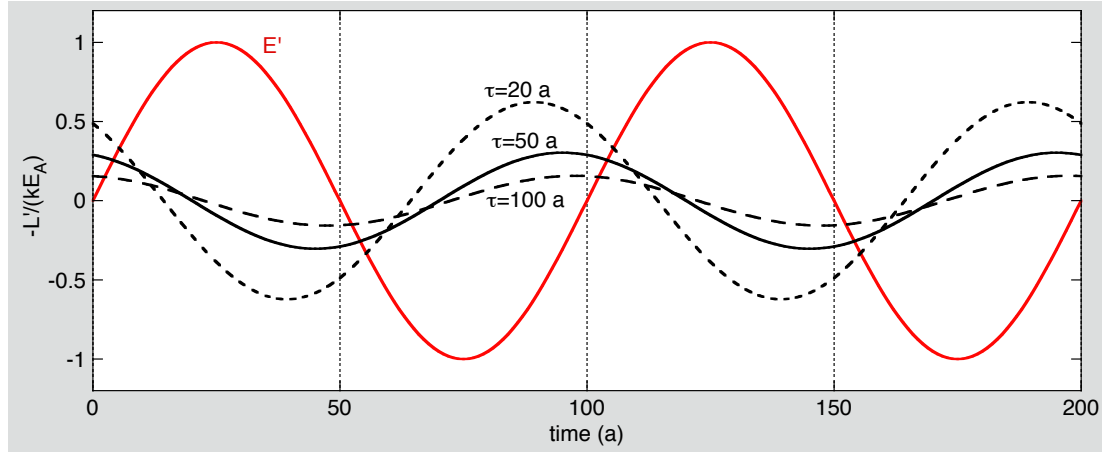


Figure 7.4. Time-dependent response of normalised glacier length for a forcing (red curve) with a period of 100 a. Glacier length is shown for three values of the response time τ .

7.3 Backward modelling

In this section we investigate how the forcing function can be derived from a length record. From different parts of the world there is a wealth of information on glacier fluctuations. The length of a valley glacier is a relatively simple parameter to measure or to infer from sketches, paintings and early maps. In many cases moraines and trimlines provide very useful additional information. It is tempting to use the theory developed above to extract climatic information from glacier length records.

Let us assume once more that the relation between glacier length and equilibrium-line altitude can be described by a linear response equation. However, a complication now has to be dealt with because in practice we are normally not sure if the reference equilibrium-line altitude E_0 corresponds with the reference glacier length L_0 . Eq. (7.2.1) is therefore rewritten as:

$$\frac{dL'(t)}{dt} = \frac{1}{\tau} \{ kE'(t) - [L'(t) - L_{imb}] \}. \quad (7.3.1)$$

L_{imb} denotes the (unknown) equilibrium length for $E'=0$ (the index ‘imb’ refers to imbalance). This equation can be solved for $E'(t)$:

$$E'(t) = \frac{1}{k} \left[\{L'(t) - L_{imb}\} + \tau \frac{dL'(t)}{dt} \right]. \quad (7.3.2)$$

There are two contributions to a reconstructed signal of the equilibrium-line altitude: one coming from the actual glacier length, and one from the time rate of change of glacier length. Note that the value of L_{imb} determines the absolute value of the equilibrium-line altitude, but not its variation in time. Because of the time derivative in eq. (7.3.2), $E'(t)$ is very sensitive to irregularities in the length record. Such irregularities can be the result of the typical small-scale variations in the bed topography normally encountered near glacier tongues. Also, sometimes real jumps in a glacier record occur because the glacier snout moves across a ramp in the bed. Anyway, annual noise in

length record has little to do with climate and should be filtered out. Generally speaking, before eq. (7.3.2) can be applied, a glacier length record has to be prepared. This implies interpolation (to fill gaps) and smoothing. A smart algorithm combines these steps, of course. A particular suitable procedure is that developed by Stineman (1980, implemented in the Kaleidagraph application). An example is shown in Figure 7.5. The length record of Bondhusbreen, southern Norway, has been selected for this purpose because it has some features typical for many glacier length records. The record is a combination of data supplied in Bogen et al. (1989), the WGMS (World Glacier Monitoring Service, Zürich) and various annual reports of the NVE (Norges vassdrags og energidirektorat, Oslo). In the first part of the record there are only a few data points, and further on there are also some gaps (notably for the period 1987-1996).

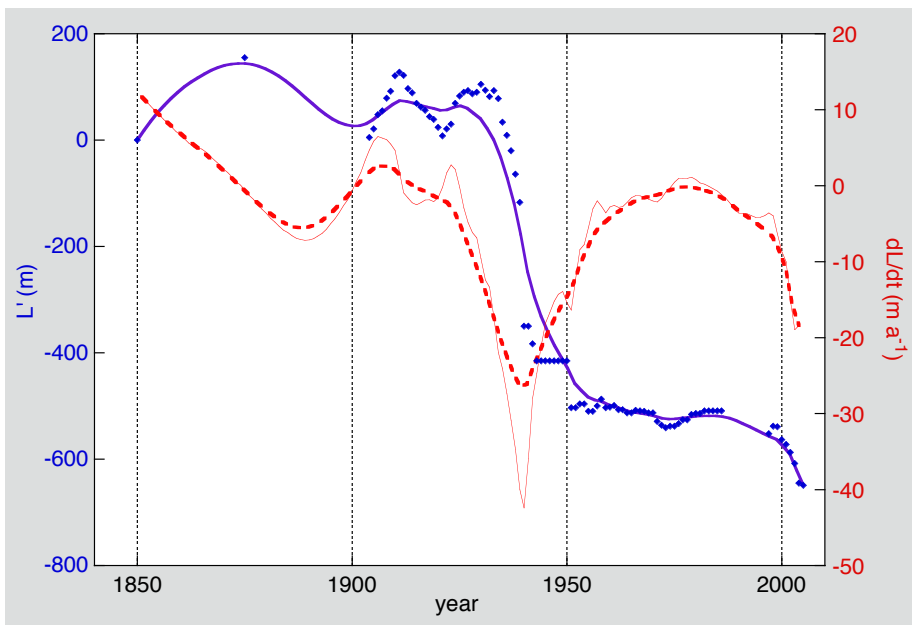


Figure 7.5. The length record of Bondhusbreen, southern Norway: data points and curve fit in blue. The red curves show the time derivative of L' (smoothed: dashed curve).

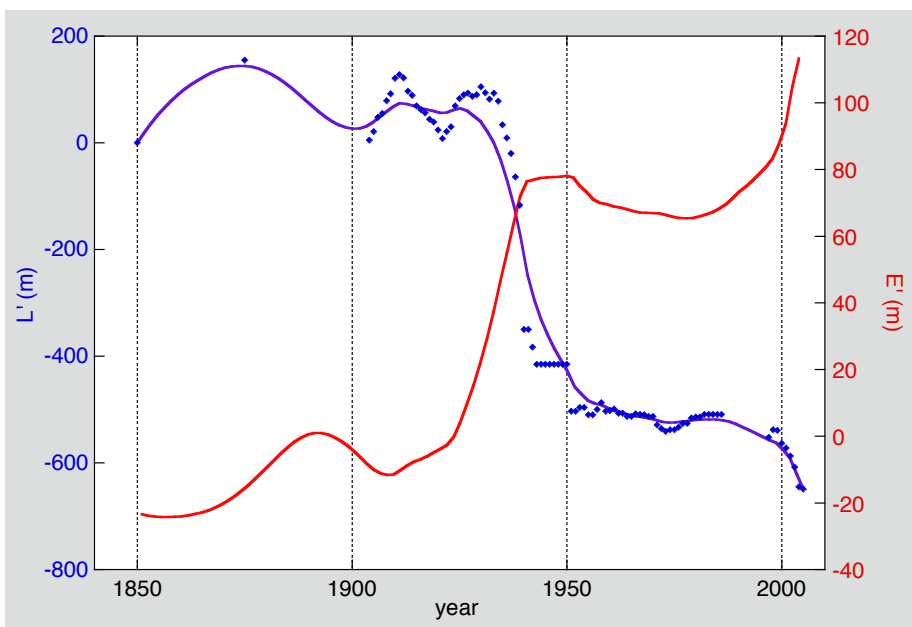


Figure 7.6. The length record of Bondhusbreen, now with the calculated equilibrium-line altitude (red curve).

In Figure 7.5 the Stineman fit is shown and the resulting data points have been used to estimate dL'/dt :

$$\frac{dL'}{dt} = \frac{L'_{yr+1} - L'_{yr-1}}{2} . \quad (7.3.3)$$

The resulting curve is still rather noisy and additional smoothing may be useful (red dashed line in Figure 7.5). Applying eq. (7.3.2), with $L_{imb} = 0$, then yields the reconstructed equilibrium-line altitude (Figure 7.6). In the calculation τ was set to 15 a, which is not more than an educated guess based on the fact that Bondhusbreen is rather steep and has a large mass turnover. The climate sensitivity k was set to -8.

The technique discussed above was used by the author to extract a temperature record from 169 glacier length records (Oerlemans, 2005a). In this study it was assumed that the effect of temperature changes is more important than changes in precipitation and other meteorological quantities when *large temporal and spatial scales* are considered. Apart from the smoothing procedure, assigning a response time and climate sensitivity to all individual glaciers constitutes a major challenge. A simple approach was taken, in which τ and k were parameterised in terms of glacier length, mean slope and characteristic annual precipitation. It is clear that there is room for improvement here, for instance by taking into account the basic hypsometry of a glacier (e.g. along the lines discussed in section 2.2). We may also wonder if a linear model should not be replaced by a (weakly) nonlinear approach for those glaciers for which the condition $\sigma_{L'} \ll L_0$ does not hold. In view of the rapid current recession of many glaciers, it has to be expected that in the near future for more and more glaciers this condition will not be fulfilled anymore.

7.4 Estimating response times from length records with linear theory

Estimating the response time of a glacier has been a subject of research for a long time. After Nye's (1965) classical paper on the application of kinematic wave theory, a now widely used approach was developed by Jóhannesson et al. (1989), see section 3.2. Harrison et al. (2001) and Oerlemans (2001; section 9.3) have modified the Jóhannesson time scale to include the effect of the height mass balance feedback (which makes the time scale larger, especially for glaciers with a small slope). Yet another method, more in line with common practice in fluid mechanics, is to estimate a response time by dividing glacier length by a characteristic ice velocity. The characteristic velocity can be taken as the balance velocity at the equilibrium line. Glaciers with a large mass-turnover will thus be faster. This is still in line with the Jóhannesson time scale, because such glaciers normally have large balance gradients and therefore high ablation rates at the snout.

Response times have also been estimated by means of numerical modelling. Models based on the shallow-ice approximation (SIA) have been used to simulate the transient response of glaciers to climate change in some detail (e.g. Budd and Jensen, 1975; Kruss, 1983; Van de Wal and Oerlemans, 1995; Oerlemans, 1997). Generally speaking, numerical models produce response times that are somewhat larger than those estimated with Jóhannesson's method. Higher-order models, in which the full stress field is considered, seem to yield somewhat smaller response times than SIA models (e.g. Leysinger-Vieli and Gudmundsson, 2004).

Validation of an estimated response time is normally difficult, because ‘clean’ data describing the response of a glacier to a precisely known change in climate forcing over a period of 100 years or more do not exist. However, in some cases it may be possible to estimate a response time from observed changes in glacier length even without knowing the forcing function *a priori*. Such a case occurs when two glaciers with a very different geometry are located in the same area and must have been subject to almost identical climatic forcing. Linear control theory can then be used to derive response times: the difference between the reconstructed climate histories for the two glacier length records can be minimised by optimising the response times (Oerlemans, 2007).

Here the procedure is illustrated by considering the length records of Briksdalsbreen and Nigardsbreen (Figure 7.7). The reconstructed equilibrium-line histories, as derived by the method discussed in the previous section, are denoted by $E'_B(t)$ and $E'_N(t)$ (the subscript B refers to Briksdalsbreen, the subscript N to Nigardsbreen). For ideal models with the appropriate response times (τ_B , τ_N) and climate sensitivities (k_B , k_N), $E'_B(t)$ and $E'_N(t)$ should be identical. However, in practice this will never be the case. A possible measure of the difference is

$$\Psi_{B,N}(\tau_B, \tau_N, k_N) = \sqrt{\frac{1}{J} \sum [E'_B(t) - E'_N(t)]^2}, \quad (7.4.1)$$

The number of data points in the record is denoted by J . For a given value of k_B , the quantities τ_B , τ_N , k_N , $E'_B(t)$ and $E'_N(t)$ can be found by minimising the cost function $\Psi_{B,N}$. Up to three control parameters can be used to minimise the cost function. It is not possible to derive values for the two response times *and* the two climate sensitivities simultaneously. In that case the system runs away in a mode with continuously decreasing sensitivities and increasing changes in the equilibrium-line altitude. So one of the four parameters has to be given as input (in this case k_B).

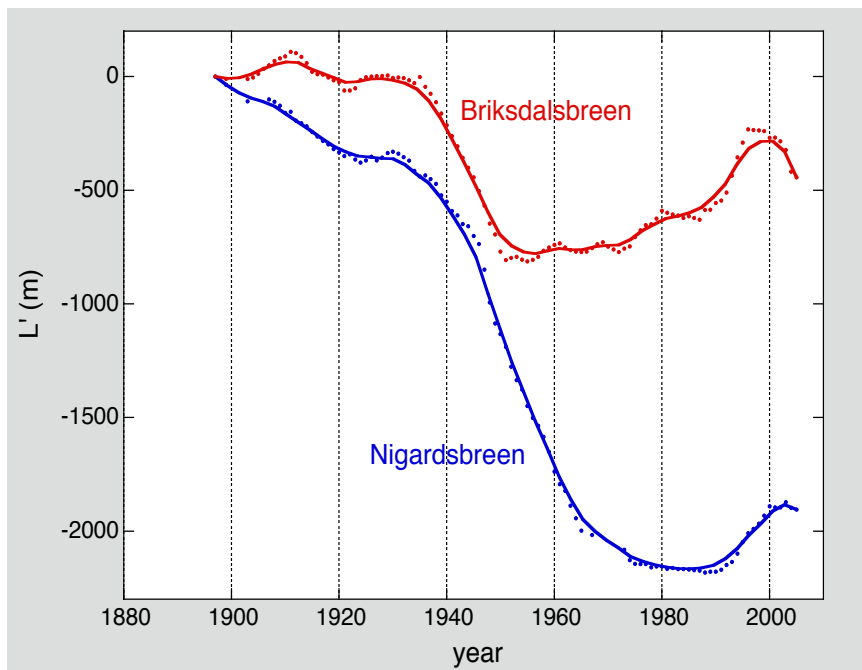


Figure 7.7. The length records of Briksdalsbreen and Nigardsbreen, Norway. data from the from Annual Reports of NVE (Norwegian Water Resources and Energy Directorate, Oslo). The curves represent Stineman fits.

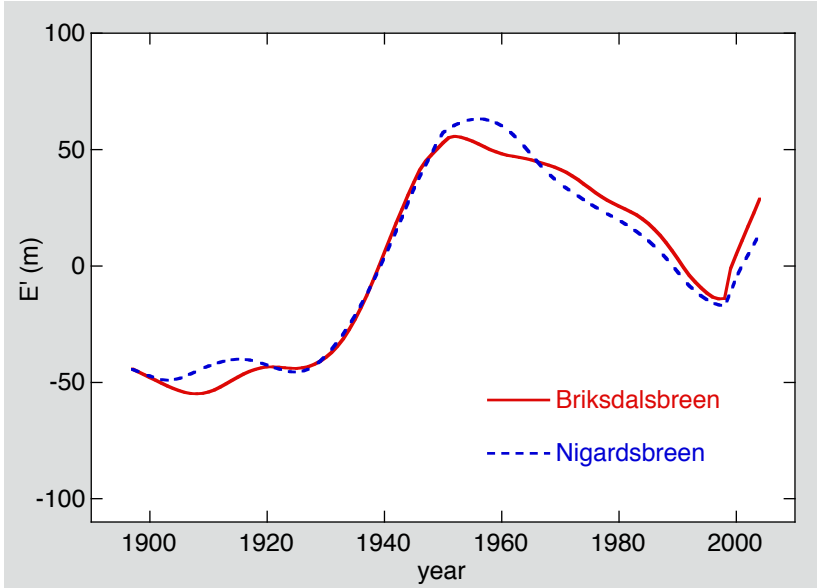


Figure 7.8. Equilibrium-line altitude reconstructed for Briksdalsbreen and Nigardsbreen.

Following the simple analysis in Chapter 2 for a glacier of constant width we have $k_B = -2/s$, where s is the mean slope along the flowline of Briksdalsbreen. If the characteristic width of the accumulation zone is larger than the width of the ablation zone, k will be larger. The analysis in Chapter 2 shows that for a glacier with an accumulation basin that is four times as wide as the ablation zone, a 50% increase of k due to converging flow has to be accounted for. Based on the geometric characteristics of Briksdalsbreen (Statens Kartverk, Norway, sheet M711-1318 II, scale 1:50000), the resulting best estimate of the climate sensitivity is: $k_B \approx -8$ (for a more detailed discussion, see Oerlemans, 2007).

A random-walk approach quickly produces a unique and meaningful solution for the climate history and associated response times. Figure 7.8 shows the equilibrium-line histories. These histories match very well for realistic response times ($\tau_B = 5.02$ a and $\tau_N = 34.82$ a), as is also demonstrated by the small minimum value of the cost function ($\Psi_{B,N} = 6.58$ m). The response time found for Briksdalsbreen is small, but one should realize that this glacier is steep and has a very large mass turnover (ablation rates on the snout are up to ~ 10 m of ice). The corresponding climate sensitivity found for Nigardsbreen is -26.1 . This is a large value, but in line with findings from numerical modelling (Oerlemans, 1997). The large sensitivity is due to the small slope of the valley in which Nigardsbreen flows, and to the relatively narrow glacier tongue as compared to the width of the accumulation basin.

For a more extensive discussion on deriving response times from glacier length records the reader is referred to Oerlemans (2007). In this paper another pair of glaciers is considered as well, namely the Vadret da Morteratsch and the Vadret da Palü in the Swiss Alps. The results are equally good, i.e. also in this case the reconstructed equilibrium-line histories match very well.

It is perhaps a bit surprising that a simple linear model with appropriate coefficients is able to map different glacier length records on the same climatic forcing. The result of Figure 7.8 suggests that at least for these records very little will be gained by more sophisticated modelling (e.g. higher-order or nonlinear). The conclusion should be that linear modelling is a powerful tool to analyse historical glacier-length records!



Vadret Pers flowing into the Vadret da Morteratsch, Switzerland

8. Further applications

8.1 Introduction

In section 3.3 we have discussed a model for a glacier of varying width on a bed with a constant slope, and in section 5.3 a model for a glacier of constant width on a concave bed. At the expense of carrying out somewhat more algebra it is possible to combine these models. Moreover, the width of the glacier can be scaled with its length. The resulting model then has a geometry that facilitates the application to real glaciers.

In this chapter we will develop the model and apply it to McCall Glacier (Alaska) and to the Vadret da Morteratsch/Pers system. In the latter case models for the Vadret Pers and the Vadret da Morteratsch will be combined, thereby demonstrating the applicability of the minimal glacier model to more complicated systems.

8.2 Model formulation

Referring to section 3.3, the width of the glacier is formulated as

$$W(x) = (L/L_0)^m \left[w_0 + w_1 x e^{-ax} \right], \quad (8.2.1)$$

where L_0 is a reference glacier length and m is the scaling exponent. Although the model can be formulated for any value of m , we will use $m = 1$ for simplicity. The bed profile is taken as

$$b(x) = b_a + b_0 e^{-x/x_l}. \quad (8.2.2)$$

Altogether there are six parameters that determine the glacier geometry, which makes it possible to represent many regularly-shaped glaciers. The parameterised geometry as described by eqs. (8.2.1) and (8.2.2) is illustrated in Figure 8.1. Although at first sight one may think that the reduction of the width for a retreating glacier is exaggerated by taking $m = 1$, observations and modelling suggest that the assumption is quite reasonable (e.g. Abermann et al., 2009; Giesen, 2009, Figure 7.7).

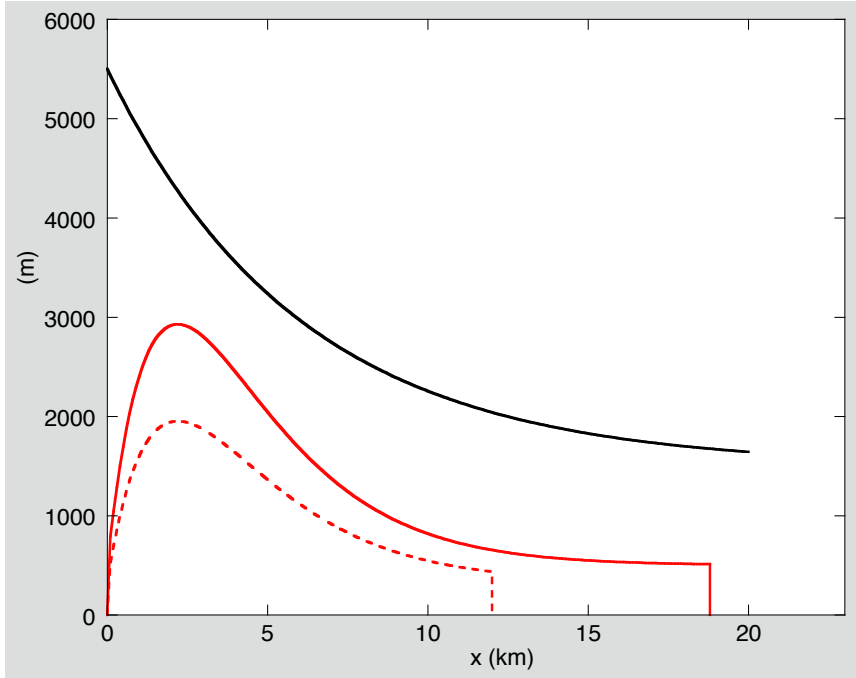


Figure 8.1. An example of a bed profile (in black) and glacier width (in red, for two different glacier lengths) as used in this chapter.

As before, the evolution of the glacier is calculated from the conservation of mass (volume):

$$B_s = \frac{dV}{dt} = H_m W_m \frac{dL}{dt} + H_m L \frac{dW_m}{dt} + W_m L \frac{dH_m}{dt} \quad (8.2.3)$$

Here W_m is the mean width of the glacier. It is easily verified by integration that

$$W_m = \frac{L}{L_0} \left\{ w_0 + w_1 a^{-2} \left(L^{-1} - a e^{-aL} - L^{-1} e^{-aL} \right) \right\}, \quad (8.2.4)$$

and

$$\frac{dW_m}{dt} = \left\{ \frac{w_0 + w_1 L e^{-aL}}{L_0} \right\} \frac{dL}{dt}. \quad (8.2.5)$$

The mean ice thickness is parameterised again as

$$H_m = \frac{\alpha_m}{1 + \nu \bar{s}} L^{1/2}, \quad (8.2.6)$$

so we have

$$\frac{dH_m}{dt} = \frac{\alpha_m}{2(1+\nu\bar{s})} L^{-1/2} \frac{dL}{dt} - \frac{\alpha_m \nu}{(1+\nu\bar{s})^2} L^{1/2} \frac{\partial \bar{s}}{\partial L} \frac{dL}{dt}, \quad (8.2.7)$$

where the mean bed slope \bar{s} is

$$\bar{s} = \frac{b_0}{L} (1 - e^{-x/x_l}). \quad (8.2.8)$$

We have now expressed all terms in the right-hand side of eq. (8.2.3) as a coefficient times dL/dt , i.e.

$$\frac{dV}{dt} = \left\{ \frac{3}{2} H_m W_m + H_m L \frac{dW_m}{dL} - H_m W_m L \frac{\nu}{1+\nu\bar{s}} \frac{d\bar{s}}{dL} \right\} \frac{dL}{dt} = \Psi \frac{dL}{dt} = B_s \Rightarrow \frac{dL}{dt} = \Psi^{-1} B_s. \quad (8.2.9)$$

The next step is to derive the expression for the total surface balance B_s . The balance profile is taken linear again, with balance gradient β and equilibrium-line altitude E . We have

$$B_s = \int_0^L W(x) \dot{b}(x) dx = \frac{\beta L}{L_0} \int_0^L (w_0 + w_1 x e^{-ax}) [b_0 e^{-x/x_l} + b_a + H(x) - E] dx \approx \frac{\beta L}{L_0} \int_0^L (w_0 + w_1 x e^{-ax}) [b_0 e^{-x/x_l} + b_a + H_m - E] dx. \quad (8.2.10)$$

Evaluating the integral yields:

$$B_s \approx \frac{\beta L}{L_0} \left\{ w_0 b_0 x_l (1 - e^{-L/x_l}) - w_0 (E - H_m - b_a) L + \frac{w_1 b_0 x_l}{(1+ax_l)^2} [x_l - e^{-L(a+x_l^{-1})} (L + L a x_l + x_l)] \right\} - \frac{\beta L}{L_0} \frac{(E - H_m - b_a) w_1}{a^2} [1 - e^{-aL} - a L e^{-aL}]. \quad (8.2.11)$$

This completes the formulation of the model. As before, eq. (8.2.9) can be integrated in time with a simple Euler scheme (see section 3.2).

8.3 Application to McCall Glacier, Alaska

McCall Glacier is a polythermal valley glacier in the Brooks Range in northern Alaska. It is currently about 7.5 km long, has an area of about 6 km^2 and extends over an altitudinal range of about 1200 m. McCall Glacier is a well studied glacier, on which several types of measurements were initiated during the International Geophysical Year (1957-58). Rabus and Echelmeyer (1997) made a detailed study of the flow of this glacier, and discussed the polythermal character and its implications. Apart from the initiation of the mass balance programme, the micro-meteorology of McCall Glacier has also been studied (e.g. Wendler and Ishikawa, 1974; Klok et al., 2006). McCall Glacier has been retreating steadily over the past hundred years (Figure 8.2). In the early 1990's the retreat accelerated (Nolan et al., 2005; Delcourt et al., 2008).



Figure 8.2. Two photographs of McCall Glacier, taken in 1958 (by A. Post) and in 2003 (by M. Nolan).

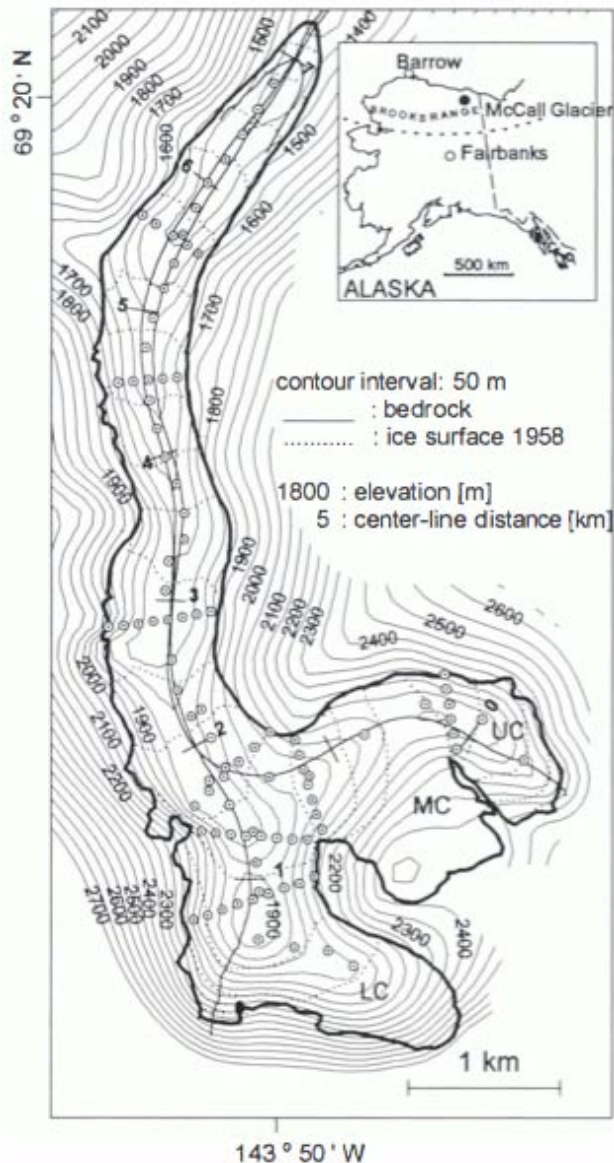


Figure 8.3. Bed topography of McCall Glacier, taken from Rabus and Echelmeyer (1997). The upper, middle and lower cirques (UC, MC and LC, respectively) have a characteristic scale of ~1 km and combine to form the valley glacier.

The bed topography of McCall Glacier is well known. Three cirques glaciers (UC, MC, LC) combine into a single well-defined flowline (Figure 8.3). Apart from some minor undulations the bed is regular and does not have significant overdeepenings.

The parameterised geometry adopted for the minimal glacier model is shown in Figure 8.4. The upper part, which has a maximum width of about 2200 m, represents the average conditions for the three cirques. The glacier width is scaled with the glacier length, as illustrated in the figure. The reference glacier length has been taken as 7.3 km in the year 2005. This is slightly shorter than the value used in Delcourt et al. (2007), which is 7.6 km. The difference is due to the fact that in the minimal model there is no flowline that goes all the way to the highest point of the glacier.

The parameter values for the geometry are: $b_a = 1280$ m, $b_0 = 1200$ m, $x_l = 3300$ m, $w_0 = 400$ m, $w_1 = 7.6$, $a = 0.0016$. The corresponding mean bed slope for a glacier length of 7.3 km is 0.146, and the glacier area 5.9 km^2 . Delcourt et al. (2008) report a mean ice thickness of about 120 m. This value can easily be matched by using $\alpha = 3.4 \text{ m}^{1/2}$ in eq. (8.2.6). In the study of Hansbreen (Oerlemans, 2010) a value of $\alpha = 3.0 \text{ m}^{1/2}$ was found to perform well. The difference is understandable if we realize that Hansbreen is an essentially temperate glacier sliding over a soft bed and McCall Glacier is a polythermal glacier that does not slide everywhere (Rabus and Echelmeyer, 1997). Other model parameters are: $v = 10$, $\beta = 0.0017 \text{ m ice a}^{-1} \text{ m}^{-1}$.

Unfortunately, mass balance observations on McCall Glacier do not constitute a continuous record. Measurements were done in the periods 1969-1972, 1993-1996, and since 2003. In view of this, here an approach is taken in which the temporal evolution of the equilibrium-line altitude is reconstructed by matching simulated and observed glacier length. In the framework of minimal glacier modelling, this technique was also used in the study of Hansbreen (Oerlemans, 2011). A piecewise linear increase in time of E , with different rates for two different periods, appears to perform well. The climatic conditions that give the best possible simulation are summarised in Table 8.1.

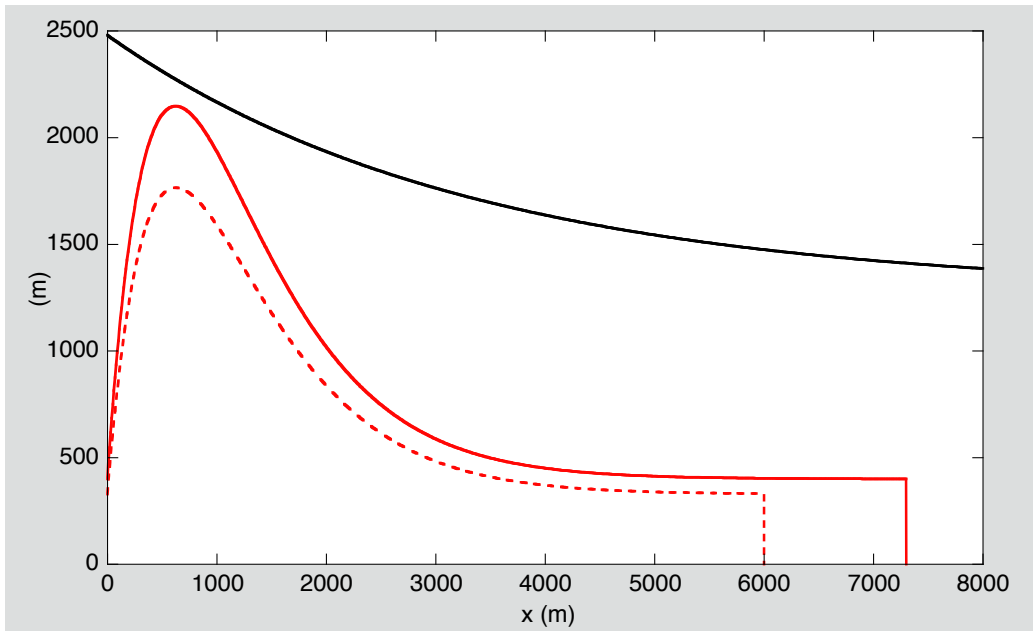


Figure 8.4. The parameterised geometry of McCall Glacier. The black solid line shows the bed profile. The glacier width is shown in red for the reference length (7300 m), as well as for a length of 6000 m (dashed).

Initial state:	$L = 7.8 \text{ km}, E = 2005 \text{ m}$
$1870 < t < 1970 \text{ (year)}$:	$\partial E / \partial t = 2.45 \text{ m a}^{-1}$
$t > 1970 \text{ (year)}$:	$\partial E / \partial t = 5.60 \text{ m a}^{-1}$

Table 8.1. Climate change scenario (in terms of equilibrium-line altitude E) that gives a very good match between observed and simulated glacier length.

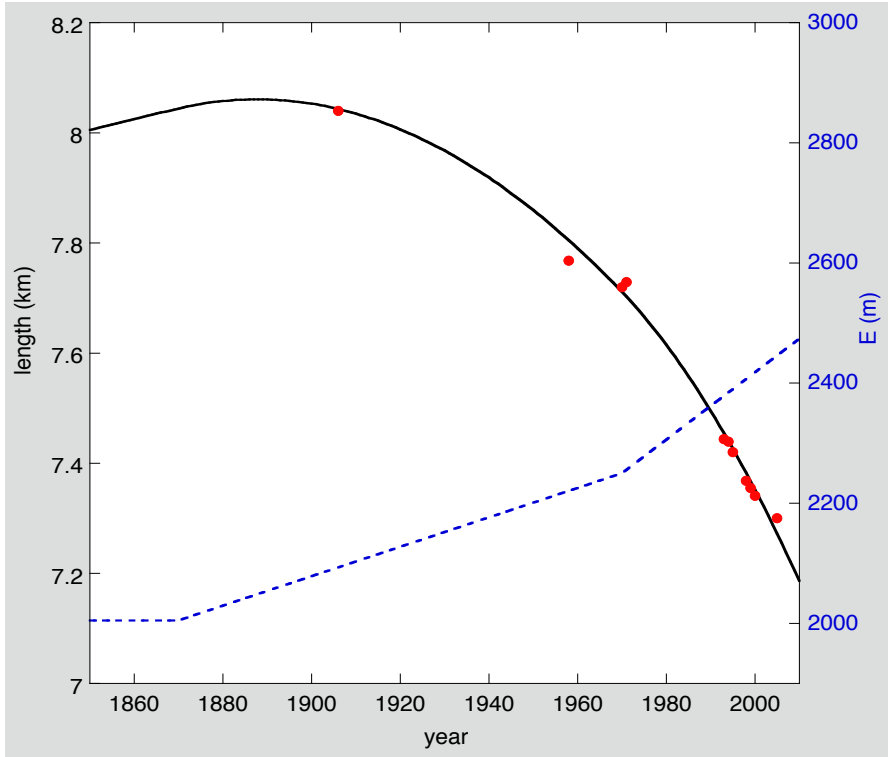


Figure 8.5. A comparison between the simulated (black line) and observed (red dots) glacier length. The dashed blue line shows the corresponding evolution of the equilibrium line altitude E .

First of all we note that the glacier length observed in 1906 is 8.04 km in our reference system (glacier length in 2005 equals 7.3 km). This is considered to be close to the Little Ice Age maximum stand. It has been suggested that McCall Glacier was more or less in a steady state towards the end of the 19th century, but there is no hard evidence for this (Nolan et al., 2005). According to the present model, a steady-state glacier length of about 8 km corresponds to an equilibrium-line altitude of about 2000 m. This is 100 m higher than the value found by Delcourt et al. (2008) in their modelling study. The reason for this discrepancy is unclear.

The typical rate at which the equilibrium line should have risen during the 20th century should be of the order of 3 m a^{-1} . A good match between observed and simulated glacier length is obtained when $\partial E / \partial t$ increases significantly somewhere in the second half of the 20th century. The best fit is obtained when $\partial E / \partial t$ has a value of 5.60 m a^{-1} from 1970 onwards, and it is interesting to see what could happen if this rise of the equilibrium line continues throughout the 21st century. In that case $E = 2978 \text{ m}$ in the year 2100, which is well above the highest point of the glacier. The model predicts an ice volume of 38% of the 2010 volume, whereas the glacier area is roughly halved. Given the fact that a 300 m increase in E may be initiated by a temperature rise of 2 to 3 K, the evolution of McCall Glacier shown in Figure 8.6 may be realistic (assuming no variations in the precipitation rate).

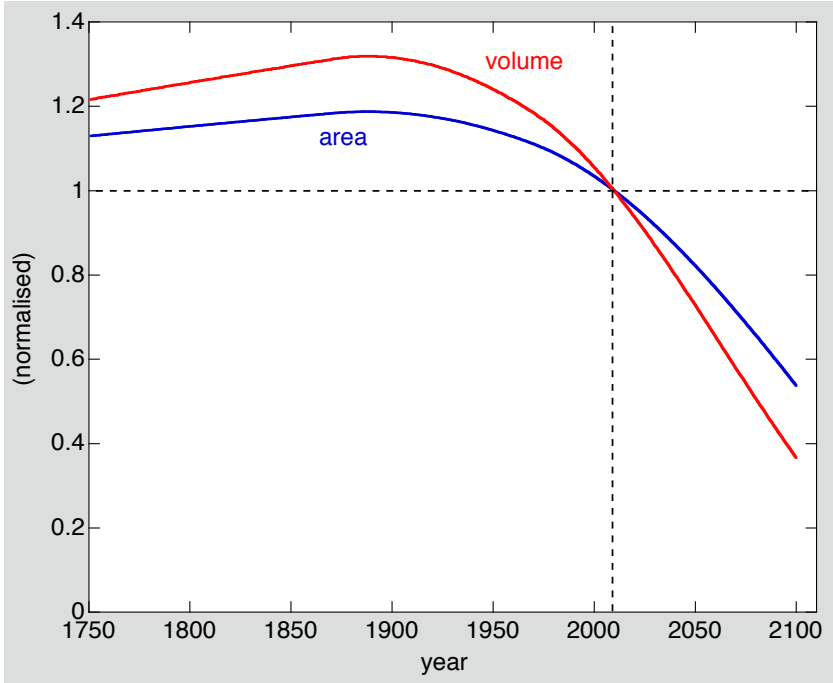


Figure 8.6. Predicted area and volume of McCall Glacier if the equilibrium line continues to rise at a rate of 3.15 m a^{-1} .

8.4 Application to the Vadret da Morteratsch system

The Vadret da Morteratsch is a typical valley glacier, located in the Swiss Alps ($46^{\circ}24'\text{N}$, $9^{\circ}56'\text{E}$; photographs on pages 55 and 83; see Figure 8.7 for a map). It is about 7 km long, has an area of about 17 km^2 and spans an altitudinal range of about 2000 m. The highest peak is the Piz Bernina (4049 m). The glacier front is found at an altitude of about 2000 m, which is somewhat below the current treeline in the region. The accumulation basin is steep and rugged, whereas the ablation zone has a smaller slope with a few crevassed areas. The equilibrium-line altitude is about 3000 m. The glacier flows in northerly direction. There is one major tributary coming in from the east, the Vadret Pers. The glacier front has retreated over a distance of about 2 km since the middle of the 19th century, as witnessed by impressive side moraines. On the Vadret da Morteratsch micro-meteorological studies have been conducted for a long time (e.g. Oerlemans and Knap, 1998; Oerlemans et al., 2009; Oerlemans, 2010), and a spatially-distributed mass-balance model with 25 m resolution has been developed and calibrated for this glacier (Klok and Oerlemans, 2002).

To further explore the possibilities of the minimal glacier model, we will consider the glacier system shown in Figure 8.7 as a two-component system: (i) the Vadret da Morteratsch (VdM) and the Vadret Pers (VP). Since the VP delivers ice mass to the VdM, the components should be coupled. In the framework of the minimal glacier model this is simple. The length of the VP is maximised by the point at which it flows into the VdM. When this maximum length $L_{P,\max}$ is reached, the total surface mass balance of the VP is added to the VdM. So, we have (note: for all variables: index M for Vadret da Morteratsch; index P for Vadret Pers):

$$\text{if } L_P < L_{P,\max} : \quad \frac{dL_M}{dt} = \Psi_M^{-1} B_{s,M}; \quad \frac{dL_P}{dt} = \Psi_P^{-1} B_{s,P}, \quad (8.4.1)$$

$$\text{if } L_P = L_{P,\max} \text{ and } B_{s,P} > 0 : \quad \frac{dL_M}{dt} = \Psi_M^{-1} (B_{s,M} + B_{s,P}); \quad \frac{dL_P}{dt} = 0. \quad (8.4.2)$$

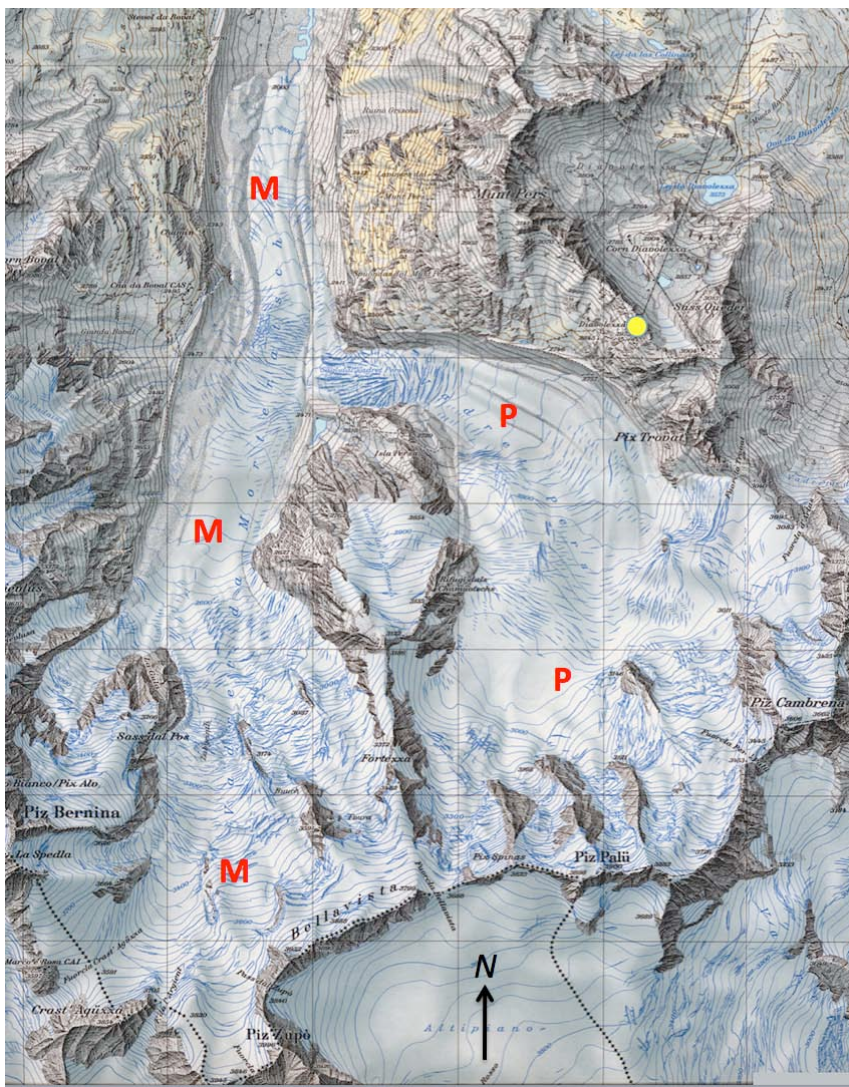


Figure 8.7. Topographic map (2006; Bundesamt für Landestopografie) of the Morteratsch (M) – Pers (P) glacier system. Peaks at the glacier head seen on the map are (from left to right): Piz Bernina (4049 m), Piz Zupò (3996 m), Bellavista (3922), Piz Palü (3905 m) and Piz Cambrena (3606 m). The yellow dot marks the upper station (~ 3000 m) of the Diavolezza cable car.

It should be noted that the VP will become shorter than its maximum length as soon as $B_{s,P} < 0$. This is a consequence of the fact that in a minimal glacier model the relation between volume and length is ‘fixed’.

The VP and the VdM have different geometric characteristics. The VP is shorter than the VdM and has a wider upper basin. The typical surface profiles of the glaciers are also somewhat different, because the topography of the VP falls off more rapidly (smaller value of x_l). The parameters chosen to represent the schematic geometry of the VP and the VdM are listed in Table 8.2.; see also Figure 8.8. Other parameter values used are: $L_{P,\max} = L_{P,0} = 4500$ m, $L_{M,0} = 8000$ m, $\alpha = 3.0 \text{ m}^{1/2}$, $v = 10$, $\beta = 0.007 \text{ m ice a}^{-1} \text{ m}^{-1}$.

	w_0	w_1	a	b_a	b_0	x_l
Vadret da Morteratsch	700 m	3.0	0.00075	1670 m	2300 m	3900 m
Vadret Pers	100 m	8.5	0.00090	1750 m	1750 m	2300 m

Table 8.2. Geometric parameters with which the VdM and the VP are characterised.

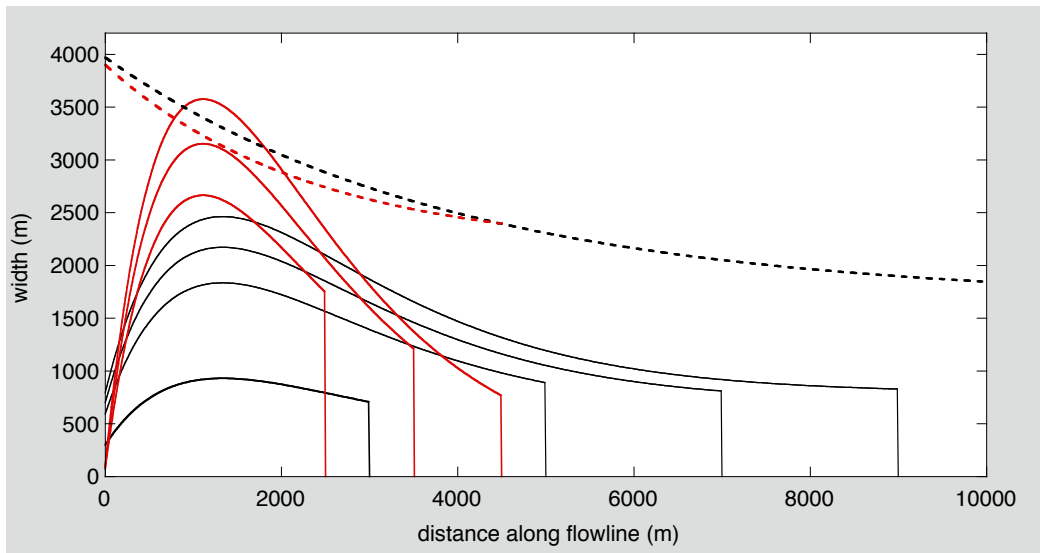


Figure 8.8. The parameterised geometry of the Pers / Morteratsch glacier system. Dashed lines show the bed profiles, solid lines the glacier width. Black lines refer to the Vadret da Morteratsch, red lines refer to the Vadret Pers. The width is shown for different glacier lengths. It should be noted that the origin of the horizontal axis (distance along flowline) is different for the two glaciers!

Figure 8.9 shows the result of a calibration procedure, in which a history of the equilibrium line $E(t)$ has been determined that yields a good match between simulated and observed length of the VdM. Data have been taken from the Swiss Glacier Monitoring Network; the last data point is for 2009. The VdM is believed to have reached its maximum neo-glacial stand around 1860. A simple functional form for $E(t)$ was chosen: a linear increase in time on which two Gaussian bumps are superimposed. By selecting the appropriate parameter values the observed record is reproduced

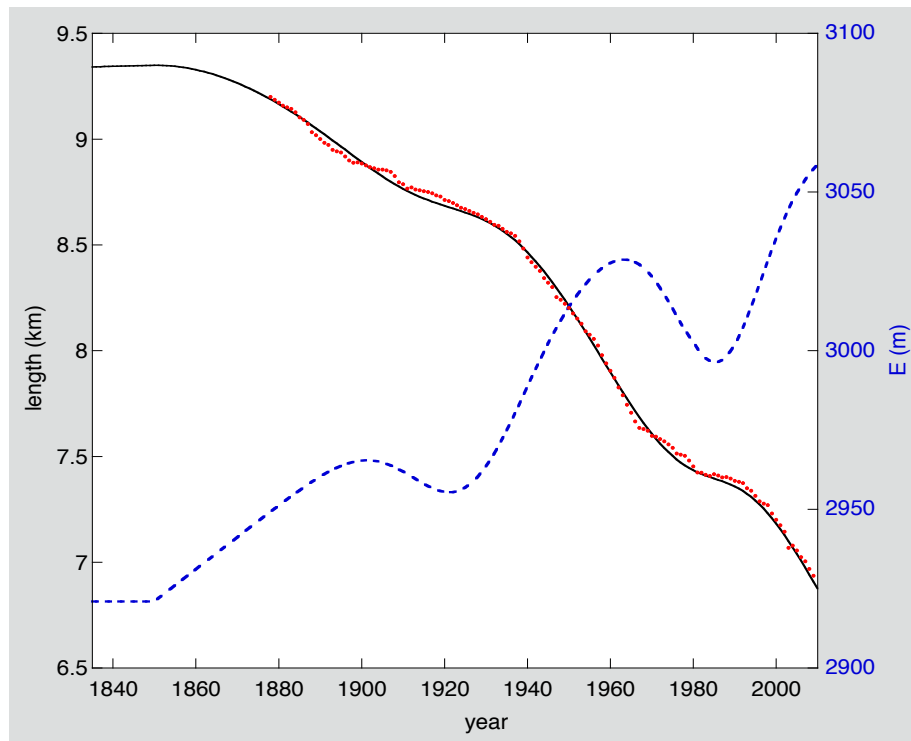


Figure 8.9. A comparison between the simulated (black line) and observed (red dots) glacier length of the Vadret da Morteratsch. The dashed blue line shows the corresponding evolution of the equilibrium line altitude E .

well. Broadly speaking, the trend of a rising equilibrium line has been interrupted twice, namely during the periods 1900–1930 and 1960–1995. The model calculation suggests that the total increase in E since the LIA is about 140 m. This is virtually the same value as found by the entirely different method described in section 7.4, applied to the Vadret da Palü and Vadret da Morteratsch (Oerlemans, 2007). It should be noted that the $E(t)$ as reconstructed here is well determined. For instance, shifting one of the Gaussian bumps by 10 years along the time axis immediately results in a significant discrepancy between simulated and observed glacier length.

The model was also integrated for a climate change scenario in which the equilibrium line rises by 1.5 m per year from 2010 onwards. The results are summarised in Figure 8.10. As expected, the strong retreat of the VdM will continue, and in 2100 the glacier length is predicted to be 4.3 km long. In 2013 the input from the VP will become zero, and the length of the VP will start to decrease (from the maximum value of 4.5 km).

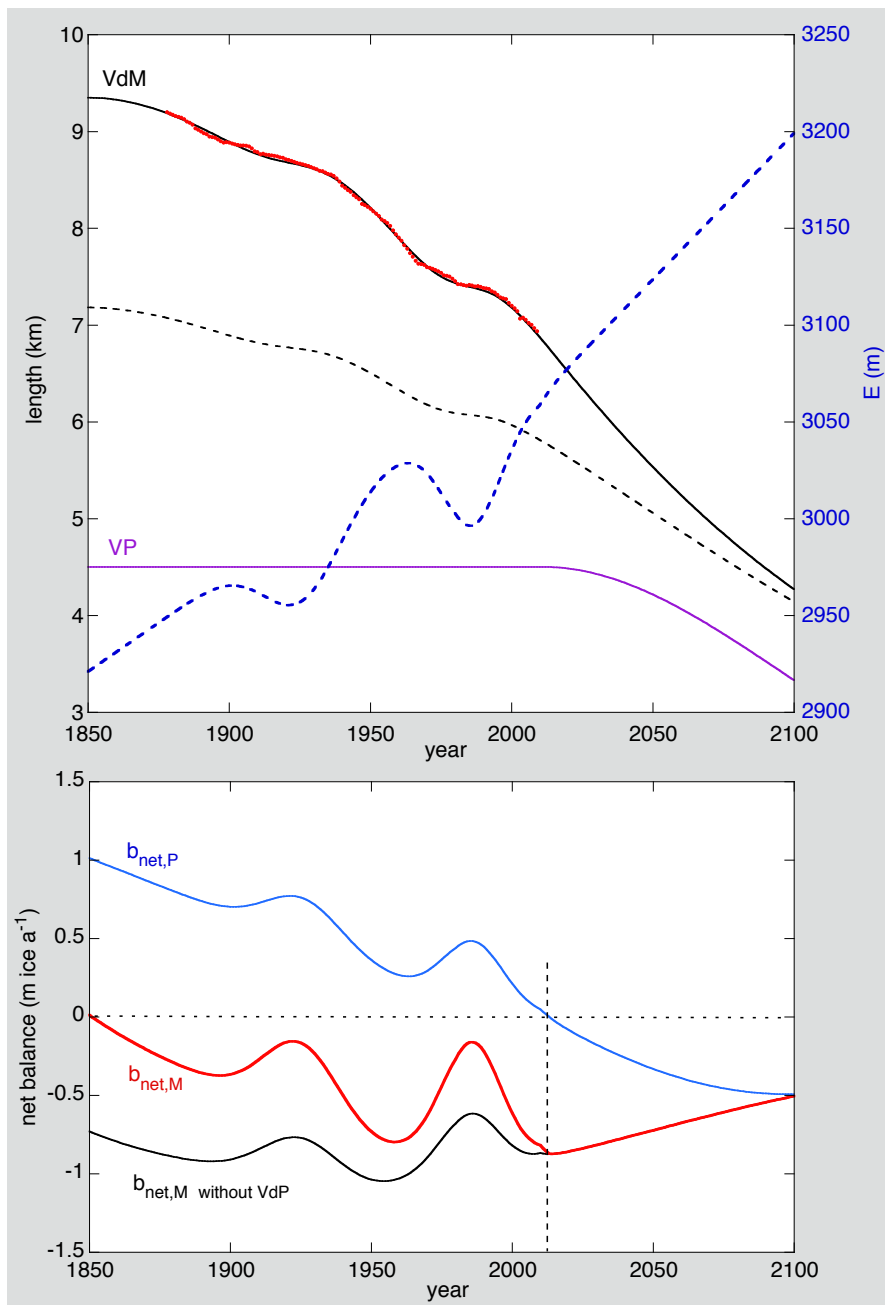


Figure 8.10. *Upper panel:* glacier length of the VdM and VP predicted for a scenario with a constant rise of the equilibrium line. The black dashed line shows the length of VdM calculated for the case without mass input from the VP.
Lower panel: net balance rates for the VP and the VdM.

The corresponding net balances are shown in the lower panel of Figure 8.10. At the LIA maximum glacier stand, the net balance of the VP was 1 m ice a^{-1} . All of the surplus ice was supplied to the VdM, which apparently had a large effect. As demonstrated by the dashed black curve in the upper panel of Figure 8.10, in 1850 the VdM would have been about 2 km shorter without mass input from the VP.

The strong climate sensitivity of the mass input from the VP into the VdM is a consequence of the hypsometry of the VP (Figure 8.8). The large contribution from the VP as calculated with the model for the early 19th century is in agreement with an old photography made in 1911 (Figure 8.11). The photo shows an interesting view on the lower part of the glacier, on which the medial moraine marks the border between ice originating from the VP (on the left) and ice from the VdM (on the right). In contrast, a comparison with the photograph at the beginning of this chapter, or with the recent topographic map (Figure 8.7), makes clear that the current mass input from the VP is very small indeed.



Figure 8.11. Photograph from 1911 showing the Pers / Morteratsch glacier system (looking south). The medial moraine marks the border between ice originating from the Vadret Pers (on the left) and from the Vadret da Morteratsch (on the right).

This photo was issued as a postcard by Wehrli A.-G., Kilchberg, Zürich, and is currently in the collection of Manfred Luckmann.

Nevertheless, it is interesting to note that the mass supplied by the VP *in the past* has some effect on the size of the VdM *in the future*, even though the mass input is predicted to be zero after 2012. This is due to the delayed response of the VdM to climate change, of course.

In 2010 the volumes of the VP and VdM were estimated to be 0.47 and 0.65 km³, respectively. Volumes as a function of time, normalised with these values, are shown in Figure 8.12.

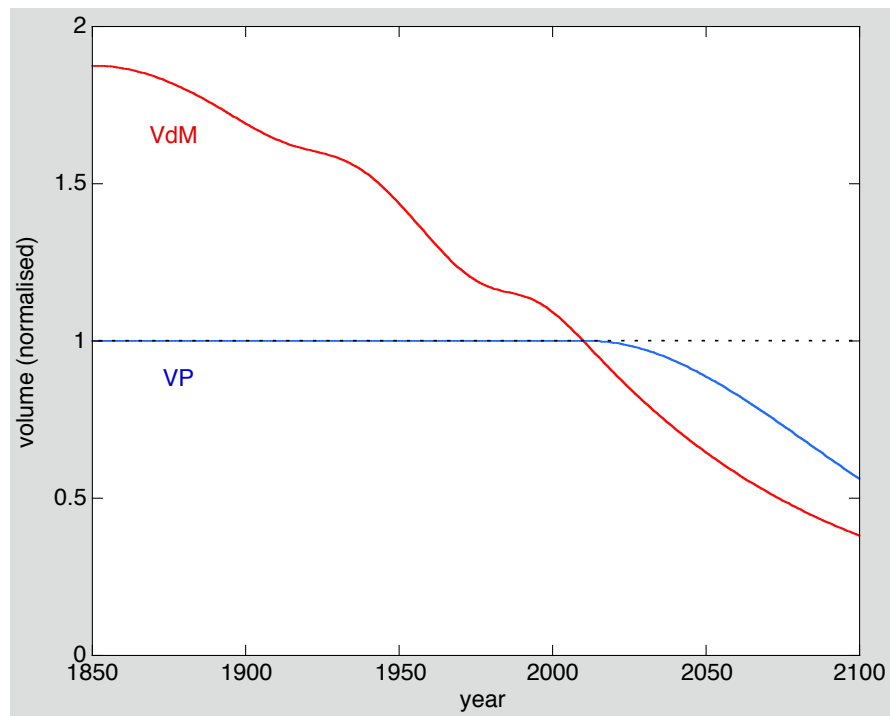
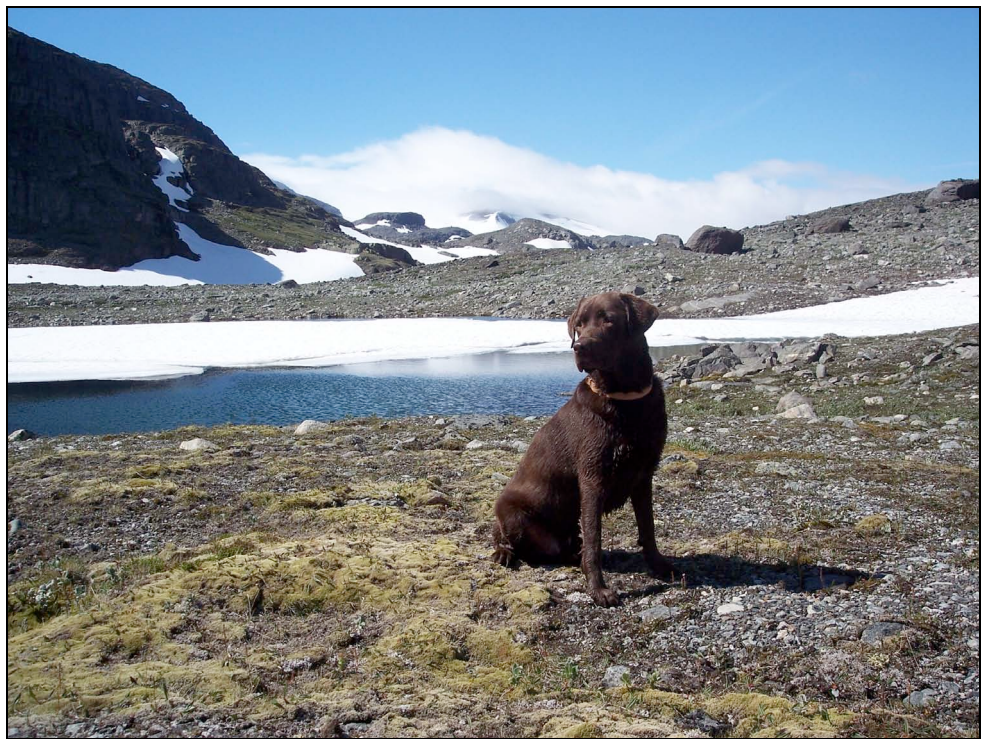


Figure 8.12. Volumes of the VP and VdM relative to the 2010 values.



Hardangervidda, Norway

Epilogue

The set of models discussed in this text are first of all meant to be learning tools. They should provide the reader with a basic feeling for what matters in the interaction of glaciers with climate. I also hope that students find inspiration to go a little bit beyond the models presented here and try, for instance, to find solutions for more complicated beds or for a more sophisticated formulation of the mass balance field.

The limitations of the approach should not be forgotten. Fundamental to the theory developed in this book is the assumption that mean ice thickness and glacier length have a one-to-one relation. Calculations with numerical models have shown that H_m may differ by typically 10% between retreating and advancing glaciers (e.g. Oerlemans, 2001). Depending on the balance gradient, this implies an error in the estimated mass budget.

Simple modelling of glaciers can also be done without assuming that volume and length (and/or area) are always in phase. Harrison et al. (2003) have developed a theory to describe the relation between volume and area. In this theory, ‘A macroscopic approach to glacier dynamics’, a second-order linear equation emerges, which supports damped oscillations and an out-of-phase relationship between volume and area. This model therefore has more possibilities to match the rapid evolution of an individual glacier.

In this second print a chapter has been added (Chapter 8), in which a minimal glacier model with varying width and bed slope has been applied to McCall Glacier (Canada) and the Vadret da Morteratsch (Switzerland). The work on Hansbreen (section 6.4) has been extended and published in a separate paper (Oerlemans et al., 2011). From these studies it appears that the power of the minimal model is the straightforward way in which calibration with historic glacier changes can be carried out.

In this text only valley glaciers were considered. I have also applied the principle of the minimal model to axisymmetric ice sheets (Oerlemans, 2003, 2004, 2005). There is a difference in scale, mass-balance conditions and forcing, but altogether the analysis is very similar. Applications include the response of the Antarctic ice sheet to temperature and sea-level forcing during the late Pleistocene, and separation of the ocean temperature and ice volume contributions to the deep-sea oxygen isotope signal through Cenozoic times.

Acknowledgements

Through the years, discussions with students and colleagues have helped to shape the ideas on which this text is based. Fortunately, I work in a group where people have a very open mind and are willing to listen when a different approach is proposed. This little book is the product of an individual, working in a stimulating research environment – it is not a deliverable of a sharply defined research project.

I am grateful to a number of people that have read the manuscript, found typos and made useful suggestions. Tómas Jóhannesson, Jojanneke van den Berg, Peter Kuipers Munneke, Paul Leclercq, Carleen Tijm-Reijmer, Roderik van de Wal, Rianne Giesen, Jean-Paul Charbonnier and Ward van Pelt should be mentioned explicitly for their helpful comments.

References

- Abermann J., A. Lambrecht, A. Fischer and M. Kuhn (2009): Quantifying changes and trends in glacier area and volume in the Austrian Ötztal Alps (1969-1997-2006). *The Cryosphere* **3**, 205-215.
- Aðalgeirs Þóttir G. (2003): *Flow dynamics of Vatnajökull ice cap, Iceland*. Mitteilungen der VAW Nr. 181.
- Aðalgeirs Þóttir G., H. Björnsson, F. Pálsson and E. Magnússon (2005): Analysis of a surging outlet glacier of Vatnajökull ice cap, Iceland. *Annals of Glaciology* **42**, 23-28.
- Ambach W. (1963): Untersuchungen zum Energieumsatz in der Ablationszone des Grönlandischen Inlandeises. *Meddelelser om Grönland* **174** (4), 311 pp.
- Anderson B., W. Lawson, I. Owens, and B. Goodsell (2006): Past and future mass balance of Ka Roimata o Hine Hukatere (Franz Josef Glacier). *Journal of Glaciology* **52** (179), 597-607.
- Björnsson H. (1988): *Hydrology of Ice Caps in Volcanic Regions*. Societas Scientiarum Islandica. 139 pp.
- Bogen J., B. Wold and G. Østrem (1989): Historic glacier variations in Scandinavia. In: *Glacier Fluctuations and Climate Change* (ed. J. Oerlemans), Kluwer Academic Publishers, 109-128.
- Brown C.S., M.F. Meier and A. Post (1982): *Calving speed of Alaska tidewater glaciers with applications to the Columbia Glacier, Alaska*. U.S. Geol. Surv. Prof. Pap. 1258-C, 13 pp.
- Budd W.F. (1975): A first simple model of periodically self-surging glaciers. *Journal of Glaciology* **14**, 3-21.
- Budd W.F. and D. Jenssen (1975): Numerical modelling of glacier systems. *IAHS-AISH Publ. No. 104*, 257-291.
- Bundesamt für Landestopographie. 1979. *Landeskarte der Schweiz, Blatt 1277, Piz Bernina*. 1:25.000. Wabern, Switzerland.
- Delcourt C., F. Pattyn and M. Nolan (2008): Modelling historical and recent mass loss of McCall Glacier, Alaska, USA. *The Cryosphere* **2**, 23-31, doi:10.5194/tc-2-23-2008.
- Dowdeswell J.A. and M. Williams (1997): Surge-type glaciers in the Russian High Arctic identified from digital satellite imagery. *Journal of Glaciology* **43**, 489-494.
- Fowler A.C. (1987): A theory of glacier surges. *Journal of Geophysical Research (Solid Earth and Planets)* **92** (9), 9111-9120.
- Giesen R. (2009): The ice cap Hardangerjøkulen in the past, present and future climate. PhD thesis, Utrecht University, The Netherlands. ISBN 978-90-393-5185-7.
- Gilmore R. (1981): *Catastrophe Theory for Scientists and Engineers*. John Wiley and Sons, 666 pp.

Greuell W., W.H. Knap and P.C. Smeets (1997): Elevational changes in meteorological variables along a midlatitude glacier during summer. *Journal of Geophysical Research* **102** (D22), 25,941-25,954.

Hamming R. (1987): *Numerical methods for scientists and engineers*. Dover Publ., 2nd edition, 721 pp.

Harrison W.D., D.H. Elsberg, K.A. Echelmeyer and R.M. Krimmel (2001): On the characterization of glacier response by a single time-scale. *Journal of Glaciology* **47** (159), 659-664.

Harrison W.D., C.F. Raymond, K.A. Echelmeyer and R.M. Krimmel (2003): A macroscopic approach to glacier dynamics. *Journal of Glaciology* **49** (164), 13-21.

Jania J., D. Mochnacki and B. Gadek (1996): The thermal structure of Hansbreen, a tidewater glacier in southern Spitsbergen, Svalbard. *Polar Research* **15** (1), 53-66.

Jóhannesson T., C.F. Raymond and E.D. Waddington (1989): Time-scale for adjustment of glaciers to changes in mass balance. *Journal of Glaciology* **35**, 355-369.

Kamb B., C.F. Raymond, W.D. Harrison, H.F. Engelhardt, K.A. Echelmeyer, N.F. Humphrey, M.M. Brugmann and T. Pfeffer (1985): Glacier surge mechanism, 1982-1983 surge of Variegated Glacier, Alaska. *Science* **227**, 469-479.

Kaser G. and H. Osmaston (2002): *Tropical Glaciers*. Cambridge University Press, 207 pp.

Kjøllmoen B. (2003): *Glaciological investigations in Norway in 2002*. NVE Report No. 3, 92 pp.

Klok E.J., M. Nolan and M.R. van den Broeke (2006): Analysis of meteorological data and the surface energy balance of McCall Glacier, Alaska, USA. *Journal of Glaciology* **51** (174), 505-518.

Klok E.J. and J. Oerlemans (2002): Model study of the spatial distribution of the energy and mass balance of Morteratschgletscher, Switzerland. *Journal of Glaciology* **48** (163), 451-461.

Kruss P.D. (1983): Climatic change in East Africa: numerical modeling from the 100 years of terminus record of Lewis Glacier, Mount Kenya. *Zeitschrift für Gletscherkunde und Glazialgeologie* **19**, 43-60.

Kuhn M. (1979): On the computation of heat transfer coefficients from energy-balance gradients on a glacier. *Journal of Glaciology* **22** (87), 263-272.

Kuhn M. (1989): The response of the equilibrium-line altitude to climate fluctuations: theory and observations. In: *Glacier Fluctuations and Climate Change* (ed. J. Oerlemans), 407-417, Kluwer Academic Publishers.

Kuipers Munneke P. (2005): *Past and future of Nordenskiöldbreen, Svalbard*. Master thesis, University of Groningen, 62 pp.

Leysinger Vieli G.J.-M.C., and G.H. Gudmundsson (2004): On estimating length fluctuations of glaciers caused by changes in climatic forcing. *Journal of Geophysical Research* **109**, F01007, doi:10.1029/2003JF000027.

Luterbacher J., D. Dietrich, E. Xoplaki, M. Grosjean, H. Wanner (2004): European seasonal and annual temperature variability, trends, and extremes since 1500. *Science* **303**, 1499 - 1503, doi: 10.1126/science.1093877.

Maisch M. (2000): The long-term signal of climate change in the Swiss Alps. Glacier retreat since the Little Ice Age and future ice decay scenarios. *Geografia Fisica e Dinamica Quaternaria* **23**, 139-152.

Marshall S., H. Björnsson, G.E. Flowers and G.K.C. Clarke (2005): Simulation of Vatnajökull ice cap dynamics. *Journal of Geophysical Research* **110**, F03009, doi:10.1029/2004JF000262.

Milana J.B. (2007): A model of the Glaciar Horcones Inferior surge, Aconcagua region, Argentina. *Journal of Glaciology* **53** (183), 565-572.

Murray T., G.W. Stuart, P.J. Miller, J. Woodward, A.M. Smith, P.R. Porter, and H. Jiskoot (2000): Glacier surge propagation by thermal evolution at the bed. *Journal of Geophysical Research* **105** (B6), 13491-13507.

Murray T., T. Strozzi, A. Luckman, H. Jiskoot, and P. Christakos (2003): Is there a single surge mechanism? Contrasts in dynamics between glacier surges in Svalbard and other regions. *Journal of Geophysical Research* **108** (B5), 2237, 10.1029/2002JB001906.

Nick F.M. and J. Oerlemans (2006): Dynamics of calving glaciers: comparison of three models. *Journal of Glaciology* **51** (177), 183-190.

Nolan M., A. Ahrendt, B. Rabus and L. Hinzman (2005): Volume change of McCall Glacier, Arctic Alaska, from 1956 to 2003. *Annals of Glaciology* **42**, 409-416.

Nye J. (1965): The frequency response of glaciers. *Journal of Glaciology* **5**, 567-587.

Oerlemans J. (1992): Climate sensitivity of glaciers in southern Norway: application of an energy-balance model to Nigardsbreen, Hellstugubreen and Alfotbreen. *Journal of Glaciology* **38**, 223-232.

Oerlemans J. (1997a): Climate Sensitivity of Franz-Josef Glacier, New Zealand, as revealed by numerical modelling. *Arctic and Alpine Research* **29** (2), 233-239.

Oerlemans J. (1997b): A flow-line model for Nigardsbreen: projection of future glacier length based on dynamic calibration with the historic record. *Annals of Glaciology* **24**, 382-389.

Oerlemans J. (2001): *Glaciers and Climate Change*. A.A. Balkema Publishers, 148 pp. ISBN 9026518137.

Oerlemans J. (2003): A quasi-analytical ice-sheet model for climate studies. *Nonlinear Processes in Geophysics* **10**, 1-12.

Oerlemans J. (2004): Correcting the Cenozoic deep-sea temperature record for Antarctic ice volume. *Palaeogeography, Palaeoclimatology, Palaeoecology* **208** (3), 191-201

Oerlemans J. (2005a): Extracting a climate signal from 169 glacier records. *Science* **308**, 675-677; doi: 10.1126/science.1107046

Oerlemans J. (2005b): Antarctic ice volume for the last 740 ka calculated with a simple ice-sheet model. *Antarctic Science* **17** (2), 281-287, doi: 10.1017/S0954102005002683.

Oerlemans J. (2007): Estimating response times of Vadret da Morteratsch, Vadret da Palue, Briksdalsbreen and Nigardsbreen from their length records. *Journal of Glaciology* **53** (182), 357-362.

Oerlemans J. (2010): *The Microclimate of Valley Glaciers*. Igitur, Utrecht University, 138 pp.

Oerlemans J., J. Jania and L. Kolondra (2011): Application of a minimal glacier model to Hansbreen, Svalbard. *The Cryosphere* **5**, 1-11.

Oerlemans J., R.H. Giesen and M.R. van den Broeke (2009): Retreating alpine glaciers: increased melt rates due to accumulation of dust (Vadret da Morteratsch, Switzerland). *Journal of Glaciology* **55**, 729-736.

Oerlemans J. and W.H. Knap (1998): A one-year record of global radiation and albedo from the ablation zone of the Morteratschgletscher, Switzerland. *Journal of Glaciology* **44**, 231-238.

Oerlemans J. and F.M. Nick (2005): A minimal model of a tidewater glacier. *Annals of Glaciology* **42**, 1-6.

Ohmura A., P. Kasser and M. Funk (1992): Climate at the equilibrium line of glaciers. *Journal of Glaciology* **130** (38), 397-411

Østrem G. and M. Brugman (1991): *Glacier mass-balance measurements: a manual for field and office work*. NHRI Science Report No. 4. Saskatoon: National Hydrology Research Institute .

Pälli A., J.C. Moore, J. Jania, L. Kolondra and P. Glowacki (2003): The drainage pattern of two polythermal glaciers: Hansbreen and Werenskioldbreen in Svalbard. *Polar Research* **22** (2), 355-371.

Pelto M.S. and C.R. Warren (1991): Relationship between tidewater glacier calving velocity and water depth at the calving front. *Annals of Glaciology* **15**, 115-118.

Plassen L., T.O. Vorren and M. Forwick (2003): Integrated acoustic and coring investigation of glaciogenic deposits in Spitsbergen fjords. *Polar Research* **23** (1), 89-110.

Post A. (1975): Preliminary hydrography and historic terminal changes of Columbia Glacier, Alaska. U.S. Geol. Sur. Hydrol. Invest. Atlas HA-559.

Rabus B.T. and K.A. Echelmeyer (1997): The flow of a polythermal glacier: McCall Glacier, Alaska, U.S.A. *Journal of Glaciology* **43** (145), 522-536.

Raymond C.F. (1987): How do glaciers surge? A review. *Journal of Geophysical Research* **92** (B9), 9121-9134.

Sharp M. (1988): Surging glaciers: behaviour and mechanisms. *Progress in Physical Geography* **12** (3), 349-370.

Smorenburg P. (2007): *Modelling tidewater glaciers: A case study of Hansbreen, a tidewater glacier on southern Spitsbergen*. Master Thesis, IMAU, Utrecht University.

Stineman R.W. (1980): A consistently well-behaved method of interpolation. *Creative Computing*. July: 54–57.

Van den Berg J., R.S.W van de Wal and J. Oerlemans (2006): Effects of spatial discretisation in ice sheet modelling using the shallow ice approximation (SIA). *Journal of Glaciology* **52**, 89-98.

Van der Veen C.J. (ed.) (1997): *Calving Glaciers: Report of a Workshop, February 28 - March 2, 1997*. Byrd Polar Research Center Report no. 5. Ohio State University (Columbus, Ohio, U.S.A.), 194 pp.

Van de Wal R.S.W. and J. Oerlemans (1995): Response of valley glaciers to climate change and kinematic waves: a study with a numerical ice-flow model. *Journal of Glaciology* **41** (137), 142-152.

Vieli A., M. Funk and H. Blatter (2001): Flow dynamics of tidewater glaciers: a numerical modelling approach. *Journal of Glaciology* **47** (159), 595-606.

Warren C.R. (1999): Calving speed in freshwater at Glaciar Ameghino, Patagonia. *Zeitschrift für Gletscherkunde und Glazialgeologie* **35** (1), 21-34.

Weertman J. (1961): Stability of ice-age ice sheets, *Journal of Geophysical Research* **66**, 3783-3792.

Wendler G. and N. Ishikawa (1974): The effect of slope, exposure and mountain screening on the solar radiation of McCall Glacier, Alaska: a contribution to the Interntaional Hydrological Decade. *Journal of Glaciology* **13** (68), 213-226.